UNIVERSITY OF CALIFORNIA SAN DIEGO

The Use of an Iron(III) Ion-Selective Electrode for Measurements of Seawater Iron Chemistry

A Dissertation submitted in partial satisfaction of the requirements
for the degree Doctor of Philosophy

in

Oceanography

by

Maxwell A. C. Fenton

Committee in charge:

Todd Martz, Co-Chair
Katherine Barbeau, Co-Chair
Andrew Dickson
Joseph Wang
Alberto Zirino

2025

The Dissertation of Maxwell A. C. Fenton is approved, and it is acceptable in quality and form for publication on microfilm and electronically.

University of California San Diego

2025

DEDICATION

To my family, especially the late Dr. Richard Fenton.

TABLE OF CONTENTS

LIST OF FIGURES

LIST OF TABLES

ACKNOWLEDGEMENTS

Chapter 1 is being prepared for submission for publication of the material. Fenton, Maxwell; Barbeau, Katherine; Martz, Todd. The dissertation author was the primary researcher and author of this material. I thank Roland De Marco for his expertise in physical chemistry, and his facilitation of the synchrotron radiation surface experiments at the Elettra synchrotron in Trieste, Italy. His past experience working with the chalcogenide glass Fe-ISE was essential for so much of this dissertation. I also thank Taylor Wirth for his help in the Martz lab, specifically with the automated pH-stat system that made our temperature tests possible.

Chapter 2 is being prepared for submission for publication of the material. Fenton, Maxwell; Barbeau, Katherine; Martz, Todd. The dissertation author was the primary researcher and author of this material.

Chapter 3 is being prepared for submission for publication of the material. Fenton, Maxwell; Barbeau, Katherine; Martz, Todd. The dissertation author was the primary researcher and author of this material. I thank the captains and crew of the R/V Sally Ride, the R/V Robert Gordon Sproul, and the R/V Roger Revelle, for their help deploying all sensor and water-sampling equipment. The science parties of Pupcycle II and P2507 were also instrumental in both seawater collection and sensor deployment. I give a special thanks to Claire Till and Adrian Marchetti, chief scientists for the Pupcycle II cruise, for welcoming me to their team and allowing me so much time to test the Fe-ISE.

I massively appreciate the efforts of Anna Lashtabeg, who manufactured all glass Fe-ISEs used in this work. None of this science would have been possible without the electrodes themselves, or her patience to deal with my endless requests. I also extend immense gratitude to Alberto Zirino. This project was largely a result of his own passion for the oceanographic potential of ISE analyses. His wisdom and intuitive sense for the workings of

these sensors was invaluable, and as one of the few people to actually use them at sea, his guidance and enthusiasm have been truly foundational for my own science. Abigail Severance deserves special recognition for her CLE-AdCSV analyses of much of the Fe-speciation samples in this work. She was a tremendous help and always had a great attitude.

Finally, I thank my advisors. Coming to Scripps, I knew that Todd and Kathy were brilliant scientists, but it is a different thing entirely to be able to work so closely to such technical, chemical, and oceanographic expertise. Though perhaps more importantly, they both foster exceptionally collaborative and friendly scientific spaces, and that is a testament to their own characters. It has been nothing but a pleasure working in their labs and with the people they have chosen to occupy them. Kathy welcomed me to her lab with a month-long research cruise in the California Current, where she and her graduate student Kiefer introduced me to science at sea with the utmost patience and kindness. I will always be grateful for such a formative experience with such amazing oceanographers.

VITA

2018 Bachelor of Science in Chemistry, University of California Berkeley

2021 Master of Science in Earth Sciences, University of California San Diego

2025 Doctor of Philosophy in Oceanography, University of California San Diego

FIELD OF STUDY

Major Field: Oceanography

Studies in Marine Chemistry, Electrochemistry

Professors Katherine Barbeau, Todd Martz

ABSTRACT OF THE DISSERTATION

The Use of an Iron(III) Ion-Selective Electrode for Measurements of Seawater Iron Chemistry

by

Maxwell A. C. Fenton

Doctor of Philosophy in Oceanography

University of California San Diego, 2025

Todd Martz, Chair
Katherine Barbeau, Co-Chair

Iron (Fe) is an essential micronutrient for marine primary producers, yet its low oceanic concentrations and complex aqueous chemistry make it difficult to measure. Current analytical techniques for assessing the ocean Fe system are rarely able to provide information about Fe-speciation at ambient seawater physico-chemical conditions. The chalcogenide glass Fe^{3+} ion-selective electrode (Fe-ISE) has emerged as a promising tool for more in-situ oceanographic Fe analyses given its ability for rapid, passive measurements of Fe activity (aFe^{3+}), a parameter

directly related to Fe lability and bioavailability. Work in this dissertation addresses the considerations for oceanographic implementation of the Fe-ISE, building from controlled laboratory experiments which establish fundamental sensor response characteristics, to in-situ measurements of seawater aFe^{3+} during several field expeditions.

In Chapter 1, an improved continuous flow analyzer (CFA) incorporating in-line pH and temperature sensors is utilized to study Fe-ISE response in well-characterized, artificial media. A solution-independent temperature coefficient is determined for the sensor system. Potentiometric calibrations are carried out using previously studied media to reexamine their applicability to seawater analyses. Synchrotron radiation experiments indicate a potential-generating mechanism in metal-chelating solutions which involves the ligand-mediated diffusion of Fe ions out of the chalcogenide membrane, and suggest that previous estimates of cross-selectivity are not relevant in seawater.

In Chapter 2, Fe-ISE acidimetric titrations of modified seawater media are used to validate values of aFe^{3+} determined by different aqueous speciation models. We present an optimized seawater-based Fe-ISE calibration system and discuss relevant aFe^{3+} modelling considerations. We conduct acidimetric titrations of natural seawater to show that the Fe-ISE is capable of resolving pH-dependent changes in Fe-speciation pertinent to ocean acidification and microbial uptake.

In Chapter 3, the Fe-ISE CFA is incorporated into shipboard systems for continuous measurements off the Californian and Oregon coasts. Parallel hydrographic sensor measurements, as well as dissolved Fe and Fe-binding ligand analyses, suggest that surface trends in aFe^{3+} appear to be driven by different physico-chemical factors than aFe^{3+} gradients associated with depth. The Fe-ISE offers a novel, uniquely in-situ lens into the complex dynamics of ocean Fe chemistry.

Introduction

Iron (Fe) is a limiting micronutrient for marine primary producers in over a third of the sunlit ocean (Martin and Fitzwater 1988, Lauderdale et al. 2020, Twining et al. 2021). Iron has been shown to facilitate electron transport in the cell during photosynthesis, respiration, and nitrogen fixation (Morel, Milligan, and Saito 2014), and it is a necessary component in various enzymes, allowing phytoplankton to process the dissolved nutrients they need to survive (Price, Andersen, and Morel 1991). Because iron is such a crucial factor in the carbon cycle, its bioavailability in different parts of the ocean has been linked to the global climate (Philip W. Boyd et al. 2004; P. W. Boyd et al. 2007; Bakker et al. 2005; de Baar et al. 2005; J. K. Moore and Doney 2007).

The dynamics of Fe chemistry are complex in the ocean. As redox-active element, Fe may be present in one of two possible states. The reduced form, Fe^{2+}, is more soluble in seawater, but is confined to reducing environments such as anoxic waters, or certain surface-ocean sites where specific organic compounds facilitate photo-reduction of Fe^{3+} (Kuma et al. 1992, 1995, Ozturk et al. 2004). In the rest of the ocean, Fe exists primarily in its oxidized form. These Fe^{3+} ions have a high affinity for hydroxides, forming insoluble Fe-(oxyhydr)oxide colloids at seawater pH (Millero et al. 1998, Liu and Millero 2002) which are scavenged from the upper water column by heavy, sinking particles (P. W. Boyd and Ellwood 2010, Tagliabue et al. 2019). This results in characteristically low, sub-nanomolar concentrations of dissolved iron in the ocean, especially in offshore regions far from benthic or lithogenic sources. The prevalence of organic Fe-binding ligands in seawater has been shown to stabilize dissolved Fe concentrations over large time and spatial scales by competing with the less-soluble hydroxide phases for Fe-complexation (Rue and Bruland 1995, van den Berg 1995).

There are a number of ways which scientists measure and quantify Fe in seawater. Due to the complexity of aqueous iron speciation and the variety of methods used by marine microbes to acquire iron, it is difficult to determine which measurements are the best indicators of iron bioavailability. Measurements of total dissolved Fe (dFe) or total dissolvable Fe (TDFe), generally utilizing robust analytical methods such as atomic adsorption spectrometry, mass spectrometry, or standardized chemiluminescent reaction, provide information about the size of certain acid-leachable pools of Fe (Achterberg et al. 2001, Worsfold et al. 2014). But dFe and TDFe are operational terms which may not represent how much Fe is truly available for microbial uptake, specifically because acidification destroys the natural Fe complexes present at seawater pH. The size, mobility, and chemical nature of these complexes, as well as the strength with which they each bind Fe, all affect how easily this Fe can be accessed by biota (Anderson and Morel 1982, Maldonado and Price 1999, Morel et al. 2008, Shaked et al. 2020). Many microbes even have receptors that specifically target certain complexes (McQuaid et al. 2018, Manck et al. 2020). In acidified samples, however, Fe^{3+} is no longer complexed, and all information about the relative bioavailability due to speciation is lost.

Certain techniques that combine specialized liquid chromatography with mass spectrometry have been able to characterize the molecular structures and association kinetics of these Fe-ligand complexes. (Boiteau et al. 2013, Boiteau and Repeta 2022). Techniques such as competitive ligand exchange – adsorptive cathodic stripping voltammetry (CLE-AdCSV) are able to assess Fe-speciation through competitive binding metal titrations, which provide information such as the concentrations and thermodynamic binding constants of the ambient ligand pool (Gledhill and van den Berg 1994, Rue and Bruland 1995, van den Berg 1995, Omanovic et al. 2015). However, this method has proven challenging to standardize, with derived parameters exhibiting clear biases related to the total dFe of the samples (Gledhill and Gerringa 2017; Laglera et al. 2013; Town and Filella 2000), the specifics of the added competing ligand (Bundy et al. 2014, Slagter et al. 2019, Gerringa et al. 2021), and the

equilibration time for the ligand exchange steps (Gledhill and Buck 2012, Laglera et al. 2015, Caprara et al. 2016,). Thus, although useful when analyzing relative speciation differences within one user's sample set, CLE-AdCSV is a fairly specialized technique.

In general, current techniques for the measurement of Fe and Fe-speciation are laborious, time-consuming, and require extensive sample preparation. Scientists lack a method for the rapid, in-situ, and potentially remote analyses of seawater Fe chemistry which would greatly facilitate their abilities to generate comprehensive global biogeochemical climate models.

Measuring Fe Activity

Studies of microorganisms in seawater and artificial seawater media repeatedly find that iron uptake is well correlated with the modeled activity of the free Fe^{3+} ion in solution (Anderson and Morel 1982, Morel et al. 2008, Lis et el. 2015, Shaked et al. 2020). This activity (aFe^{3+}) is regularly estimated by CLE-AdCSV and aqueous metal speciation models to be on the order of 10^{-22} M and below in marine environments (Gledhill and van den Berg 1994, Rue and Bruland 1995, Gerringa et al. 2015, Gledhill et al. 2022). This would correspond to just 10s of Fe^{3+} ions in a liter of seawater – a nonsensical value when considering actual chemical species. Because virtually all Fe^{3+} ions are complexed, predominately by hydroxides and organic ligands, what an equilibrium value of aFe^{3+} really represents in an aqueous solution is the overall *accessibility* of this Fe. At higher values of aFe^{3+}, the Fe is more weakly complexed, making it more available to microorganisms. Lower values of aFe^{3+} on the other hand imply either less total Fe, or stronger or more abundant complexation. Thus, aFe^{3+} appears to function as a master variable for the complex and dynamic Fe system, representing the availability of Fe to biota.

An attractive option for the in-situ measurement of the ionic activity of a system is the potentiometric ion-selective electrode (ISE). Potentiometric measurements require minimal power and simple, inexpensive instrumentation. When calibrated and conditioned correctly, an

ISE allows for continuous measurements at low ionic activities. Because they function passively without disturbing the chemical or physical behavior of a system, they are the optimal way to monitor dynamic equilibrium processes over various timescales.

Although functional ISEs are available for many ions of great importance in marine science (H^+, NO_3^-, PO_4^{3-}, NH_3, Ca^{2+}, F^-, Cu^{2+}, Fe^{3+}), they have been of limited use in oceanographic analyses (Warner 1969, Zirino et al. 1998, Mortensen et al. 2000, De Marco, Clarke et al. 2007, Privett et al. 2008, Vlasov et al. 2010). For Fe^{3+} specifically, ISEs were initially developed for the analyses of higher Fe systems such as waste water (Baker and Trachtenberg 1971, Jasinski and Trachtenberg 1973). Their potential for in-situ seawater measurements was realized following marked improvements in the detection limits of ISEs. By buffering metal ion concentrations using organic chelators, or by thinning electrode diffusion layers using turbulent flow analytical regimes, a number of studies found that it was possible to measure extremely low ionic activities relevant to that of Fe^{3+} in seawater (Avdeef et al. 1983, Schefer et al. 1986, Belli and Zirino 1987, Sokalski et al. 1997, De Marco and Shackleton 1999).

Roland De Marco and colleagues were the first to test an Fe^{3+} ISE (Fe-ISE) with natural seawater analyses ultimately in mind. Specifically, they examined electrodes of chalcogenide glass (ChG) membranes of the formulation $Fe_{2.5}(Ge_{28}Sb_{12}Se_{60})_{97.5}$, which had been shown to be sensitive, durable, and resistant to degradation even in complex and saline solutions (Baker and Trachtenberg 1971, Jasinski and Trachtenberg 1973, Koenig and Grabner 1995). Using organically buffered saline media, a chalcogenide Fe-ISE in a specialized flow-system was calibrated down to an aFe^{3+} of 10^{-25} M (De Marco and Mackey, 2000). Over the next 15 years, De Marco's calibration solutions gradually increased in chemical complexity in attempts to better mimic Fe-ISE surface chemistry in seawater (De Marco and Martizano 2007; 2008; Maric et al. 2015). These studies also entailed select Fe-ISE measurements of UV photo-oxidized and natural seawater samples, which agreed with modeled aFe^{3+} values, or were in the range of literature CSV-derived aFe^{3+}.

While no Fe-ISE experiments to date have examined variations in ambient aFe^{3+} between different seawater samples, jalpaite Cu-ISEs have been effectively employed to explore Cu speciation in natural seawater systems (Zirino et al. 1998, Zirino et al. 2002, Blake et al. 2004, Rivera-Duarte et al. 2005, Neira et al. 2011, Marcinek et al. 2021). These investigations continually show that distributions of metal ion activity as measured by an ISE tell a very different story about metal ion availability and toxicity than parallel measurements of total metal concentrations are able to deduce. Outfitting the chalcogenide Fe-ISE for such in-situ analyses of ocean Fe chemistry would offer a novel, high-resolution perspective into an extremely complex system, and could provide new information regarding the cycling of Fe and its bioavailability to marine organisms.

To that end, the goal of this dissertation is to increase our familiarity with the response of the chalcogenide Fe-ISE in seawater and similarly buffered systems such that we are able to fully interpret its signal in complex media, and to then use this knowledge to make in-situ measurements of Fe activity in natural seawater. In Chapter 1, an improved Fe-ISE continuous-flow analyzer (CFA) is described which incorporates in-line pH and temperature sensors for more precise measurement of aFe^{3+}. This system is utilized to reexamine the fundamental response characteristics of the Fe-ISE, many of which had never been directly assessed in the flowing, organically buffered media relevant to seawater analyses. Calibration of the Fe-ISE in artificial buffer solutions is reinvestigated in the context of its applicability to the Nernstian response of the sensor. Potentiometric measurements by the Fe-ISE CFA system are used in conjunction with a temperature controlled pH-stat to determine a revised solution-independent temperature coefficient for the chalcogenide Fe-ISE. The results of synchrotron radiation surface studies of the chalcogenide membrane are discussed as they relate to possible potentiometric interference by Cu ions, and to the overall potential-generating mechanism of the sensor in seawater-like systems.

In Chapter 2, the focus shifts from Fe-ISE response in artificial media to that in seawater and modified seawater solutions. An optimal seawater-based calibration system is presented which is well-modeled and allows for reliable calculation of aFe^{3+}. Fe-ISE acidimetric titrations are carried out to observe changes in aFe^{3+} over a large range in pH, and to examine how these trends differ in modified seawater of varying Fe/chelator ratios. These titrations are also used to validate the aqueous speciation models necessary for Fe-ISE calibration and calculation of aFe^{3+}, particularly in their handling of the precipitation of Fe-hydroxide and Fe-oxyhydroxide species. Similar acidimetric titrations of natural seawater samples show that the Fe-ISE may be used in this manner for the analysis of the pH-dependent Fe-binding properties of the natural ligand pool, which are likely relevant for studies of ocean acidification and deoxygenation.

Finally, Chapter 3 presents the first in-situ oceanographic measurements of aFe^{3+} by an Fe-ISE. A trace metal clean shipboard pumping technique combined with the Fe-ISE CFA system is used for continuous at-sea analyses during two separate research cruises. Surface gradients in aFe^{3+} are observed during a number of transects into and across sites of deep-water upwelling off the coasts of Oregon and northern California. Gradients in aFe^{3+} with depth are measured during pumped vertical profiles of the upper (<100 m) water column at several sites near the San Pedro Basin in the Southern California Bight. Fe-ISE measurements are discussed in the context of parallel measurements of pH, sea surface temperature, salinity, fluorescence, and oxygen concentrations, as well as analyses of discrete samples for dFe and organic Fe-binding ligands.

Chapter 1. Response Characteristics of the Chalcogenide Glass Fe(III) Ion-Selective Electrode in Fe-Chelating Media

Abstract

The chalcogenide glass Fe^{3+} ion-selective electrode (Fe-ISE) is a promising tool for in-situ analysis of marine Fe chemistry. However, many features of the sensor's response essential to understanding its signal have only been evaluated in solutions of markedly different Fe chemistry compared to that of natural seawater. Here, we reexamine the response of the Fe-ISE in well-characterized artificial media with Fe-binding properties similar to seawater, utilizing an improved continuous-flow analyzer with in-line pH and temperature sensors. A series of potentiometric calibrations are carried out which utilize previously studied Fe-ISE calibration solutions, and we revisit their applicability to the determination of seawater Fe^{3+} activity. We find that the curvature observed in voltage vs Fe^{3+} activity calibration plots is likely attributable to variations in the potential-generating mechanism associated with the changing speciation of facilitating ligands, and/or to intrinsic errors in the calculation of the Fe species present in alkaline solutions. Through the use of a temperature-controlled pH-stat system, we determine a revised temperature coefficient for the Fe-ISE of -0.82 mV/°C, to be applied to all measurements in organically-buffered media. We report the results of synchrotron radiation (SR) surface studies of the Fe-ISE chalcogenide glass exposed to buffered and unbuffered media, and reassess the possibility of a cross-selectivity to Cu^{2+} ions in seawater-like solutions. We find that the presence of metal chelators in solution prevents any infiltration of Cu into the glass matrix, proof that there is no Cu ion-exchange reaction with the solid state membrane – the well-known mechanism for ion interferences in these types of membranes. Similar SR experiments examining the Fe chemistry of the glass surface layers suggest that the potential-generating mechanism in low aFe^{3+} solutions involves the ligand-mediated diffusion of Fe^{3+} ions

from the modified surface layer of the Fe-ISE. In these systems, the Fe-ISE signal is a measurement of the Fe-binding tendencies of the ligand pool.

Introduction

Studies of chalcogenide glass ion-selective electrodes began in the early 1970s when Baker and Trachtenberg (1971) first described their synthesis. They showed that an Fe-doped chalcogenide matrix of 60% selenium, 12% antimony, and 28% germanium resulted in a glass which was potentiometrically sensitive to Fe^{3+} ions. Their early manuscripts tested a variety of Fe^{3+}-selective electrodes and reported fairly consistent Nernstian slopes averaging 57.6 mV/dec, differing considerably from the 19.8 mV/dec response that would be expected for the simple exchange of trivalent Fe^{3+} ions (Baker and Trachtenberg 1971, Jasinski and Trachtenberg 1973). These calibrations were conducted in acidic KCl solutions of varying total Fe concentration, and showed sensitivity down to 10^{-6} M Fe. Importantly, Jasinski and Trachtenberg (1973) noted several crucial steps in the functioning of the Fe-ISE. Namely: an oxidation of the glass surface which created an active modified surface layer (MSL); an exchange of Fe^{3+} ions in this MSL with the solution; and a slower, irreversible adsorption of ferric ions which would eventually “deactivate” the electrode. These discoveries first emphasized the complexity of the overall potential-generating mechanism of the Fe-ISE.

Koenig and Grabner’s 1994 reexamination of the Fe-ISE included notable contributions to this discussion. Their experiments investigated a number of glass compositions by varying the mol% Fe doped into the chalcogenide matrix. They measured electrode slopes from 32 to 110 mV/dec, which appeared to increase with added Fe content and were postulated to be related to differing resistivities and susceptibilities to surface oxidation. That said, Trachtenberg had also tested several glass compositions and had found no correlation between iron content and electrode slope (Jasinski and Trachtenberg 1973). In fact, his reported values of close to 60

mV/dec were for electrodes of <2 mol% Fe, while Koenig and Grabner's 2 mol% Fe electrodes gave slopes of 32 mV/dec. It was only with electrodes of much higher mol% Fe that Koenig and Grabner reported slopes close to 60 mV/dec. Thus, the Fe doping itself likely has less of an effect on the sensitivity than other aspects of the manufacturing of the glass and perhaps the conductive contact.

Koenig and Grabner supplemented their potentiometric measurements with cyclic voltammetry (CV) and X-ray photoelectron spectroscopy (XPS) studies of the electrode's surface to propose a potential-generating process that involved the selective exchange of ferric ions from the solution into the MSL. A given Fe^{3+} exchange event would then induce the injection of a single hole into the bulk glass matrix as a charge carrier, which would produce a nominal Nernstian response of 59 mV/dec. The chalcogenide glass, behaving as a p-type semiconductor, displayed a negative temperature coefficient as expected – reported by Koenig and Grabner to be -3 mV/°C. Their study also determined selectivity coefficients for major interfering ions, the highest being a value of 10^{-3} for Cu^{2+} ions.

While these early Fe-ISE tests were not conducted with seawater analyses in mind, the 70s and 80s also marked several important developments toward significantly lowered detection limits of solid-state and membrane-based sensors, which were relevant for environmental applications. Researchers realized that the often-reported detection limits for these sensors, around 10^{-7} M analyte ion, were due to contamination by primary ions leaching from the sensor membrane into solution (Smith and Manahan 1973, Jasinski et al. 1974, Schefer et al. 1986, Belli and Zirino 1993, Sokalski et al. 1997). By buffering the solution with an organic chelator, primary ion activity could be regulated to much lower values, and sensor detection range could be expanded (Avdeef et al. 1983). Additionally, primary ion saturation of an ISE's diffusion layer could be mitigated by incorporating a turbulent flow regime such as a rotating disk electrode or a continuous flow analyzer (Zirino et al. 1998, Zirino et al. 2002). Given the extremely low

activities of Fe^{3+} in seawater, these developments toward improved detection limits had important implications for potential oceanographic implementation of the Fe-ISE.

Over the past two decades, De Marco and colleagues have taken steps toward this application of the Fe-ISE by incorporating a continuous-flow analyzer to limit membrane contamination, and by moving away from tests in acidic, high Fe solutions. Instead, in an attempt to adequately mimic the ISE's behavior in seawater, De Marco has carried out a series of calibrations in low Fe ligand-buffered media of increasing chemical complexity (De Marco et al. 1999; De Marco and Mackey 2000; De Marco and Martizano 2007; 2008; Maric et al. 2015). As in seawater, the inorganic and organic Fe chelators in these buffers behave as acid-base species, such that Fe^{3+} activity (aFe^{3+}) can be controlled by changing the pH. An aqueous speciation modeling software equipped with Fe(III) binding constant data is then used to calculate aFe^{3+} for a given pH. Early calibrations utilized buffers that were simply an Fe-spiked saline solution with an added organic Fe-binding ligand, such as citrate, salicylate, or EDTA. In these calibrations, the Fe-ISE displayed a linear response to $\log[aFe^{3+}]$ values from 10 to 25 (De Marco and Mackey 2000).

Calibrations in these simple buffers, as well as in UV photo-oxidized seawater, gave calibration slopes of 24-29 mV/dec, again suggesting a more involved mechanism than simple Fe^{3+} ion-exchange. De Marco and Pejcic proposed a model to explain this sensitivity, envisioning a potential-generating process which is a combination of ion exchange *and* charge transfer reactions (De Marco and Pejcic 2000). This leads to theoretical slope of 29.6 mV/dec according to the following Nernst equation:

$$E = E^{\circ} + \frac{2.303RT}{2F}\log[a_{Fe^{3+}}] \quad (1)$$

where E represents the measured electrochemical potential in solution, E° is the standard electrode potential, R is the universal ideal gas constant, T is the temperature in Kelvin, and F is Faraday's constant. Further, electrochemical impedance spectroscopy (EIS) and XPS revealed

that the organic ligands exert a significant influence on the response mechanism – appearing to affect the kinetics of both ion-exchange and charge transfer to various extents dependent on the nature of the ligand (Pejcic et al. 2002a, Pejcic et al. 2002b, Pejcic et al. 2004) Notably, lower impedance values in seawater suggested these natural Fe-chelators had a facilitating effect on both processes.

The most recent calibrations by De Marco et al. made use of a more complex buffer solution they dubbed the alternative calibration system (ACS), which comprised some amounts of copper sulfate and ethylene diamine added to prevent corrosion of the ISE surface (De Marco and Martizano 2007; Maric et al. 2015). Spectroscopic investigations of the Fe-ISE indicated that the ACS was better able to mimic the MSL Fe chemistry observed in seawater as compared to previous calibration buffers (Maric et al. 2014, Maric et al. 2015). Although the ISE responded quickly and reproducibly to ACS, and again gave slopes close to 30 mV/dec, the resulting potential vs log[aFe^{3+}] calibration plots exhibited slightly more curvature, perhaps indicating some sensitivity to the abundant Cu^{2+} ions in solution.

De Marco's work has been instrumental in moving us closer to environmental Fe-ISE applications through the use of organically buffered media and novel analytical strategies for lowered detection limits. But some of the sensor characteristics most relevant to natural seawater measurements (temperature sensitivity, Cu cross-selectivity) came from the earliest tests of the Fe-ISE, which were undertaken in acidic media, at concentrations of Fe^{3+} no less than 10^{-7} M and often much higher (Baker and Trachtenberg 1971, Jasinski and Trachtenberg 1973, Vlasov and Bychkov 1994, Vlasov et al. 1994, Koenig and Grabner 1995). In natural seawater at ambient pH, however, the activity of Fe^{3+} ions is extremely low, on the order of 10^{-21} (Rue and Bruland 1995). Investigations of ocean trace metal chemistry find that overall Fe activity is moderated less by total Fe concentrations, and more so by the low solubility of Fe in oxygenated seawater coupled with pH-dependent chelation by a variety of both organic and inorganic Fe-binding ligands (Millero et al. 1995, Liu and Millero 1999, 2002, Gledhill and Buck

2012, Zhu et al 2021a, 2021b). Accordingly, it is necessary to reexamine the early experiments which were conducted in vastly different media, yet which provide such fundamental parameters. As we move toward the Fe-ISE analyses of natural seawater, a dynamic medium of changing temperature and myriad trace metal species, we need a clear understanding of all contributions to the sensor signal.

Here, we reexamine the fundamental response characteristics of the Fe-ISE using low Fe, organically buffered solutions at environmentally relevant pH values. We carry out a series of calibrations utilizing an improved continuous-flow analyzer with in-line pH and temperature sensors, allowing for more precise aFe^{3+} determination. This affords a reassessment of the linearity and applicability of Fe-ISE calibrations in artificial solutions, especially as they relate to the Nernstian response of the sensor. With additional potentiometric experiments, we determine a revised solution-independent temperature coefficient for the Fe-ISE, to be used for all temperature corrections to seawater measurements. We use data from synchrotron radiation (SR) surface studies of our chalcogenide membranes to reexamine the potential for Cu cross-selectivity in the context of organically-buffered, flowing media, and to discuss the fundamental detection mechanism for the Fe-ISE.

Experimental

Fe(III) Chalcogenide Glass ISE

High purity (>99.5%) metal powders of selenium, germanium, antimony and iron were mixed and added to a 10 mm diameter quartz tube. Unless otherwise specified, the metal mixture was of the following ratio: $Fe_{2.5}(Se_{60}Ge_{28}Sb_{12})_{97.5}$ (Baker and Trachtenberg 1971, Koenig and Grabner 1995). The tube was sealed under vacuum, then heated in a calibrated furnace for 24 hours at 1030°C. The resultant melt was air quenched and annealed for 2 hours at 240°C to remove excess stress within the glass. The quartz tube was cut down to expose a flat section of

the chalcogenide glass 3 – 4 mm thick, which was polished to a mirror finish. A shielded copper wire was attached to the back of the chalcogenide glass with a silver epoxy contact. Photographs of the Fe-ISE and chalcogenide surface are visible in Figure 1.1.

Electronics

All potentiometric measurements with the Fe-ISE were made against a Ag/AgCl liquid junction reference electrode (BASi MF-2056). Measurements of pH were made in line with a glass combination pH/reference electrode (Orion 8102 BN). Both working electrode signals were passed through unity-gain operational amplifiers (LMC6041) before being fed into an analog-to-digital converter (ADC, National Instruments 9219) connected to a computer. Temperature measurements were made in-line using an threaded thermistor probe (Omega), which connected to the same ADC. Figure 1.2 details the circuit layout of these electronics.

A Labview interface was designed which processed, saved, and plotted all data real-time. One “measurement” by the ADC consists of a rapid 5000-reading burst which appears as a waveform for each sensor. The DC average of each waveform is recorded as a data point, while the waveform itself can be viewed to assess sensor noise. Unless otherwise specified, the ADC was set to take a measurement once every three seconds.

Fe-ISE Continuous Flow Analytical System

A flow cell (~25 mL volume) was designed and 3D-printed from a stereolithography (SLA) photopolymer resin to house the Fe-ISE, reference electrode, and combination pH electrode. The solution stream was exposed to the sensor elements in that order to avoid contamination of the Fe-ISE. A separate flow cell housed the thermistor probe further downstream. Flow cell, plastic connectors, and tubing (flexible PVC, 1/8” internal diameter) were all acid-washed before use. A peristaltic pump (Masterflex) was used to pump the sample through the system at 300 mL per minute. For tests of buffered calibration solutions and

modified seawater where total [Fe] > 1 μM, samples were recirculated to conserve volume, as any possible contamination by the Fe-ISE itself was deemed negligible. For tests using natural, low Fe seawater, samples were expelled to waste after passing through the flow cell. All Fe-ISE analyses described in this chapter make use of this continuous flow analytical (CFA) system. A schematic of the full Fe-ISE CFA system is displayed in Figure 1.3.

Reagents

Analytical grade reagents were used for all experiments, and all solutions were prepared with high purity Milli-Q deionized water. For all artificial solutions discussed in this chapter, an ionic background was provided by 0.55 – 0.60 M NaCl. The pH of each solution was adjusted using concentrated HCl or NaOH, and was measured on a separate, external glass combination pH electrode (Orion 8102 BN) which was calibrated to three Orion pH buffer solutions traceable to NIST standards.

The aqueous speciation modeling software Visual MINTEQ was employed for all calculations of aFe^{3+} and other free metal activities. This software is free and publicly available, and uses a database of chemical equilibrium binding constants from continually updated literature sources. All database information can be found online at https://vminteq.com.

Potentiometric Calibrations

Calibrations in this chapter primarily utilized organically-buffered solutions examined in previous studies of the Fe-ISE. Namely, De Marco and colleagues' initial calibration solutions detailed in De Marco and Mackey (2000), here referred to as Simple Buffer Solutions (SBS), and the Alternate Calibration Solution (ACS) as described in Maric et al. (2015). The components for each calibration solution are shown in Table 1.1.

For a given calibration system, a bulk solution was prepared and brought to pH 2 for at least 24 hours to improve the stability of the system. The solution was then partitioned into

several smaller (100 mL) acid-clean vials, which were each brought to a desired pH and allowed to equilibrate. By adjusting the pH, the aFe^{3+} is also changed according to the acid-base properties of the Fe-complexing organics and hydroxy components of the solution, and can be calculated using the MINTEQ speciation software. This generates calibration standards in the aFe^{3+} range of interest.

Prior to a calibration, the Fe-ISE was polished on nylon and micro-cloth pads using a Buehler alumina slurry of decreasing particle size, and subsequently rinsed in Milli-Q. The Fe-ISE was then conditioned in its flow cell for at least 24 hours in either seawater, or an aliquot of the calibration solution, until a stable potential (< 0.5 mV/hour drift) had been reached. After conditioning, the calibration was carried out, circulating each standard through the flow system until a stable potential was reached, moving from low aFe^{3+} to high aFe^{3+} standards unless otherwise specified.

Temperature Dependence Tests

Four liters of the EDTA-based SBS defined in Table 1.1 was prepared and brought to pH 7.1 using NaOH. This solution was placed in an in-house pH-stat system as described in Wirth et al. (2024). Briefly, temperature is controlled through a water bath and jacketed beaker, while pH is controlled by bubbling either gaseous CO_2 or O_2-scrubbed air into the solution. A pH sensor (Honeywell Durafet) and temperature probe are connected to a LabView interface, which automatically adjusts the pH and temperature to set points input by the user. Figure 1.4 displays a schematic of the pH-stat system.

The pH of the solution was held constant at 7.095, while the temperature was adjusted to four points between 6°C and 20°C. Temperature was held at each point for several hours, allowing for complete equilibration of the system. The Fe-ISE continuous flow system was plumbed into the pH-stat, continually circulating the pH-stat solution through the analytical flow cell. The flow cell housed the Fe-ISE as well as its own pH and temperature sensors to account

for any differences as the solution stream left the jacketed beaker. The Fe-ISE was set to take a potentiometric measurement every 10 seconds throughout the experiment.

The aFe^{3+} of each temperature point was calculated using Visual MINTEQ software. The software makes temperature corrections using the Van't Hoff equation to modify the log *K* binding constant of all aqueous species based on their enthalpies of formation (ΔH values). This modeled change in aFe^{3+} over temperature was converted to a change in potential using the experimentally determined calibration slope for this solution, *21.6 mV/dec*. The difference between the model-based temperature effect and the measured temperature effect was taken as the overall temperature coefficient for the Fe-ISE.

Surface Studies

To evaluate the presence of specific chemical species in the chalcogenide glass and help further elucidate its detection mechanism, a series of surface studies was carried out at the Elettra synchrotron light source in Trieste, Italy, as part of a Central European Research Infrastructure Consortium (CERIC) grant awarded to collaborator Roland De Marco. The Elettra Materials Science Beamline (MSB) offers an ultra-high vacuum chamber (10^{-10} mbar base pressure) equipped with a multichannel electron energy analyzer (Specs Phoibos 150). SR XPS and NEXAFS (near edge x-ray adsorption fine structure) spectroscopic analyses were conducted to probe the elemental composition of the chalcogenide glass surface layer after prolonged exposure to a variety of solutions. Detailed technical descriptions of the synchrotron radiation methods and the subsequent spectral processing involved in this work are available in De Marco et al. (2025, in prep). Briefly, all photon energies were calibrated against a Cu foil standard, and XPS peak intensities were normalized across samples using gold mesh currents recorded at each photon energy. KolXPD software (https://www.kolibrik.net/en/solutions-products/kolxpd) was utilized for curve fitting to deconvolute spectra into constituent species. XPS peak intensity data were corrected for photon energy effects as well as electron kinetic

energy effects to provide final values of mol% for all elemental species. The theory behind this quantitative elemental resolution is described in detail in Cuartero et al. (2016).

In the first experiment, chalcogenide glass chips (~4 mm^2) were polished on one side and exposed to one of four treatments. Each treatment consisted of an overnight soak in a 40 mL saline solution of varying composition. Two solutions were brought to pH 2 and contained either unbuffered Fe or Cu. The other solutions contained the same total metal concentration, but were brought to pH 8 and also included equivalent amounts of EDTA metal chelator. Table 1.2 details these four treatments. One chalcogenide piece was left untreated as a control.

The second experiment investigated variations in surface Fe composition of the chalcogenide pieces as a result of seawater exposure time and exposure regime. Chalcogenide pieces were aged in filtered seawater (total Fe < 5 nM) at ambient pH for either 4, 19, 28, or 48 hours. One set of chalcogenide pieces underwent this aging in a 40 mL vial of “static” seawater. Another set of pieces were placed in a flow-cell akin to that of the Fe-ISE CFA system, such that they were exposed to continuously flowing seawater from a 20 L reservoir which was replenished every several hours.

When removed from their treatments, all pieces were immediately placed in the MSB sample chamber and subjected to XPS and NEXAFS analyses. NEXAFS spectra for the Fe 2p electronic transitions were measured over a photon energy range of 706.5 to 714.5 eV, while Cu 2p spectra were measured over a photon energy range of 929 to 952 eV. Using the KolXPD software, integrated intensities for Cu(I), Cu(II), Fe(II), and Fe(III) species were used to calculate relative percentages of Fe and Cu speciation as a function of conditioning treatment.

Results and Discussion

Fe-ISE Calibrations

To show the typical response of the Fe-ISE during a calibration using ACS standards, a representative experiment is shown in Figure 1.5, which displays the raw voltage signal from both the Fe-ISE and the glass pH electrode as the sensors are exposed to six ACS standards. These standards spanned an aFe^{3+} range from roughly 10^{-15} to 10^{-28}, as determined by Visual MINTEQ. The Fe-ISE responded quickly, reaching a stable potential generally within 3 minutes of the introduction of each standard. The associated calibration standard data and calibration plot are visible in Table 1.3 and Figure 1.6, respectively.

Table 1.4 shows the results of six ACS calibrations of this same Fe-ISE, as well as three calibrations of this Fe-ISE in SBS of differing organic ligand. The ACS-derived calibration slopes are in close agreement with the value reported by Maric et al. of 28.8 mV/dec. However, it is worth noting that the chosen pH range for these calibration standards has a significant effect on the calculated slope. As visible in Figure 1.6, and characteristic of all calibrations utilizing the ACS, the mV vs log[aFe^{3+}] plot is not perfectly linear and exhibits a slight curvature over the range of the calibration. This means that extending the calibration to higher pH standards (thus lower aFe^{3+}), biases the slope toward a lower absolute value. This is evident in Table 1.4, where the April 2023 and May 2023 ACS calibrations, which include standards up to pH ~10.8, have slopes closer to 24 mV/dec. Calibrations utilizing a lower pH range on the other hand consistently give slopes of around 30 mV/dec. This trend is therefore very reproducible, and must be considered when interpreting any ACS-based calibrations.

Calibrations in SBS generated a slightly lower slope – consistently around 21 mV/dec regardless of the organic ligand in the solution. These calibrations are subject to aFe^{3+} range-dependent biases as well, although the calibration plots display the opposite curvature as that of ACS. Table 1.5 and Figure 1.7 shows the data table and calibration plot for a citrate-based SBS

calibration, while Table 1.6 and Figure 1.8 show the same for an EDTA-based SBS calibration. In both calibrations, a slight curvature is visible that bias response slopes to *greater* absolute mV/dec values with the inclusion of higher pH standards.

That said, the SBS-derived calibration slopes exhibit greater overall consistency across different ligand backgrounds *and* different standard pH ranges. These simpler solutions mean fewer components in the speciation model, and perhaps a more valid calculation when attempting to determine the true thermodynamic activity of these aqueous species.

There are a few possible explanations for the calibration curvature observed in both the SBS and ACS matrices; the first being related to the response mechanism of the Fe-ISE itself. De Marco and Pejcic used their 30 mV/dec value to propose a potential-generating process for the Fe-ISE which is a combination of Fe^{3+} ion-exchange and single electron charge-transfer, and thus resulted in an expected Nernstian response of 29.6 mV/dec (De Marco and Pejcic, 2000). It may be that this mixed response mechanism changes slightly over the course of a calibration. In fact, De Marco and Pejcic's findings that organic ligands can facilitate or hinder both charge transfer and ion-exchange processes would suggest that the relative dominance of these processes may shift as the speciation and Fe-binding capacity of the ligand background is altered across differing pH and aFe^{3+} regimes. This would appear as curvature in the mV/log[aFe^{3+}] slope, with regions close to 30 mV/dec indicating an equal contribution from charge transfer and ion-exchange mechanisms, and regions of lower slope representing Fe and ligand chemistry more conducive to ion-exchange.

It is also very important to note that the aqueous speciation calculations used to determine values of aFe^{3+} are based on thermodynamic constants for all involved species. In actual aqueous systems, there are almost certain to be kinetics-related discrepancies from this equilibrium model. Figures 1.9 and 1.10 display the log activities of the dominant Fe species in the EDTA-based SBS and ACS systems respectively, as calculated by MINTEQ over the pH range of the calibrations. In both matrices, as is the case for natural seawater, the changes in

speciation that occur between pH 7 and pH 9 are especially complex due to rising hydroxyl activities (Millero et al 1995, Millero 1998). As pH increases in this region, the most abundant Fe species shifts from $FeEDTA^-$ to its hydroxylated form. The dominant inorganic Fe species shifts from $Fe(OH)_2^+$ to $Fe(OH)_4^-$, while the electrochemically neutral $Fe(OH)_3$ reaches its solubility limit. As the activities of these species are all at least ten orders of magnitude larger than that of the free Fe^{3+}, any small inaccuracy at the higher-activity end would propagate to larger errors in aFe^{3+}. The precipitation of Fe-hydroxy species in particular is exceptionally difficult to constrain in an environment of assumed equilibrium, yet has a significant effect on the total concentration of dissolved Fe species (Kuma et al. 1996, Liu and Millero 1999, Rose et al. 2003). If the model overestimates (or underestimates) the extent of this process over certain ranges of pH, true aFe^{3+} in those regimes would be higher (or lower) in the actual solution than calculated values. This would manifest as a curvature in the mV vs log[aFe^{3+}] plot.

To use any calibration to determine natural seawater aFe^{3+}, we must be confident that the standard potential of the Fe-ISE is consistent between our calibration solution and seawater. Otherwise, there will be an offset in measurements made in the different media. Figure 1.11 displays the Fe-ISE response during an experiment where the sensor is exposed to a natural seawater sample, then three ACS standards, followed by re-exposure to the initial seawater sample. Notably, the measured potential of the seawater sample jumped 100 mV in the positive direction after exposure to the ACS. It took over 24 hours for the seawater potential to return to its pre-ACS value (Figure 1.11b). This phenomenon is observed during all ACS calibrations during seawater analyses. Thus the ACS indeed imparts a significant offset to the standard potential of the Fe-ISE, making it difficult to relate modeled aFe^{3+} data in the ACS to measured seawater potentials. Conducting an SBS calibration during seawater analysis (not pictured here) has a similar effect on standard potential, the extent of which appears to vary with the chosen ligand background.

The response slope for a given Fe-ISE in a given calibration system is consistent (Table 1.4), suggesting that artificial solutions may be helpful in assessing the reproducibility of a sensor's response over time, or in comparing sensitivities between sensors. However, the variability in intercept (aka "reference" or "standard" electrode potential) limits the use of these media as traditional calibration solutions. That said, if a calibration slope must be used to gauge the Fe-ISE's sensitivity to changes in aFe^{3+}, it is recommended that calibration standards span as large a range of pH (and therefore aFe^{3+}) as possible. This will cover multiple regions of Fe-speciation as well as any different regimes of the sensor's detection mechanism, and will generate an overall slope that is less prone to bias from any one factor. While calculating specific values of aFe^{3+} is unreliable due to aforementioned offsets to the standard potential, the slope and thus overall sensitivity of the Fe-ISE appears to be a more robust parameter even across different media. In summary, it may be of greatest value to use the sensor to examine relative changes in Fe activity (ΔaFe^{3+}).

Temperature Coefficient of the Fe-ISE-Ag/AgCl Electrode

The Fe-ISE response over a range of temperature (Figure 1.12) was used to establish the solution-independent temperature coefficient of the sensor (Figure 1.13). This term is similar to the temperature dependence of the standard potential, E°, of established sensors, but we avoid using the term standard potential here because, as described above, the MINTEQ-derived aFe^{3+} at each temperature includes Van't Hoff corrections to all binding constants, and is converted to a potential in mV using the experimentally determined response slope for EDTA (Table 1.4). Subtracting the thermodynamic temperature dependence from the measured temperature dependence gives a solution-independent temperature coefficient for the standard potential of -0.82 ± 0.04 mV/°C.

The largely uncharacterized pool of Fe-chelators in seawater and their unknown enthalpies of formation would make it impossible to estimate a temperature effect on the

thermodynamic equilibria for Fe-speciation in seawater. Thus, while we can easily observe the *overall* Fe-ISE voltage dependence on temperature, it is only with a well-characterized artificial solution that we are able to partition this dependence into its two constituents: that of the Fe(III) chemistry, and the sensor's temperature coefficient itself.

The importance of determining the solution-independent temperature coefficient of the sensor (similar to the temperature dependence of the standard potential for well-established systems) is demonstrated by Figure 1.14, which displays the flow-cell temperature and Fe-ISE response during several hours of conditioning in a large volume (>10 L) of recirculated raw seawater. As the laboratory climate control cycled on-and-off, the temperature of the non-insulated volume of recirculated seawater oscillated by roughly 0.5°C. Averaged over 11 temperature swings, the associated Fe-ISE potential changed -1.16 mV/°C. Thus, 70% of the observed change in sensor voltage is due to factors inherent to the sensor and unrelated to its chemical response to Fe or Fe ligands. This temperature dependent term reflects all of the components of the measurement system other than the interactions at the chalcogenide/liquid interface that contribute to the measured potential and may change with temperature, including factors such as the sum resistivity of the chalcogenide material, circuitry, and changes in the activity of the reference electrolyte. This is a significant difference from Koenig and Grabner's (1995) value of -3 mV/°C, determined in acidic, non-flowing media with high concentrations of total Fe. We recommend that the value of -0.82 mV/°C be used for all temperature corrections to Fe-ISE measurements made in organically buffered, low Fe systems such as seawater.

Surface Studies

For the metal-buffering experiment detailed in Table 1.2, marked differences in metal chemistry between the control sample, buffered treatments, and unbuffered treatments were evident in both XPS and NEXAFS spectra. Figures 1.15a and 1.15b display Cu 2p XPS and NEXAFS spectra for treatments 3 and 4, showing the effect of the EDTA buffer on the Cu

chemistry of the chalcogenide glass surface. The XPS data represent the outer surface layer (1 – 2 nm) of the chalcogenide piece, and reveal the presence of Cu(I) in the unbuffered treatment. This indicates that Cu(II) from solution has undergone a reductive ion-exchange with this outermost layer of the glass. Similarly, the NEXAFS spectra reveal both Cu(I) and Cu(II) signals originating from deeper (5 – 10 nm) layers of the chalcogenide piece exposed to the unbuffered treatment. These suggest both direct and reductive ion-exchange of Cu(II) from solution into the MSL. Both the XPS and NEXAFS spectra for treatment 4 however show no evidence of Cu in the glass. The presence of EDTA, a Cu-chelator, appears to prevent this Cu exchange in both the outermost layers and the MSL as a whole. This is a strong indication that Cu^{2+} interference is not an issue in well-buffered, low metal activity solutions such as seawater, where kinetic limitations of the Cu ion-exchange reaction occur at ultralow Cu^{2+} activities. A similar effect was noted with the Cl^- interference effect on the chalcogenide glass Cu-ISE at low ion activities (Belli and Zirino 1993, De Marco 1994).

Figure 1.16 shows the L-edge NEXAFS spectra of the Fe 2p electrons in the control sample and in treatments 1 and 2. A distinct excess of Fe(III) is observed in the unbuffered treatment, suggesting an exchange of Fe^{3+} ions from the solution into the MSL. The buffered treatment shows significantly less Fe in the MSL, depleted even compared to the control sample. SR XPS core level binding energies for both the Cu and Fe treatments are shown in Supplemental Table 1.2, indicating an absence of these metals in the membranes exposed to the EDTA-buffered solutions. According to these comparative analyses, the strong Fe-binding capacity of the EDTA causes a net diffusion of Fe^{3+} ions *out of* the chalcogenide glass. This is to be expected in all strongly-complexing systems, where the relatively abundant free Fe^{3+} ions in the Fe-ISE have the tendency to migrate toward the much lower aFe^{3+} of the solution.

In Figure 1.17, NEXAFS signals for the chalcogenide pieces aged in seawater are plotted as differences from the signal magnitude of the polished control piece. The pieces aged in static conditions (Figure 1.17a) clearly display a surplus of surface Fe which increases with

longer seawater exposure, resulting from the adsorption of membrane-released Fe. In contrast, the chalcogenide pieces aged in CFA conditions showed a *decrease* in surface Fe content as compared to the control (Figure 1.17b). As hypothesized, turbulent flow at the glass surface appears to cleanse the membrane of released Fe, leading to the gradual removal of Fe from the chalcogenide MSL.

Evidently, the lower concentration of natural Fe chelators in our static seawater solution (likely on the order of 10s to 100s nM), as compared to our 1 mM static EDTA solution, is not able to fully complex the totality of Fe released from the chalcogenide membrane. In a 40 mL volume, our ligands become saturated, and Fe begins to accumulate in the MSL. This membrane contamination is well-documented for ISEs which comprise some amount of analyte ion (Smith and Manahan 1973, Jasinski et al. 1974, Schefer et al. 1986, Sokalski et al. 1997). In a regime of flowing seawater however, fresh chelators are continually brought to this glass-solution interface region, and the outward diffusion of Fe can continue indefinitely. In the context of the Fe-ISE, this process generates a steady-state potential proportional to the Fe-binding tendencies of the ligand pool. Zirino and colleagues similarly utilizing turbulent flow regimes to lower the detection limit of Cu-ISEs for effective environmental analyses (Belli and Zirino 1993, Zirino et al. 1998, Zirino et al. 2002, Blake et al. 2004, Rivera-Duarte et al. 2005, Neira et al. 2011).

Although the results are not reported here, ultra-high surface sensitivity SR XPS showed that a 0.6 nm thick calcium/magnesium/silicate/chloride scale was formed on the ISE surface after continuous ageing in seawater under static conditions, while this effect was almost practically eliminated with the exception of the formation of minute amounts of $MgCl_2$, as a result of the surface cleansing effect experienced under turbulent flow conditions in the CFA system. If analyzing seawater under static conditions, it would be essential to simulate this seawater scaling phenomenon in calibration standards, while continuous flow analysis obviates this

problem. This also demonstrates that continuous flow is the optimal analytical conditions for use of the ISE in seawater analysis.

From our SR studies, it is evident that in these flowing, buffered systems, the Fe-ISE signal is not caused by metal ions from the solution interacting with the sensor, be these Fe^{3+} ions or Cu^{2+} ions. Instead, the ions active in this potential-generating process are only those mobile Fe^{3+} ions already in the chalcogenide glass matrix. These ions are available for exchange in the MSL, driven toward the solid-liquid interface by the electromotive attraction of the Fe-chelators in solution.

The Cu^{2+} cross-selectivity coefficient reported by Koenig and Grabner is therefore not relevant in these systems. The concept of interference as a whole takes on a different meaning when dealing with such strongly metal-complexing media. In fact, the Fe-ISE becomes a fundamentally different sensor in these solutions, where the electrode itself contributes an overwhelming flux of Fe to the ligand pool in what is essentially a complexometric titration. Ions or other ligands that could inhibit this process may be deemed to “interfere” with the potentiometric signal, and such species should be considered as analyses progress. But this is not the same as cross-selectivity in the traditional sense. What Koenig and Grabner measured was a proclivity for similarly-exchangeable metal ions to migrate *into* the MSL from solutions in which those ions are abundant. Their cross-selectivity coefficients only apply to such systems.

Conclusion

In this work we have conducted a necessary reexamination of some of the fundamental features of the response of the chalcogenide glass Fe-ISE in the context of eventual measurements of natural seawater. Synchrotron radiation studies of the chalcogenide glass surface have shown that the Fe-ISE behaves as a fundamentally different sensor in strongly metal-complexing systems such as seawater, such that some early findings regarding the Fe-

ISE's response in acidic, high Fe media are not relevant to studies in seawater. Specifically, NEXAFS results indicated that previous estimates of interference by Cu^{2+} ions do not apply in systems where the Fe-ISE signal relates to *outward* diffusion of mobile ions in the glass matrix. Our studies support the notions put forth by early investigations of metal-ISE measurements of exceptionally low metal activities – that the activities determined are relative measurements of the metal binding properties of the predominant complexes as they mediate the diffusion of metal ions from the ISE surface (Jasinski et al. 1974, Avdeef et al. 1983, Zirino et al. 1998)

Utilizing organically-buffered media in an in-house pH-stat combined with the Fe-ISE CFA system, we have reported a revised value for the Fe-ISE's temperature coefficient of -0.82 mV/°C. This value will be critical to interpreting in-situ seawater measurements, where any signal response to changes in temperature must be accounted for.

The optimal calibration procedure for the Fe-ISE had not been revisited for a decade. By conducting a suite of our own potentiometric calibrations, we have addressed several important points concerning these procedures. First, we have established the impact of the chosen pH range of the calibration standards. We propose that observed biases are likely attributable to errors in the speciation model or to variations in the potential-generating mechanism of the sensor commensurate with changes in ligand speciation over the course of a calibration. Additionally, we have shown that the standard potential determined from a calibration in these artificial solutions displays a strong dependence on the ligand background. In so doing, we have revealed the challenges that arise from treating the Fe-ISE as a traditional "ion-sensing" electrode and attempting to calibrate it as such.

In systems where the Fe^{3+} activity is merely a factor of the total Fe concentration, i.e. low pH solutions, calculating aFe^{3+} is fairly trivial. This is the framework for most ISEs, where a standard addition of the analyte ion produces a regular voltage change. In solutions with an excess of Fe-chelators, where essentially all of the Fe^{3+} is complexed, the concept of Fe activity takes on another meaning altogether. Though aFe^{3+} can theoretically be calculated, the

infinitesimally small values have little weight, and attempting to relate these values to measured Fe-ISE potentials may be more trouble than it is worth, especially since we have established that the sensor is not responding to the free Fe^{3+} ions in solution. But the general trends in activity as they relate to concentrations of organic and inorganic Fe-chelators are certainly still valuable as we move toward analyses of natural seawater. In these systems, the "activity" measured by the Fe-ISE represents the *tendency or capacity of the ligand pool to bind additional Fe*. This capacity is quite relevant to the accessibility and bioavailability of Fe in the ocean, and may provide clues as to how a marine environment will respond to fluxes of Fe. Chapter 2 of this work will explore techniques to better quantify this capacity, especially in seawater-based matrices.

Acknowledgements

This chapter, in part, is currently being prepared for submission for publication of the material, Fenton, Maxwell; Barbeau, Katherine; Martz, Todd. The dissertation author will be the primary author. All work was supported by grant NSF OCE 1924386. We would like to thank collaborator Dr. Roland De Marco for his helpful comments and discussion during much of this work, and his facilitation of the Elettra synchrotron experiments. We thank Anna Lashtabeg for the manufacturing of all electrodes used in this work.

Figures and Tables

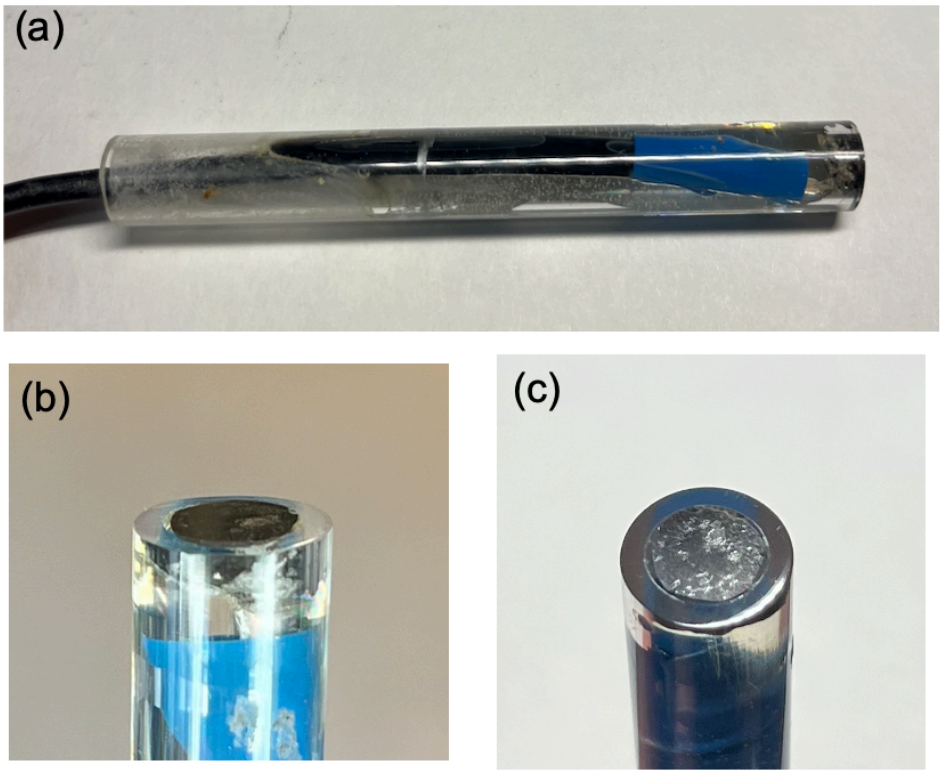

Figure 1.1: Photographs of the $Fe_{2.5}(Se_{60}Ge_{28}Sb_{12})_{97.5}$ chalcogenide glass Fe-ISE wired probe (a) and freshly polished surface (b, c).

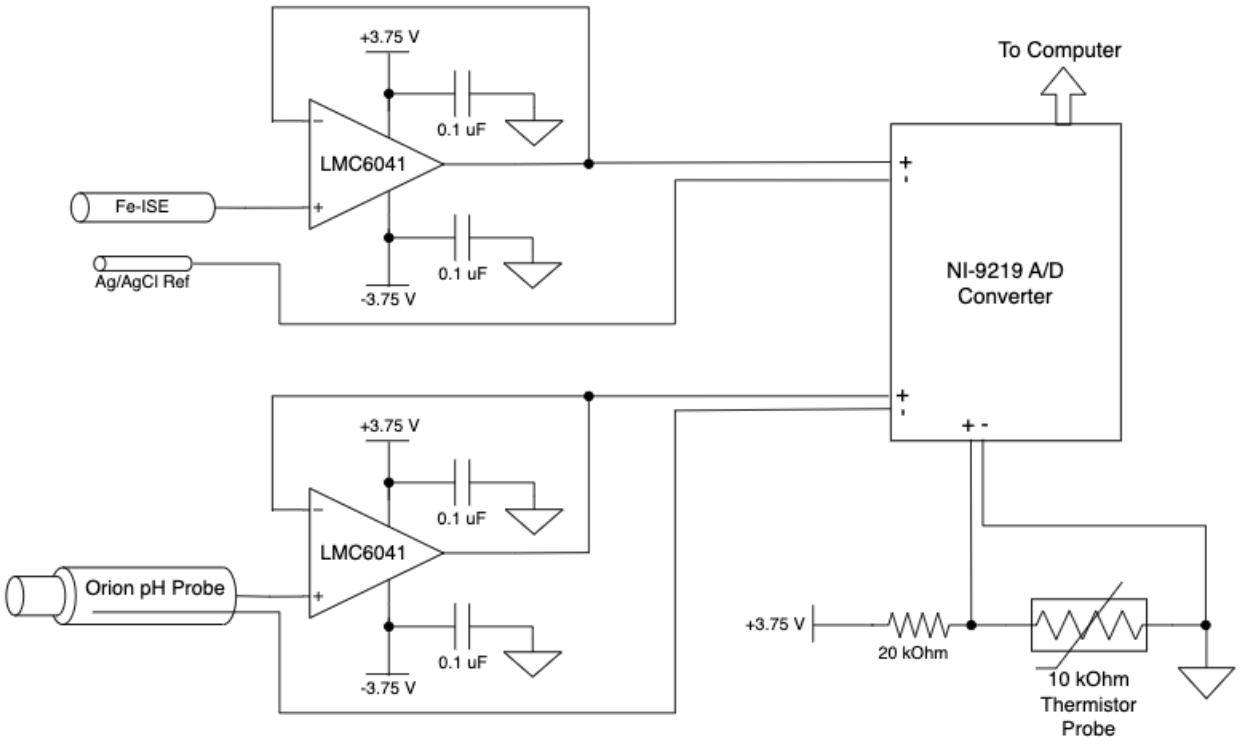

Figure 1.2: Circuit diagram detailing the wiring of the Fe-ISE potentiometric cell, glass pH sensor electrochemical cell, and thermistor. Two regulated 9V batteries were the sources of all power.

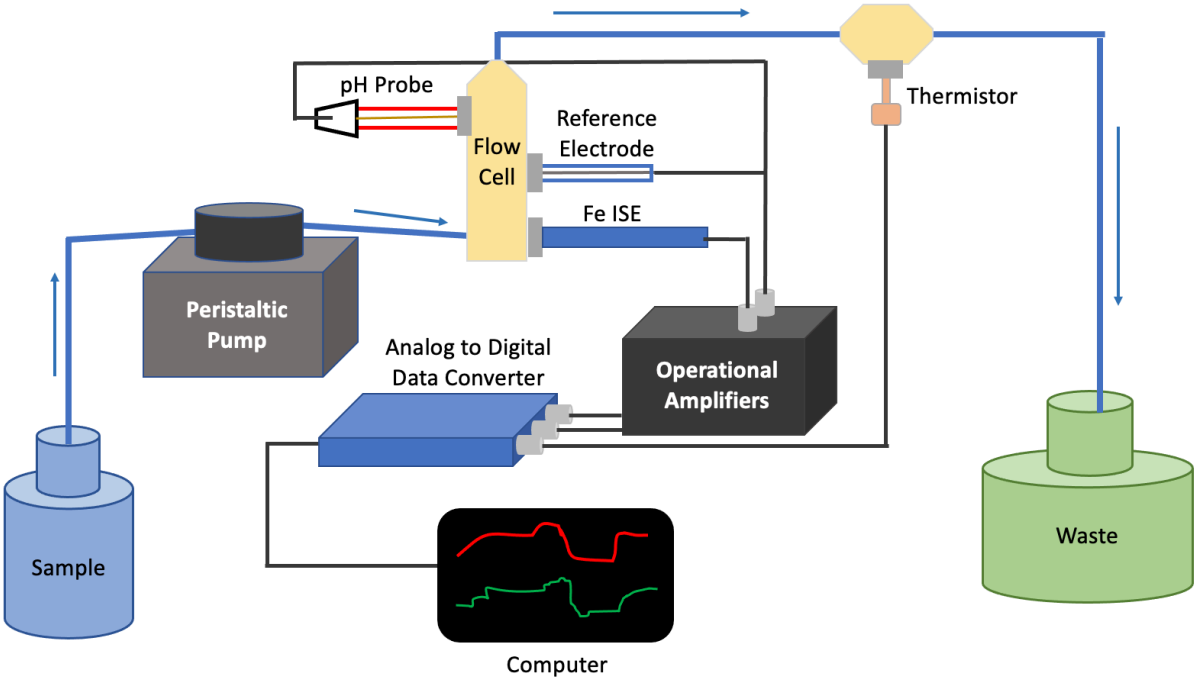

Figure 1.3: Schematic for the Fe-ISE continuous-flow analytical system.

Table 1.1: Components of the ACS and SBS calibration buffers. *In SBS standards, EDTA was replaced by citrate or salicylate chelators where specified. ACS standards only used EDTA.

Component	Concentration ACS	Concentration SBS
Iron (III) Chloride	10^{-4} M	10^{-4} M
EDTA*	10^{-4} M	10^{-2} M
Copper (II) Sulfate	10^{-3} M	*N/A*
Ethylene Diamine	$5x10^{-3}$ M	*N/A*
Sodium Chloride	0.55 M	0.55 M

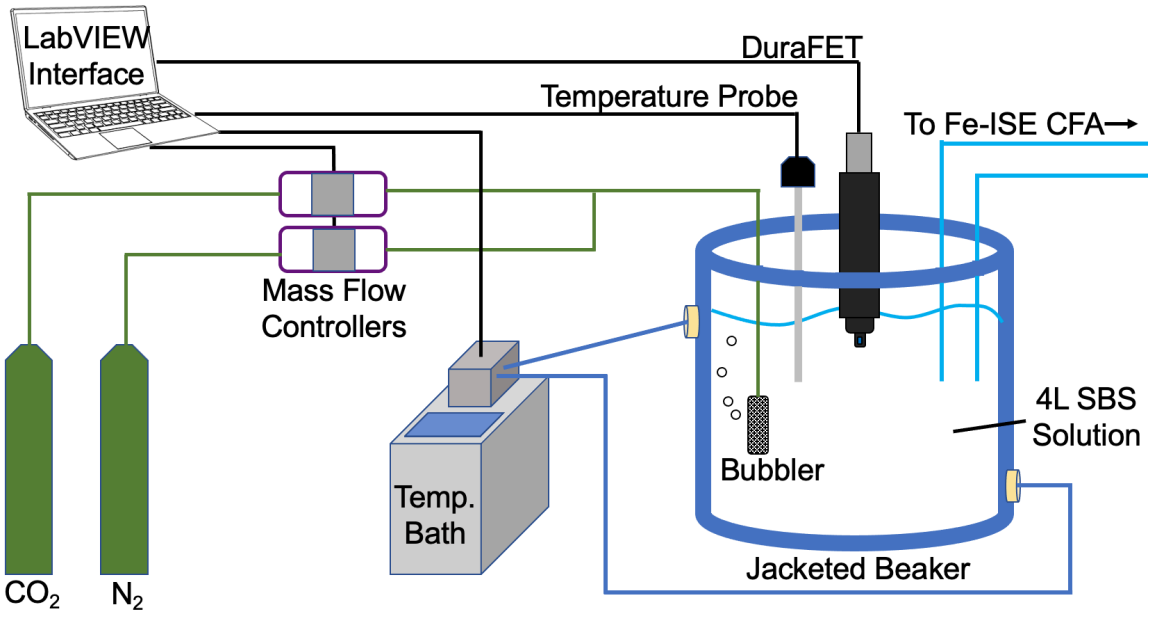

Figure 1.4: Schematic of the pH-stat system used in conjunction with the Fe-ISE CFA for determination of the sensor's temperature coefficient.

Table 1.2: Chalcogenide glass solution treatments for synchotron radiation surface studies.

Treatment	Salt	Metal	Chelator	pH
1	0.6 M NaCl	10^{-3} M FeCl	*N/A*	2
2	0.6 M NaCl	10^{-3} M FeCl	10^{-3} M EDTA	8
3	0.6 M NaCl	10^{-3} M $CuSO_4$	*N/A*	2
4	0.6 M NaCl	10^{-3} M $CuSO_4$	10^{-3} M EDTA	8

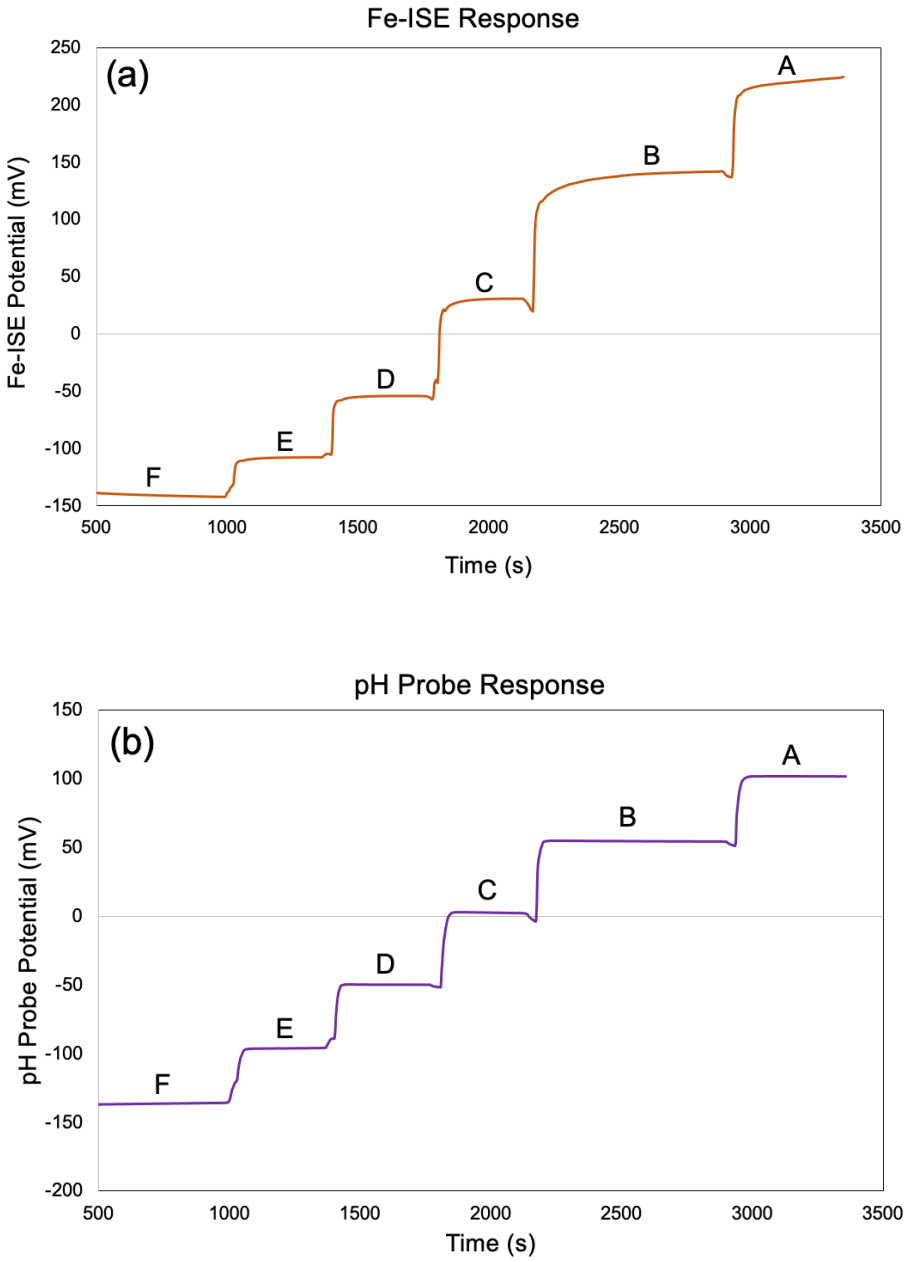

Figure 1.5: Fe-ISE (a) and pH probe (b) response in the CFA system during an ACS calibration. Capital letters above each stabilized potential denote each of the six ACS standards used for the calibration which are detailed in Table 1.3.

Table 1.3: Calibration data for ACS calibration of the Fe-ISE displayed in Figures 1.5 and 1.6

Std	pH	*log*[aFe^{3+}]	ISE Potential (mV)
A	4.77	-15.78	228
B	5.64	-18.12	143
C	6.58	-20.66	30
D	7.58	-23.44	-55
E	8.30	-25.60	-108
F	9.04	-27.82	-143

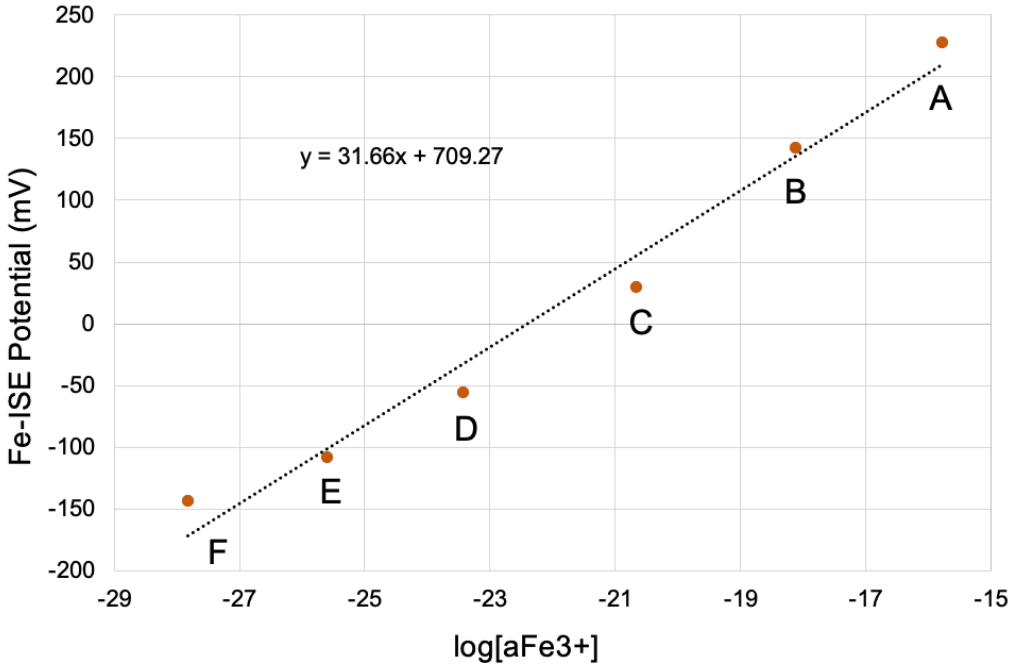

Figure 1.6: Calibration plot for ACS calibration of the Fe-ISE conducted December, 2024, showing the linear trendline and calculated regression. Capital letters correspond to the calibration standards detailed in Table 1.3.

Table 1.4: Compilation of calibration results for a single Fe-ISE probe in ACS and SBS systems.

Date	Solution	pH Range	Slope (mV/dec)	y-intercept (mV)
Sep 2022	ACS	4.87 - 9.5	32.0	705
April 2023	ACS	5.03 - 10.85	24.5	567
May 2023	ACS	4.96 - 10.8	23.7	508
June 2023	ACS	5.17 - 9.56	32.5	767
June 2023	ACS	4.91 - 9.67	29.4	670
Dec 2024	ACS	4.77 - 9.04	31.7	709
Aug 2022	SBS - Salicylate	5.42 - 10.34	21.8	475
Sep 2022	SBS - EDTA	4.26 - 9.26	21.0	483
Sep 2022	SBS - Citrate	4.88 - 10.97	21.1	411

Table 1.5: Calibration standard data for citrate-based SBS calibration of the Fe-ISE depicted in Figure 1.7

Std	pH	*log*[aFe^{3+}]	ISE Potential (mV)
A	4.88	-16.07	67
B	5.95	-18.96	4
C	7.00	-21.80	-48
D	7.89	-24.37	-85
E	8.98	-27.64	-164
F	9.79	-30.07	-236
G	10.97	-33.61	-302

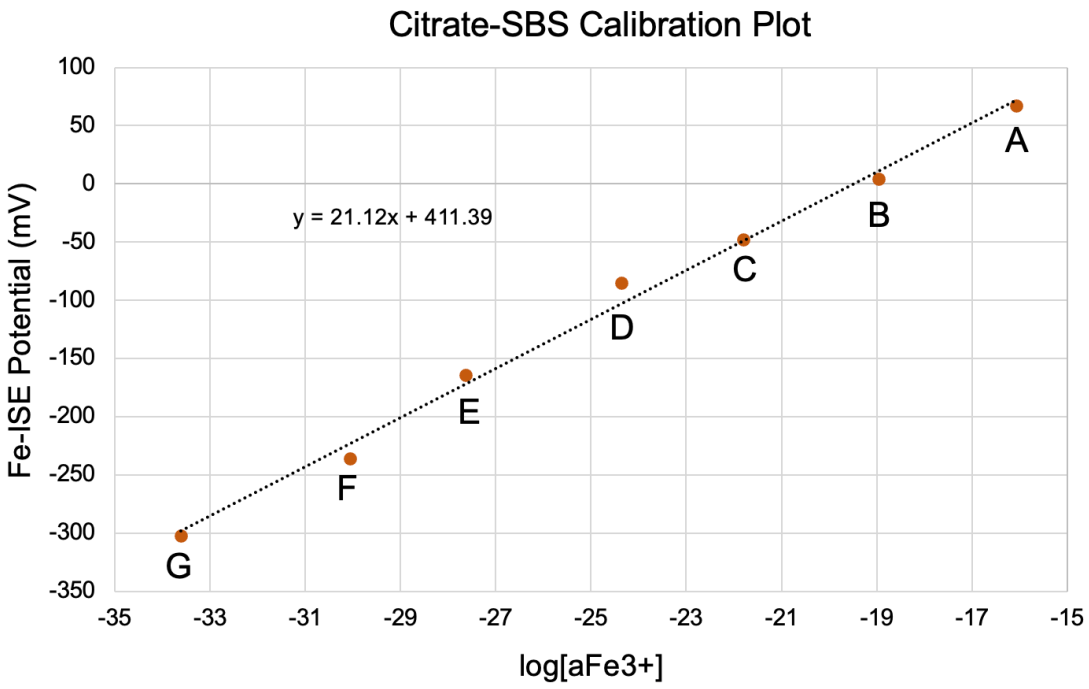

Figure 1.7: Calibration plot for citrate-based SBS calibration of the Fe-ISE, showing the linear trendline and calculated regression. Capital letters correspond to the calibration standards detailed in Table 1.5.

Table 1.6: Calibration standard data for EDTA-based SBS calibration of the Fe-ISE depicted in Figure 1.8

Std	pH	*log*[aFe^{3+}]	ISE Potential (mV)
A	4.26	-20.53	43
B	5.82	-23.27	6
C	7.04	-24.82	-27
D	8.22	-26.64	-77
E	9.26	-28.48	-120

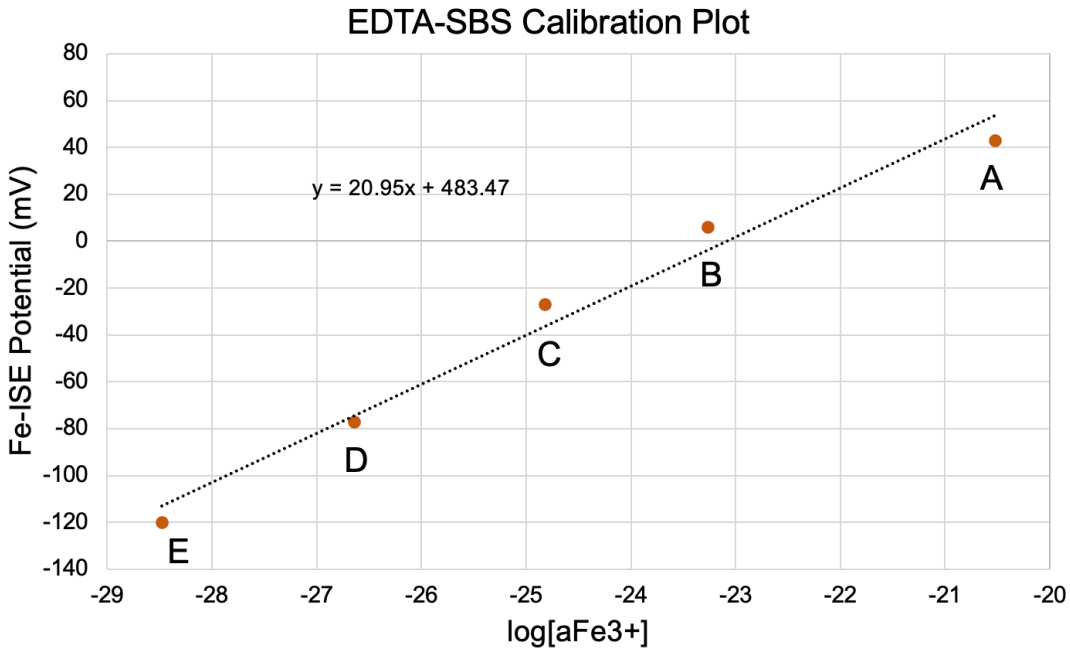

Figure 1.8: Calibration plot for EDTA-based SBS calibration of the Fe-ISE, showing the linear trendline and calculated regression. Capital letters correspond to the calibration standards detailed in Table 1.6.

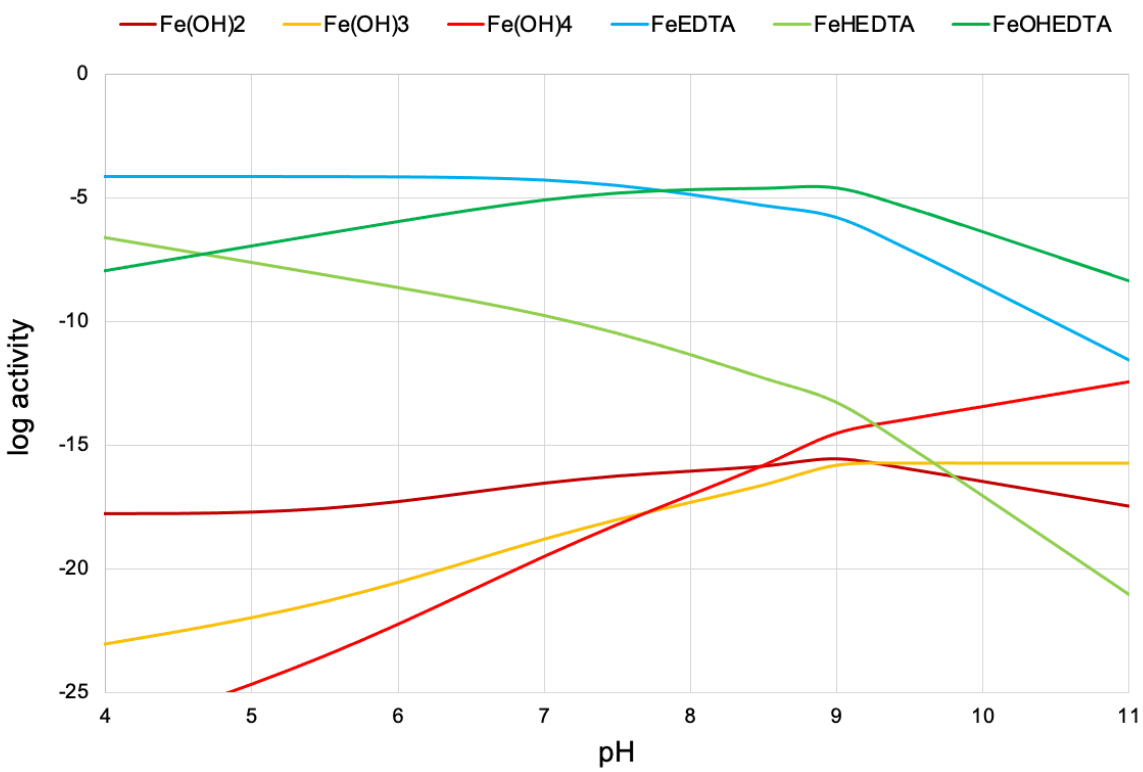

Figure 1.9: Activities of the dominant Fe species in the EDTA-based SBS matrix over the pH range of a typical calibration. Calculated by MINTEQ aqueous speciation modelling software according to the SBS components described in Table 1.

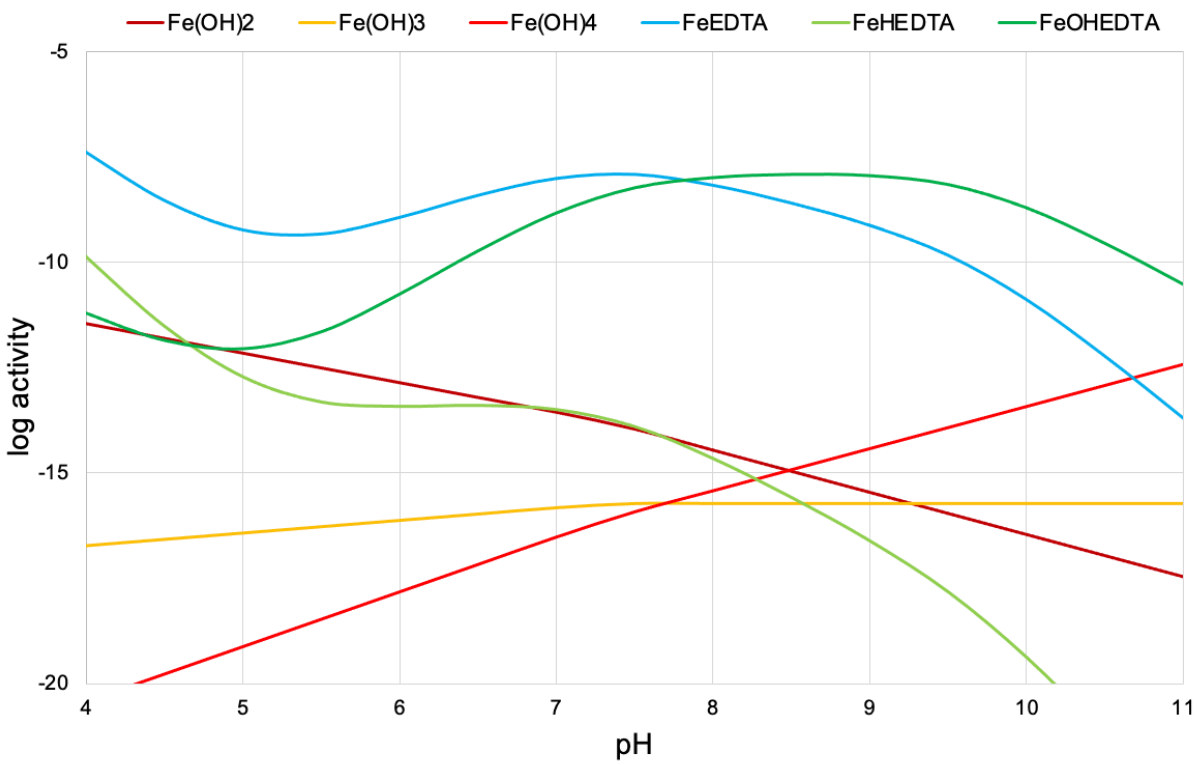

Figure 1.10: Activities of the dominant Fe species in the ACS matrix over the pH range of a typical calibration. Calculated by MINTEQ aqueous speciation modelling software according to the ACS components described in Table 1.

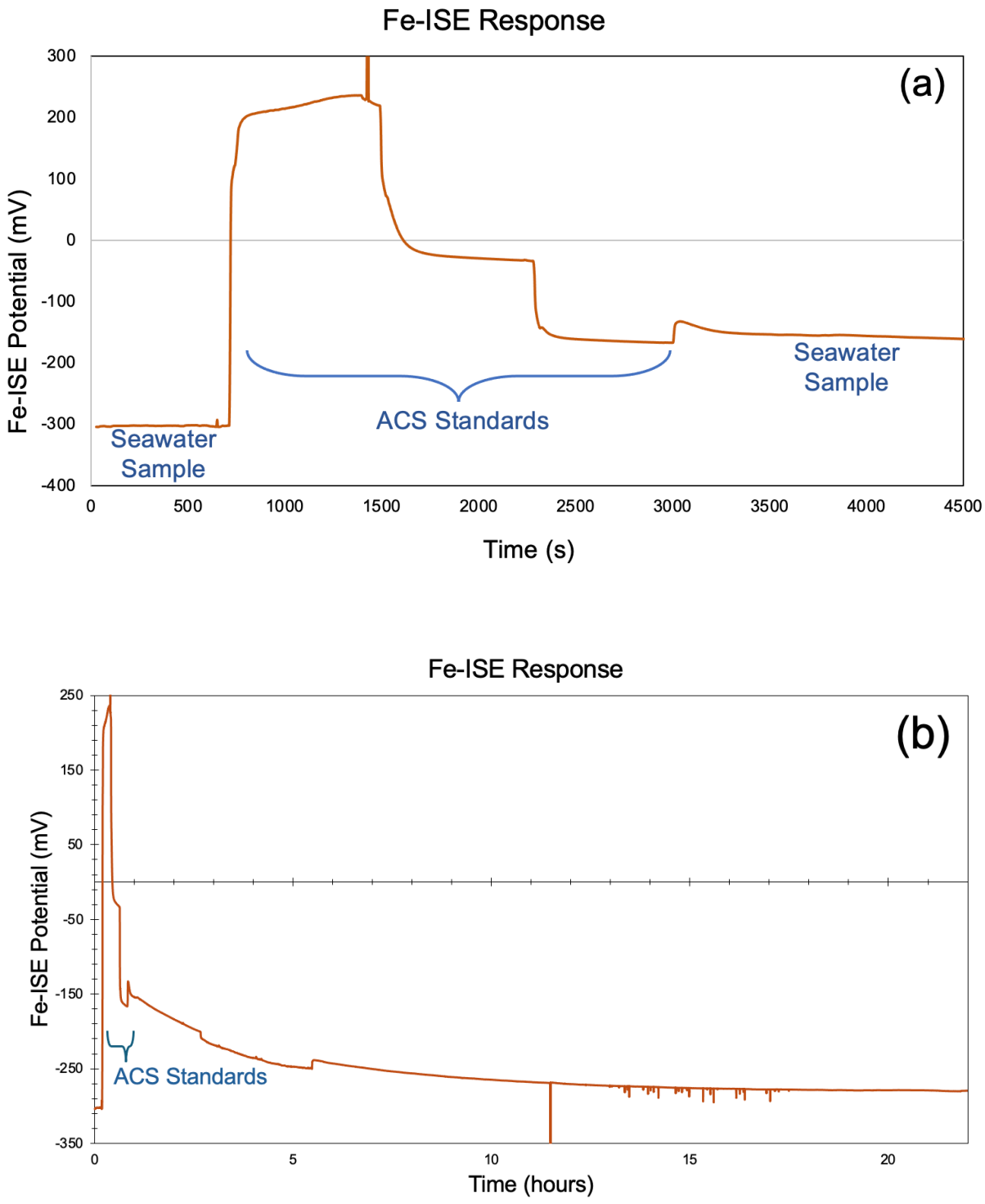

Figure 1.11: a) Fe-ISE response showing a seawater measurement before and after a 3-point ACS calibration. b) The same analysis, including the following 21 hours of reconditioning back to the seawater sample.

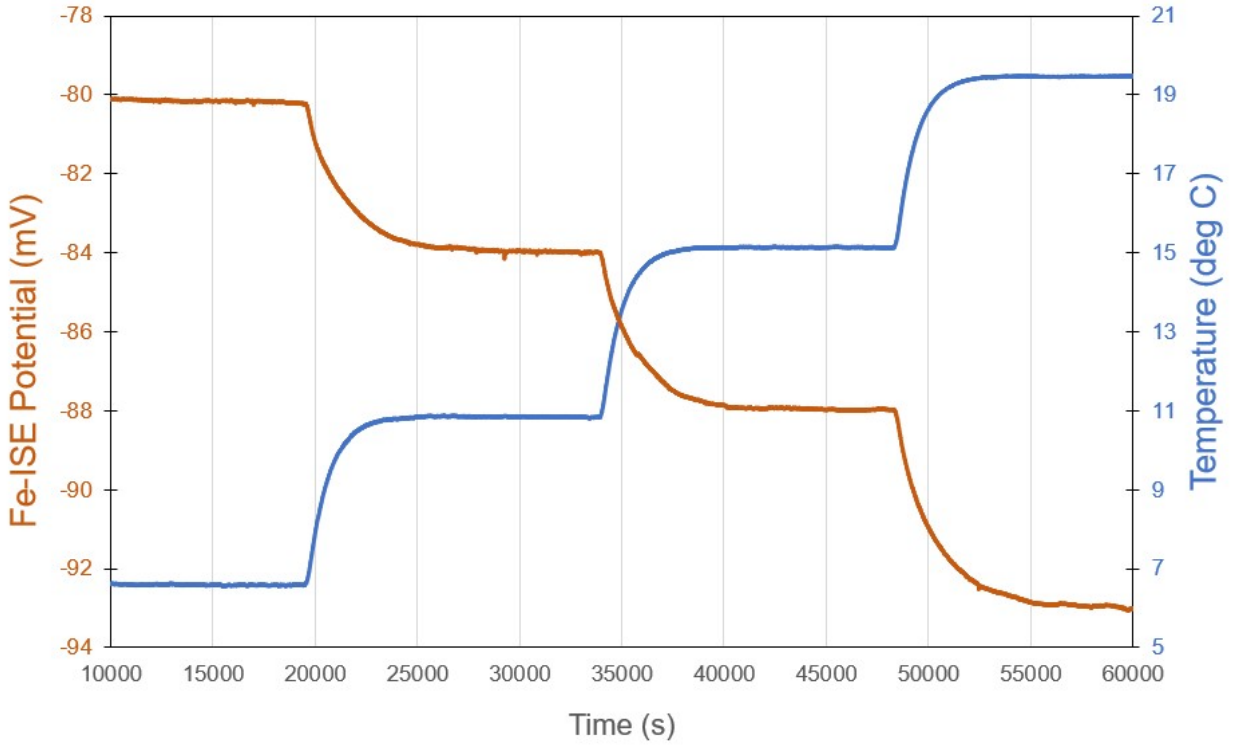

Figure 1.12: Fe-ISE response (orange) and temperature (blue) as measured by in-line thermistor probe during pH-stat temperature-sweep experiment with an EDTA-based SBS at pH 7.095.

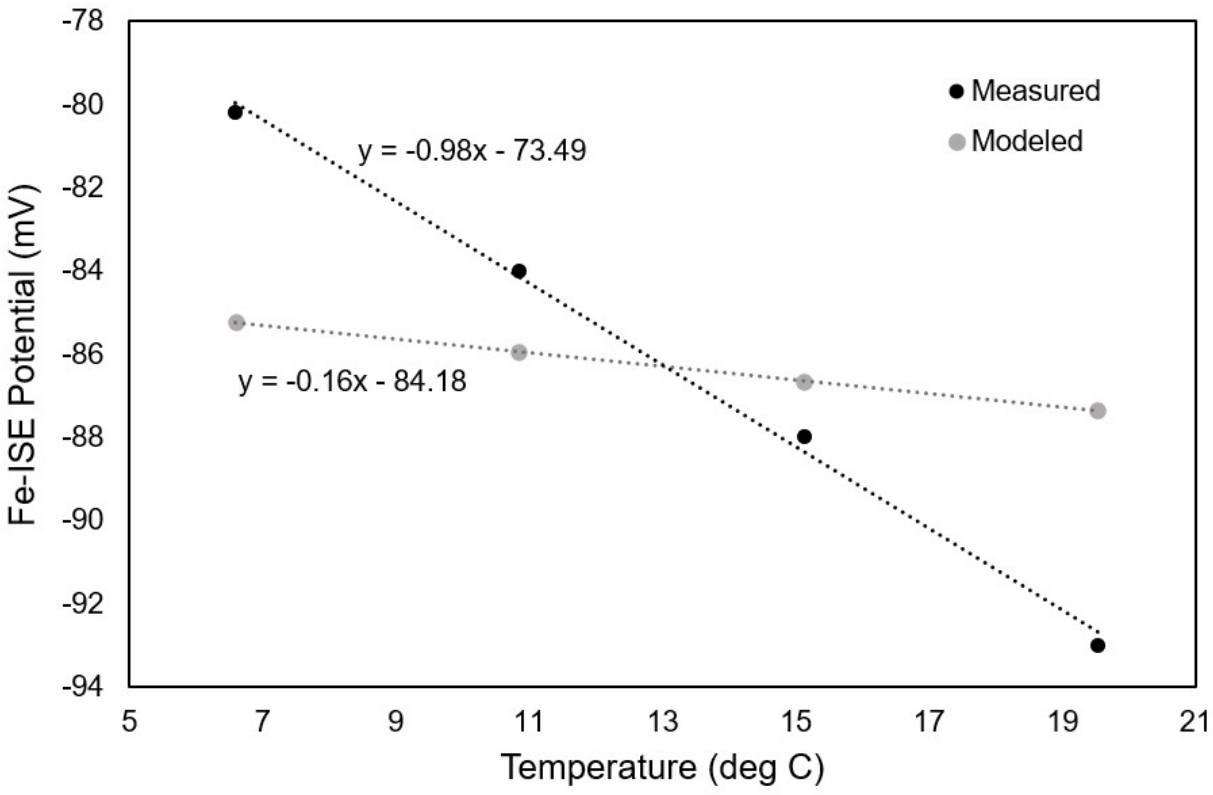

Figure 1.13: Plotted data and linear regression trendline for measured ISE voltage (black) at four temperatures during the temperature-sweep experiment in an EDTA-based SBS held at pH 7.095. Grey points represent the calculated aFe^{3+} expected at each temperature based on the MINTEQ speciation model for the solution, converted to potential using the calibration slope for this solution and offset to the mean measured potential.

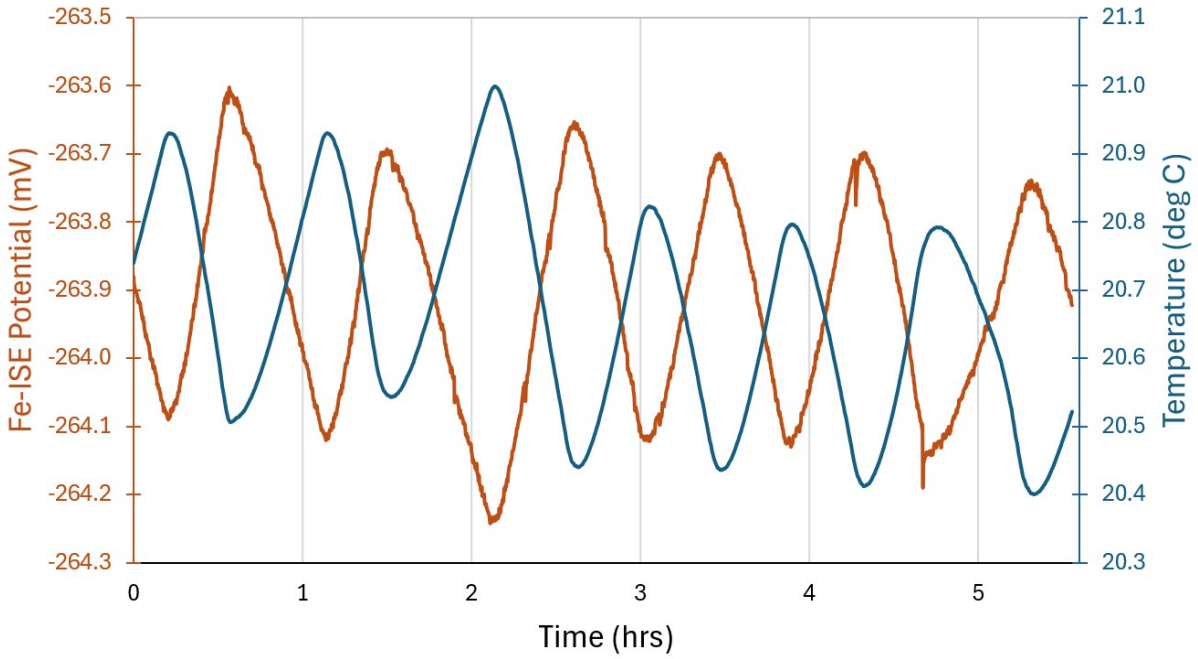

Figure 1.14: Fe-ISE response and thermistor-measured temperature during seawater conditioning in the CFA system while laboratory room temperature fluctuated.

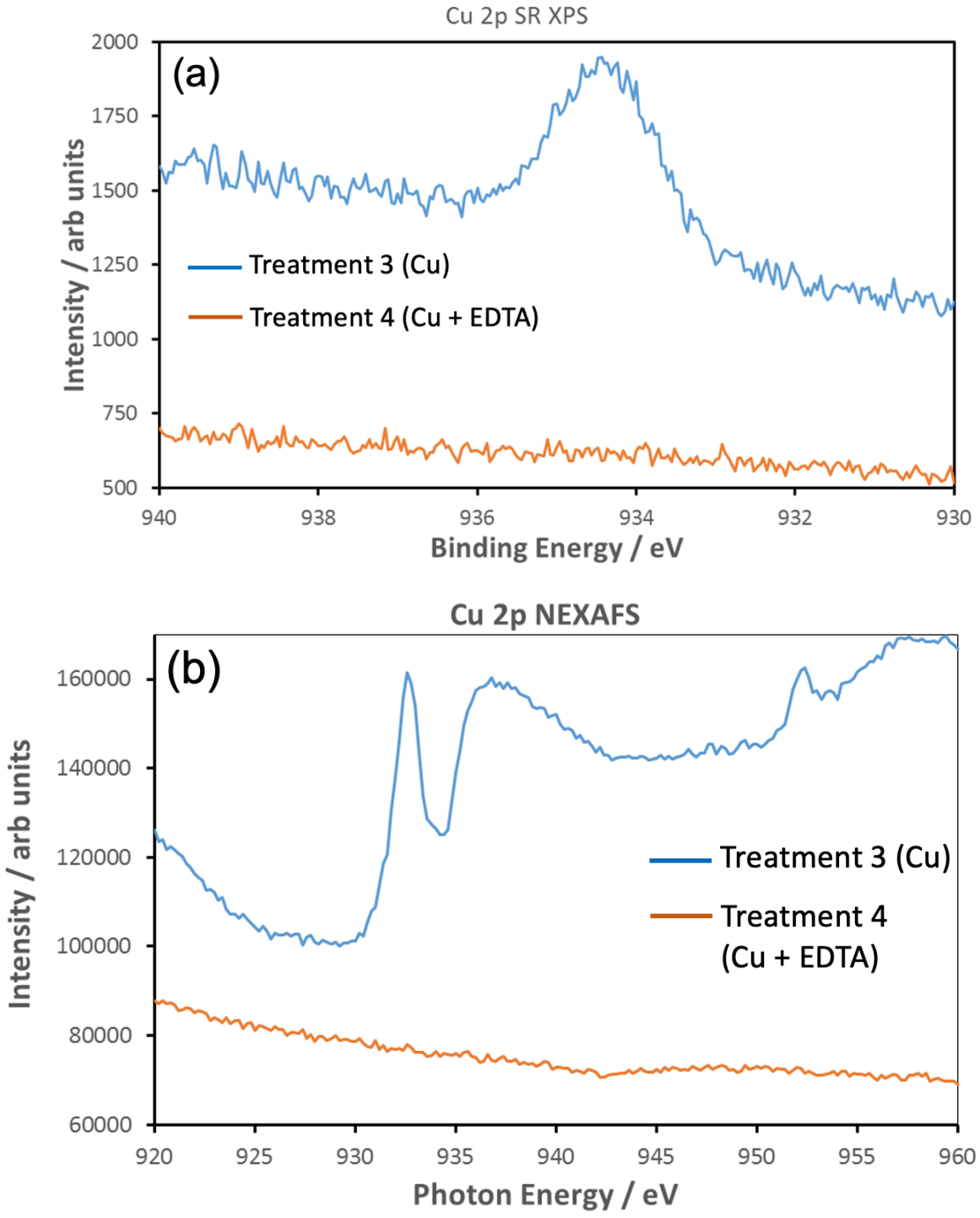

Figure 1.15: Cu 2p XPS (a) and NEXAFS (b) spectra of chalcogenide glass pieces exposed to organically-buffered and unbuffered saline Cu solutions (treatments 3 and 4 in Table 1.2), showing Cu species present in the surface layers of the unbuffered treatment, yet no evidence of Cu infiltration in the buffered treatment.

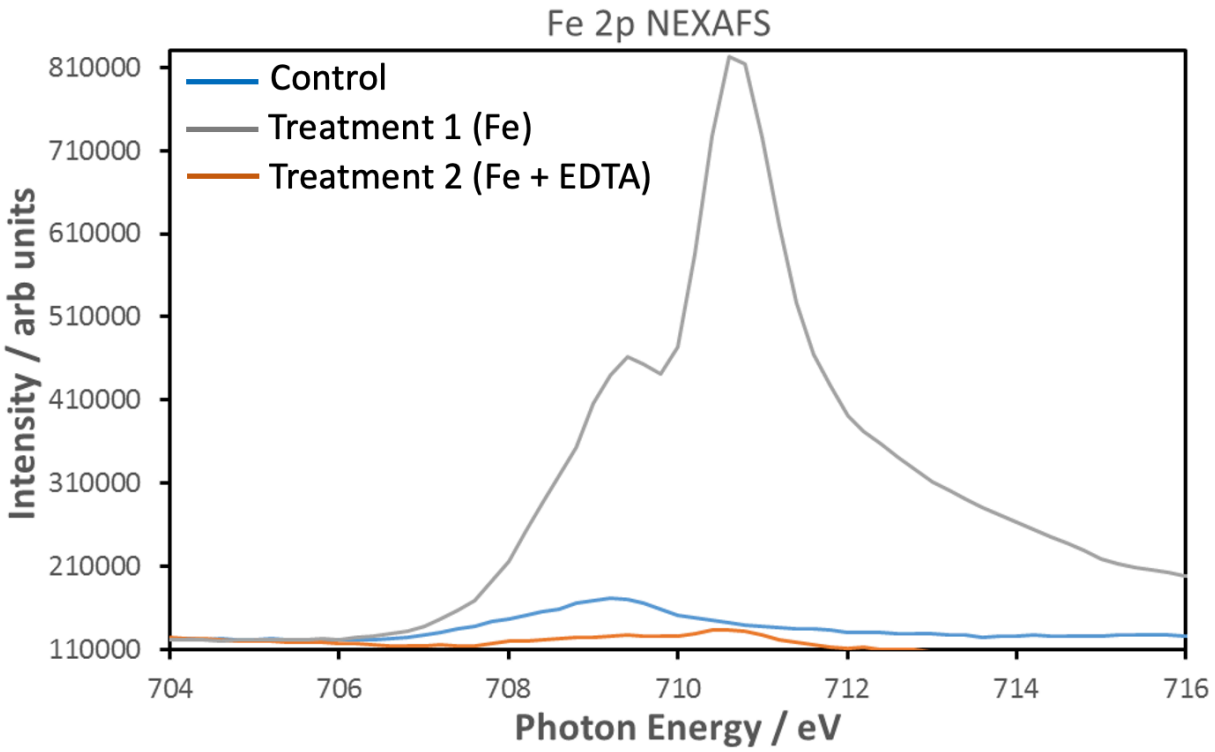

Figure 1.16: Fe 2p NEXAFS spectra of chalcogenide glass pieces exposed to organically-buffered and unbuffered saline Fe solutions (treatments 1 and 2 in Table 1.2) and an untreated control piece. An excess of Fe is present in the unbuffered treatment relative to the control, while the buffered treatment shows Fe deficient surface layers.

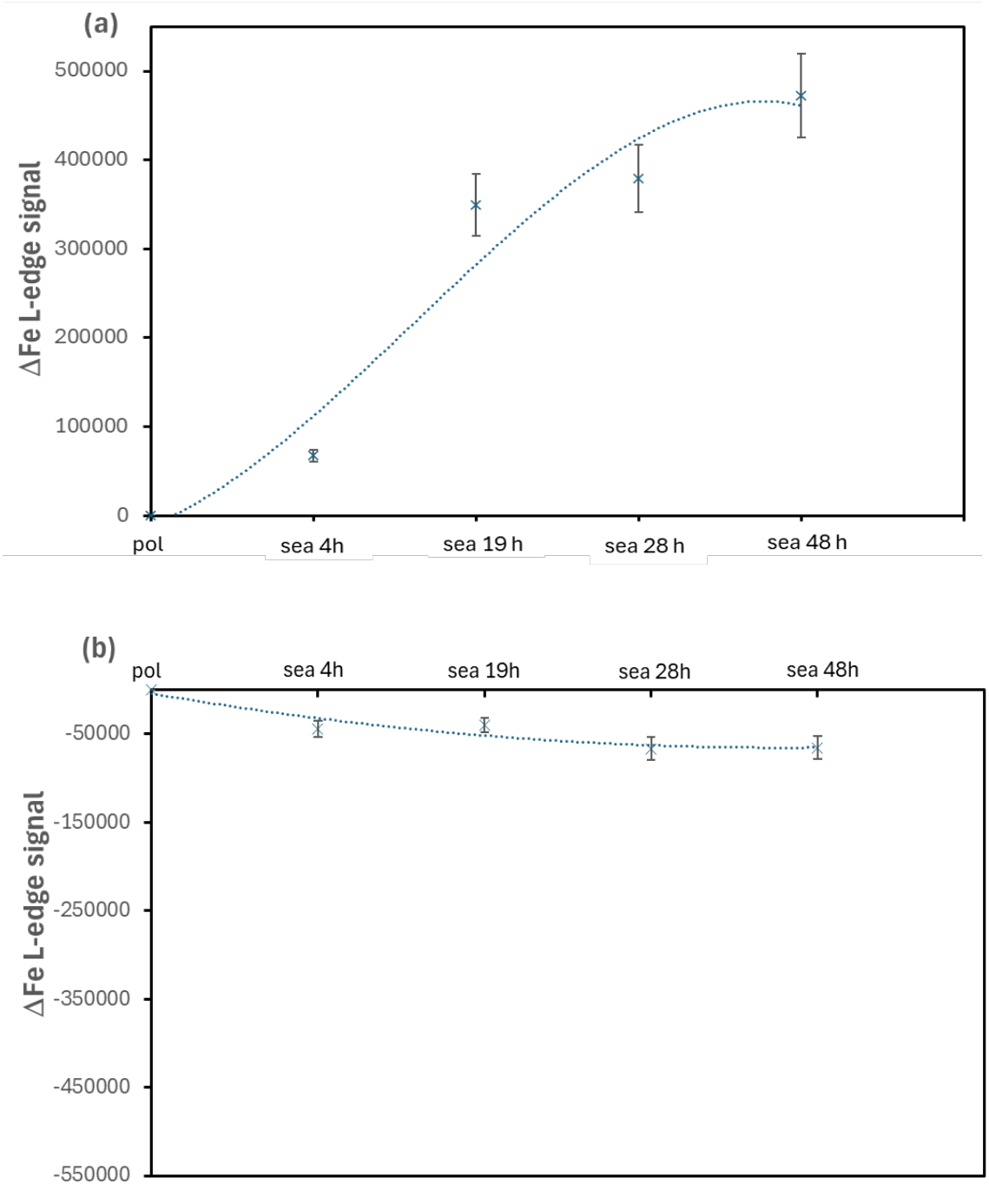

Figure 1.17: Difference in Fe L-edge NEXAFS signal magnitude as compared to the polished control, for chalcogenide pieces aged in static (a) or flowing (b) seawater at four different time points.

Supplemental Information

Supplemental Table 1.1: Compiled calibration results for ACS calibrations of six different Fe-ISE probes. Results shaded in yellow highlight calibration results that differ significantly from expected values, and likely indicate a manufacturing flaw.

Date	Electrode	pH range	Slope (mV/dec)	y-intercept (mV)
Oct 2021	St. Petersburg	5.43 - 9.47	28.6	637
Nov 2021	Unshielded Black AUS	5.66 - 9.72	25	519
July 2022	St. Petersburg	5.04 - 10.25	24.8	590
July 2022	Unshielded Green AUS	4.45 - 10.63	9.4	161
July 2022	Unshielded Blue AUS	4.45 - 10.12	18.7	330
April 2023	AUS April S1	4.95 - 10.43	15.8	261
April 2023	AUS April S2	4.77 - 10.73	23.8	524

Supplemental Table 1.2: SR-XPS core level binding energies of membranes treated in unbuffered and buffered Cu media using a photon energy of 210 eV (a) and unbuffered and buffered Fe media using a photon energy of 830 eV (b)

a	Se $3d_{5/2}$	Se $3d_{3/2}$	Ge $3d_{5/2}$	Ge $3d_{3/2}$	Sb $4d_{5/2}$	Sb $4d_{3/2}$	Cu $3p_{3/2}$	Cu $3p_{1/2}$
unbuffered Cu	53.7, 54.4, 55.1	54.6, 55.3, 56.0	30.4, 32.0	31.0, 32.6	-	-	74.8, 76.6	77.1, 78.9
buffered Cu	54.2, 55.1	55.0, 56.0	30.8, 32.5	31.4, 33.1	33.1	34.4	-	-

b	Se $3d_{5/2}$	Se $3d_{3/2}$	Ge $3d_{5/2}$	Ge $3d_{3/2}$	Sb $4d_{5/2}$	Sb $4d_{3/2}$	Fe $2p_{3/2}$	Fe $2p_{1/2}$
unbuffered Fe	54.1, 55.0, 56.0	55.0, 55.9, 56.9	30.6, 32.6	31.2, 33.2	34.3	35.5	711.6	725.7
buffered Fe	54.1, 54.9, 55.8	55.0, 55.8, 56.6	30.6	31.2	33.0	34.3	-	-

Chapter 2. Fe-ISE Acidimetric Titrations of Seawater Media: Calibrations, Model Validations, and Seawater Analyses

Abstract

The chalcogenide Fe^{3+} ion-selective electrode was analyzed through the context of novel measurements in seawater and seawater-based media. An improved calibration system is presented, optimized for the analysis of natural seawater, based on a filtered seawater solution comprising 10 µM added Fe and 100 µM added EDTA. These calibrations reproducibly generate slopes of around 25 mV/dec, which are in excellent agreement with previous calibrations of the Fe-ISE, yet do not impart the potential offset to seawater measurements that has been observed in calibrations utilizing more artificial systems. Plots showing the modeled change in aFe^{3+} vs pH are compared to commensurate Fe-ISE potentiometric pH titrations to illustrate the good agreement between modeled and measured aFe^{3+} trends in seawater media, provided chemical speciation models adequately account for Fe solubility effects. Natural seawater samples of varying Fe speciation are analyzed using Fe-ISE acidimetric titrations. This technique proves to be a powerful new method to evaluate seawater Fe chemistry and the effects of pH on Fe parameters.

Introduction

The Fe-ISE is a promising tool for oceanographic analysis given the relatively simple instrumentation required for its operation, and the ease with which it could be incorporated into shipboard flow-through systems or autonomous sensor suites. But while Fe-ISE response has been thoroughly studied in artificial, well-characterized solutions (Baker and Trachtenberg 1971,

Jasinski and Trachtenberg 1973, De Marco and Mackey 2000, De Marco and Pejcic 2000, De Marco and Martizano 2007, 2008, Maric et al. 2015) there is still some uncertainty as to the sensor's performance in natural seawater, a far more complex medium.

The extent of Fe-ISE usage in seawater thus far has amounted to several studies undertaken by De Marco and colleagues. These early, proof-of-concept experiments involved the UV-oxidation of the seawater samples to remove any organics and simplify speciation modeling. De Marco et al. (1999) measured an acidified, UV-oxidized seawater sample using an Fe-ISE calibrated in a saline citrate buffer system and determined a value of aFe^{3+} (activity of the free Fe^{3+} ion) in good agreement with their speciation model. De Marco and Mackey (2000) conducted what was essentially a calibration of the Fe-ISE using UV-oxidized seawater brought to various pH (and modeled aFe^{3+}) values, obtaining a calibration slope of 24.2 mV/dec which agreed well with their calibrations using artificial media. Measurements of natural, un-oxidized seawater at ambient pH have been limited to single point analyses following the sensor's calibration in an artificial organically-buffered system (De Marco and Martizano 2008, Maric et al. 2015). The aFe^{3+} determined by these measurements (~10^{-20}) were comparable to common values obtained by CLE-AdCSV analyses of natural seawater (Rue and Bruland 1995, Van den berg 1995, Ven den berg et al. 2006). Although, we note our results in Chapter 1 which indicate that these artificial calibration solutions appear to impart a significant potential offset to seawater measurements, such that it becomes difficult to relate calibration potentials to that of seawater analyses. Therefore, if our goal is in fact to use the Fe-ISE to determine aFe^{3+} of natural seawater samples, the optimal calibration system would be based in seawater itself.

The artificial media used for previous tests of the Fe-ISE comprise fairly simple Fe-speciation, with generally only one or two organic Fe-binding species, and a basic ionic background of sodium chloride. In UV-oxidized seawater, Fe-speciation depends only on relatively high concentrations of well characterized inorganic Fe-chelators (Byrne and Kester 1976, Millero et al. 1995). This means that calculation of aFe^{3+}, the activity of the free Fe^{3+} ion,

is straightforward, and may be more directly related to the Fe-saturation and concomitant Fe-binding capacity of the ligand pool – what the Fe-ISE appears to be measuring. In a more complicated, natural seawater calibration system with myriad strong Fe-chelators (Bundy et al. 2014, Velasquez et al. 2016, Slagter et al. 2019, Whitby et al. 2020, Forsch et al. 2021), it is unknown how well calculated aFe^{3+} values will agree with potentiometric data from the Fe-ISE.

Fe Activity in Seawater

Fe activity, or aFe^{3+}, as it pertains to an organically-buffered aqueous solution is a single parameter which best represents the overall Fe-binding nature of the system. Total Fe, ligand strengths, ligand concentrations, pH, temperature, and any Fe-precipitation are all taken into account in the calculation of aFe^{3+}. As discussed in Chapter 1, in seawater and similarly buffered solutions, aFe^{3+} should not be taken to denote a particular fraction of Fe. Rather, it is a fundamental thermodynamic master-variable for the Fe-system, and is relevant to the overall availability of Fe to microorganisms (Anderson and Morel 1982, Avdeef et al. 1983, Zirino et al. 1998).

Because aFe^{3+} is so dependent on the Fe-chelators in solution, our main empirical measurements of seawater aFe^{3+} come from Fe-speciation studies employing the CLE-AdCSV technique. However, these studies have moved away from quantifying Fe-binding by natural ligands in terms of Fe^{3+} itself, instead focusing on Fe′, which represents all soluble inorganic Fe species. Conversion from Fe′ to Fe^{3+} relies on the inorganic side reaction coefficient which is usually taken to be $\alpha_{Fe'}$ = 10^{10} (Hudson et al. 1992, Rue and Bruland 1995, Van den Berg et al. 2006) but this assumes no neutral $Fe(OH)_3$ species present in solution, which may not be entirely accurate (Liu and Millero 1999, 2002, Kuma et al. 1996). Thus, while not of utmost importance in the CSV method where the goal is largely to examine relative ligand strengths among a sample set, there is still some uncertainty on actual aFe^{3+} values. In most CSV

analyses, seawater samples are buffered to a standard pH, generally 8.2, to utilize established log K binding constants during competitive ligand exchange calculations (Boye et al. 2001, Buck et al. 2015, Mahieu et al. 2024). Recent CSV studies measuring the effect of pH on Fe-speciation show that pH has a significant influence on the Fe-binding parameters elucidated by the technique, and suggest that in certain marine systems, natural pH variations account for more of the observed gradients in aFe^{3+} than those caused by variations in ligand strength or concentration (Heimstra and van Reimsdijk 2006, Avendano et al 2016, Gledhill et al. 2015, Zhu et al. 2023)

The other way to gain an idea of seawater Fe activity is through chemical speciation models. These models allow us to neatly visualize the major controls of aFe^{3+} in seawater, and how they affect other aspects of the Fe system. Figures 2.1 and 2.2, for example, show the effects of pH and two different organic ligands on aFe^{3+} (Figures 2.1a, 2.2a) and associated total dissolved Fe concentrations (Figures 2.1b, 2.2b), as calculated by Visual MINTEQ aqueous speciation modeling software. As pH increases, aFe^{3+} decreases due to increased complexation by hydroxides, as well as increased complexation by any organic species as their Fe-binding sites are deprotonated. The binding strength and concentration of these organic species, as well as their particular acid-base properties (pK_a values), determine the shape of the $log[aFe^{3+}]$ vs pH curve. This is illustrated well by the difference between the DTPA and EDTA curves. Although increased binding by organic ligands serves to decrease aFe^{3+}, it also results in higher concentrations of total dissolved Fe species (Figures 2.1b, 2.2b), noting that maximum dissolved Fe concentrations are limited by the insolubility of $Fe(OH)_3$ species.

If the Fe-ISE could be used alongside a pH sensor during an acidimetric titration of natural seawater, it would generate a characteristic $log[aFe^{3+}]$ vs pH curve (as in Figures 2.1a and 2.2a) that could be used to identify and describe the Fe-binding ligand pool. These potentiometric pH titrations would be particularly relevant in understanding the changes in Fe-speciation that may arise due to ocean acidification. Studies have shown that concentrations of

free Fe ions as well as concentrations of organically complexed Fe may both increase in response to decreasing ocean pH (Breitbarth et al. 2010, Millero et al. 2009, Gledhill et al. 2015, Stockdale et al. 2016) but the specifics of these dynamics are complex and vary both spatially and temporally (Ye et al. 2020). Most of these predictions rely on aqueous speciation models which incorporate metal binding by marine dissolved organic carbon (WHAM, NICA-Donnan), while the experimental studies utilize laborious and time-intensive CLE-AdCSV techniques (Gledhill et al. 2015, Zhu et al. 2021). A simple, rapid method to probe pH-related effects on Fe-speciation would massively facilitate scientists' abilities to forecast and study the influence of ocean acidification.

Additionally, there is growing evidence that physico-chemical properties (pH, O_2) of the phycosphere, the aqueous microenvironment surrounding phytoplankton cells, can differ significantly from the properties of the bulk seawater matrix (Liu et al. 2020, Liu et al. 2022). Given the implications for phytoplankton Fe uptake, an improved understanding of pH-Fe dynamics under different seawater conditions is required to be able to predict metal bioavailability, and the Fe-ISE is uniquely suited to such studies.

Thus, this work highlights three main scientific efforts in advancing our understanding of the Fe-ISE as it pertains to measurements of seawater. First, we present an optimal, seawater-based Fe-ISE calibration system which can be accurately modeled and allows for reliable calculation of aFe^{3+}. Next, we discuss several Fe-ISE acidimetric titrations of modified and unmodified seawater solutions to examine exactly when modeled aFe^{3+} is most relatable to Fe-ISE potential, and how to adjust our models to that end. Here, we make use $\log[aFe^{3+}]$ vs pH curves, which prove to be valuable tools for model validation. Finally, we present data from a series of acidimetric titrations of different natural seawater samples, to assess whether the Fe-ISE can be used in this way to glean useful information regarding the natural Fe-binding ligand pool.

Experimental

Trace-Metal Clean Seawater Collection

All sampling efforts adhered to the trace-metal clean sampling and bottle-cleaning protocols detailed in the GEOTRACES cookbook (https://www.geotraces.org/methods-cookbook/). Offshore surface seawater was obtained during two separate research cruises: the Pupcycle II cruise on the R/V Sally Ride in May/June of 2023, with sampling offshore of Cape Blanco, Oregon; and the P2402 CCE LTER process cruise on the R/V Roger Revelle in February/March of 2024, with sampling offshore of Point Conception.

For Pupcycle, bulk (~20 L) surface seawater was collected using a trace-metal clean towed-fish system and metal-free diaphragm pump. As the ship steamed at 5 kts, the fish was towed outside the ship's wake and surface seawater was pumped directly into a trace-metal van (HEPA-filtered air, metal-free). Seawater was filtered in-line through a 0.2 µm Acropak 200 capsule filter (VWR) into acid-clean low-density polyethylene (LDPE) plastic cubitainers.

During P2402, surface seawater was collected using a trace-metal clean coated sampling rosette equipped with 5-L Niskin sampling bottles (General Oceanics). Niskin bottles were secured in a trace-metal van and pressurized with ultra-filtered air, such that sample filtration could occur directly from the bottle. Bulk seawater was then filtered and collected as described above.

At the Scripps Institution of Oceanography pier, seawater was collected by lowering an acid-clean carboy into the water using trace-metal clean line. The carboy was brought back into a trace-metal clean lab space, pressurized with ultra-filtered air such that the seawater could be filtered in-line through an Acropak (as above) and collected in a secondary, polycarbonate carboy.

At the time of analysis on the Fe-ISE system, aliquots of these bulk seawater samples were taken for measurements of total dissolved Fe (dFe). Dissolved Fe samples were collected in 250 mL low-density polyethylene (LDPE) bottles and acidified to pH 1.8 with optima HCl.

Determination of dFe and Fe-L Parameters of Unmodified Seawater

All seawater samples used to make modified seawater solutions were analyzed at Scripps Institution of Oceanography using in-house methods for determination of total dissolved Fe (dFe) and Fe-binding ligands. Measurements of dFe were made using a flow-injection with chemiluminescence (FI-CL) system based on the manifold by Lohan et al. (2006). Briefly, dissolved Fe is oxidized to Fe^{3+} with 10 mM Q-H_2O_2 (Suprapur grade). An ammonium acetate solution buffers the sample to pH 3.5 in-line, where it is preconcentrated on a chelating resin column (Toyopearl AF-Chelate-650M). The salt matrix is removed, and the Fe is eluted from the column using 0.14 M HCl (Optima grade, Fisher Scientific). The Fe catalyzes a chemiluminescent reaction between H_2O_2 and luminol (Sigma Aldrich), and this luminescence is recorded by a photomultiplier tube (Hamamatsu Photonics).

Fe standards were made with an ICP spectrometry standard (TraceCERT, ultra-high purity, in 2% HNO_3) added to Pacific ocean surface seawater to match the sample matrix, to final concentrations of 0, 0.4, 0.8, 3.2, and 10 nM Fe. Standards were measured at the beginning and end of each analytical run, and precision and drift were assessed with replicate analyses of aliquots of a large volume of reference seawater measured throughout each run.

Preparation of Modified Seawater Solutions

In order to test Fe-ISE response in seawater matrices with varying overall Fe-binding capacities, seawater from both the Scripps Pier and offshore regions was modified with $FeCl_3$ and a strong organic Fe-complexing agent, EDTA (analytical grade, Fisher Scientific). The

ambient dissolved Fe concentrations as measured by FI-CL (described above) are shown in Table 2.1 for all seawater used in this work. For all modified seawater solutions, enough Fe and EDTA were added such that the electrochemical signature of the ambient Fe or ligand pool in each sample would be swamped. In this way, we assure that aFe^{3+} is not affected by possible variations in the ambient Fe or ligand pool of a given sample, and is only dependent on our additions, as well as the concentrations of the major ions of seawater and the carbonate system. All formulations of modified seawater are detailed in Table 2.2, noting that EDTA was always in excess of Fe as is the case for natural Fe chelators in seawater, ensuring a metal-buffered system (Gledhill and Buck 2015, Taglibue et al. 2017)

For seawater-based calibration experiments and pH-based potentiometric titrations, a bulk solution of natural seawater or modified seawater was partitioned into up to nine aliquots (200 mL for modified seawater, >2 L for unmodified seawater). Each aliquot was brought to a desired pH (and associated aFe^{3+}) using concentrated HCl or NaOH, measured on a separate, external glass combination pH electrode (Orion 8102 BN) which was calibrated to three Orion pH buffer solutions traceable to NIST standards. Aliquots were then left at the adjusted pH for at least 24 hours to allow added EDTA and Fe to equilibrate with the natural seawater species prior to Fe-ISE measurements.

Fe-ISE Potentiometric Measurements

The chalcogenide glass electrode used in all measurements was of the formulation $Fe_{2.5}(Se_{60}Ge_{28}Sb_{12})_{97.5}$ and was manufactured exactly as described in Chapter 1 (Baker and Trachtenberg, 1971). Similarly, all potentiometric electric circuits, as well as the Fe-ISE CFA system itself, were identical to those detailed in Chapter 1. For measurements of unmodified seawater samples, large enough volumes were used such that a stable signal could be reached without circulating the sample. Modified seawater samples were recirculated through the CFA

system as total Fe was in excess of 10 μM, and contamination of a given sample by the Fe-ISE itself was negligible over the course of a measurement (De Marco and Mackey 1999).

Prior to any series of measurements, the Fe-ISE was polished on nylon and micro-cloth pads using a Buehler alumina slurry of decreasing particle size, and subsequently rinsed thoroughly in Milli-Q. The Fe-ISE was then conditioned in its flow cell for at least 24 hours in unmodified filtered seawater until a stable potential (<0.5 mV/hour drift) had been reached. After conditioning, the Fe-ISE was exposed to each pH aliquot until a stable potential (<0.1 mV/min) was reached, moving from high aFe^{3+} to low aFe^{3+} (low pH to high pH) solutions unless otherwise specified.

Aqueous Speciation Modeling

Visual MINTEQ chemical equilibrium modelling software was employed for all calculations of aFe^{3+} and other chemical species in our modified seawater solutions. This software is free and publicly available, and utilizes a database of chemical equilibrium binding constants from continually updated literature sources. All database information can be found online at https://vminteq.com.

For modified seawater calibration solutions and pH-based potentiometric titrations, model inputs were pH, concentrations of the major ions of seawater, concentrations of select trace metals, and concentrations of added Fe and EDTA. Visual MINTEQ calculates ionic strength based on all ionic species, and makes corrections using the Davies equation (extended Debye-Huckel equation). Input concentrations of all species are shown in Table 2.3, and assume a salinity of roughly 35.9 ppt (Morel et al., 1971). It should be noted that changes to salinity (and thus ionic strength) within 2-3 ppt have a negligible effect on the aFe^{3+} output, and do not change the shape of the aFe^{3+} vs pH curve, which is the main interest of this work.

Visual MINTEQ allows for the inclusion of “possible solids”, which accounts for the precipitation (effectively, the removal from solution) of any selected solid if the species reaches

oversaturation with respect to its solubility product (K_s). For models where we assumed precipitation, we selected *all* solids in the solution that reached oversaturation. Models that included no precipitation mean that even oversaturated species remained in solution. Implications of these assumptions as they relate to our experiments are explored in the Results and Discussion section.

For attempted modeling of the unmodified filtered Scripps pier seawater, inputs were identical but also included the addition of NICA-Donnan dissolved organic matter (Kinniburgh et al. 1999, Koopal et al. 2006, Dudal et al. 2004, Lodeiro et al. 2020). We used a total dissolved organic carbon (DOC) concentration of 75 μM, a typical value measured at Scripps pier during the month of our seawater collection (Shimadzu TOC analyzer). This led to final binding site concentrations of 8.73 μM DOM1, and 2.76 μM DOM2. Thermodynamic constants for Fe(III) binding by DOM were taken from Zhu and Hopwood et al. (2021), such that $\log K_{Fe(III)DOM1} = 2.94$, $n_{Fe(III)DOM1} = 0.32$, and $\log K_{Fe(III)DOM2} = 9.60$, $n_{Fe(III)DOM2} = 0.30$. All other NICA-Donnan parameters were left unchanged in Visual MINTEQ, which uses values from Milne et al. (2003 and 2001) for acid-base constants and DOM binding of other cations.

Results and Discussion

Fe-ISE Calibration with Seawater-Based Solutions

Figure 2.3 shows calibration curves for B5 seawater modified from filtered seawater from Scripps pier and the Pupcycle II cruise, as well as linear regression trendline data for each calibration. Calibration slopes were 26.7 $\pm$ 1.6 mv/dec and 24.9 $\pm$ 1.1 mV/dec for Scripps pier and Pupcycle II B5 modified seawater respectively. These slopes are in good agreement with those obtained by De Marco and colleagues in artificially buffered media and UV-oxidized seawater (De Marco et al. 1999, De Marco and Mackey 2000, De Marco and Martizano 2007, 2008, Maric et al. 2015) as well as those of our own calibrations in similar artificial solutions

described in Chapter 1. Slopes are again between 20 and 30 mV/dev, which would imply some combination of Fe^{3+} ion-exchange and charge transfer potential-generating mechanisms as per De Marco and Pejcic (2000). Again, we stress that calibrating the sensor voltage to a theoretical (model-determined) aFe^{3+} requires an assumption that the sensor signal induced by Fe^{3+} ions present in the modified surface layer of the Fe-ISE, which are interacting with ligands in bulk solution, reflects the aFe^{3+} in bulk solution, which is an unmeasurable property by direct means. That said, the linearity of the sensor to theoretical log[aFe^{3+}] is unmistakable, and thus may prove useful in studying, e.g. the ligand-pool of a sample. So, while we hesitate to use the specific mV/dec slope to read too much into the sensor's potential-generating mechanism, it is reassuring that the slopes as related to aFe^{3+} are consistent and reproducible, even in vastly differing media.

It should be noted that the speciation model used to calculate aFe^{3+} for the B5 seawater calibration curves in Figure 2.3 does allow for the precipitation of solids. When precipitation was not included in the model, aFe^{3+} outputs lead to a less linear calibration, and a calibration slope almost 5 times larger – in poor agreement with all past calibrations of this type of electrode. As we move toward modified seawater solutions with higher concentrations of EDTA, however, the inclusion of precipitation appears to generate less accurate values of aFe^{3+}. With our highest EDTA concentrations, A1 seawater calibration curves look most linear and show the best agreement with characteristic Fe-ISE calibration slopes when aFe^{3+} is calculated *without* any inclusion of precipitation. Figures 2.4 and 2.5 compare the calibration curves for A1 and B5 systems based in Pupcycle seawater, utilizing both types of models (precipitation and no-precipitation) for each modified seawater system.

In summary, a functional Fe-ISE calibration must use an appropriate model to estimate aFe^{3+}. A calibration slope established in B5, A1, etc. is only functional if the intercept of the calibration function does not shift when the sensor is moved from the calibration medium into natural seawater. A typical sensor voltage for a natural seawater sample is around -250 mV

(discussed below), resulting in a calculated log[aFe^{3+}] of -25.1 using the B5 system (with precipitation) or -24.8 using the A1 system (without precipitation). This level of agreement across different calibration systems is highly encouraging. Figure 2.6 displays the compiled calibration trendlines for A1 and B5 modified seawater systems utilizing both models, as well as that of the artificial calibration solution from Maric et al. (2015) for comparison. We highlight the observed range of voltage and expected Fe-activity for measurements of unmodified seawater to emphasize the agreement between A1 (no-precipitation) and B5 (precipitation) calibrations in this region, especially as related to the other calibrations. We also note the calibration voltage and log[aFe^{3+}] ranges spanned by these two calibration solutions to show that natural seawater measurements fall well within the range of a B5 calibration, while calibrating to A1 seawater would require significant extrapolation. Thus B5 modified seawater is perhaps a more reliable calibration system.

Acidimetric Titrations as Speciation Model Validation

The various modified seawater systems and corresponding speciation models can be further validated by examining the Fe-ISE signal over a wide range of pH during an acidimetric titration. In Figures 2.7 and 2.8, we examine the same Fe-ISE calibrations in A1 and B5 Pupcycle seawater from Figures 2.4 and 2.5, now displayed as plots of log[aFe^{3+}] vs pH. Colored data points represent the measured calibration standards. Black lines show modeled log[aFe^{3+}] values which were calculated using the two speciation models over the range of pH, either including precipitation (dotted lines) or assuming no precipitation (dashed lines). Measured voltages are converted to the colored log[aFe^{3+}] points using the calibration slopes from the optimal speciation model for each seawater system (precipitation for B5, no-precipitation for A1). Visualizing the data in this way allows us to better observe the effect of pH on a given Fe-chelator system, and how the precipitation of Fe (or lack thereof) would affect the measured signal. Also, the relatively constant voltage-per-aFe^{3+} sensitivity between seawater

systems (Figures 2.4b, 2.5a) despite significant variation in aFe^{3+}-per-pH, and thus voltage-per-pH (Figures 2.6, 2.7) suggests that the Fe-ISE is in fact responding to these unique aFe^{3+} curves and not simply exhibiting a direct response to protons.

The fact that A1 and B5 seawater are best represented by such different models suggests that precipitation is inhibited, at least on the timescales of this experiment, only at high enough concentrations of EDTA. Considering that the vast majority of EDTA in a seawater-based solution will complex Ca and Mg, it appears that the 10 mM addition in A1 modified seawater provides enough excess EDTA for Fe chelation even at higher pH, where Fe-hydroxy precipitation would otherwise remove Fe from solution. B5 seawater lies at the other end of this spectrum, with very low values of aFe^{3+} at higher pH that seem to result from the uninhibited precipitation of Fe-hydroxide and Fe-oxyhydroxide species.

We are able to more directly compare our modified seawater formulations to one another in Figure 2.9, which displays four acidimetric titrations measured on the Fe-ISE as part of one analytical run. Rather than polishing and reconditioning, the Fe-ISE was exposed to a flowing solution of the unmodified seawater at ambient pH between titrations. By keeping the Fe-ISE conditioned in this way, we limit changes to the standard electrochemical potential of the sensor, and we are able to better compare the titrations to one another in terms of their absolute potential. Here we observe titrations of three modifications of Scripps pier seawater, and a titration of the unmodified Scripps pier seawater itself.

The initial takeaway from these curves is that the Fe-ISE is in fact capable of distinguishing between seawater samples based on this type of pH-related signature. The unmodified seawater curve contains multiple inflections that are likely related to the acid-base properties of the natural ligand pool. These features may be of some use in identifying the dominant Fe-binding species, especially with a higher resolution of Fe-ISE measurement points. In comparing the unmodified seawater curve to those of the modified seawater, it appears that between pH 5 and pH 8, the major control on Fe activity is the total Fe in the seawater, where

more Fe = higher measured potential. Below pH 5, it may be that total Fe-chelator becomes more consequential, such that more EDTA = lower measured potential. But it is difficult to say definitively without greater pH-point resolution and additional modified seawater variations.

As we further examine the modified seawater data in Figure 2.9, it is again helpful to reference modeled aFe^{3+} curves, visible in Figure 2.10a (precipitation) and Figure 2.10b (no precipitation). As mentioned earlier, B5 and B4 seawater follow their precipitation-inclusive modeled curves fairly well, with a potential/pH slope steepening around pH 6.5, and an overall measured potential range that implies a drop of over 10 orders of magnitude in aFe^{3+} (based on a characteristic Fe-ISE calibration, Figure 2.6). Although, it is worth noting that the drop in potential from pH 7 to pH 9 is not as perfectly linear as their models (Figure 2.10a) would imply, with features around pH 8 perhaps indicating kinetic limitations not included in the model. The strong overall convergence of B5 and B4 seawater however, especially at higher pH, is in agreement with the model (Figure 2.10a) and suggests that aFe^{3+} is largely precipitation-controlled.

The A2 seawater titration on the other hand appears to share notable features with both the precipitation-inclusive model *and* the precipitation-free model. As in A1 seawater (Figure 2.7), the measured A2 seawater potential is essentially unchanged from pH 4.5 to pH 7 (Figure 2.9) – in excellent agreement with calculations of aFe^{3+} that assume no solid formation (Figure 2.10b). But above pH 8, A2 seawater potential drops sharply, eventually converging with B5 and B4 seawater at the highest pH point. Thus, the overall potential range does seem to imply precipitation, but it seems that the increased EDTA as compared to B5 and B4 seawater is enough to stave off that precipitation until a slightly higher pH point. In conclusion, while the incorporation of a pH titration provides a new dimension to the sensor's interaction with seawater, interpreting the voltage over a broad pH range may require the inclusion of kinetic processes rather than the binary choice of "complete precipitation" and "no precipitation" currently available in the thermodynamic model.

Because we do not know the acid-base properties of the dominant Fe-chelators in our natural Scripps pier seawater, we are unable to precisely model Fe-speciation and aFe^{3+} over the full pH range of our unmodified seawater titration. However, the NICA-Donnan model has emerged as a promising method to estimate the effect of pH on Fe-binding by marine DOM, assuming binding by phenolic- and carboxylic-like functional groups with established ion-binding constants and pK_a values (Milne et al. 2001, 2003). Here, we use the NICA-Donnan model to compare aFe^{3+} values to our Fe-ISE measurements (see **Experimental**). Total Fe for the speciation model was input as 6.1 nM, as measured by FI-CL for this sample, while total DOC was set to 75 μM, a typical value measured at Scripps pier at the time of year this seawater was collected (December). We convert titration points to aFe^{3+} by calibrating to the model which assumes no solid formation. This calibration curve exhibited improved linearity and a sensitivity (~27 mV/dec) in better agreement with characteristic Fe-ISE slopes than our calibration using the precipitation-inclusive model (Figure 2.11a vs Figure 2.11b). Figure 2.12 shows the unmodified seawater titration curves, with the colored points representing our measured data, and the black dashed/dotted lines showing model aFe^{3+} outputs.

It is immediately clear that the assumption of complete precipitation generates a model lacking many of the features visible in the measured curve. This model suggests that solid formation is limiting aFe^{3+} all the way down to pH 5, and that the 75 μM DOC does not provide strong enough Fe-binding to alter Fe solubility. The precipitation-free model does predicts the major feature observed by the sensor over the full pH range, but with a clear offset in aFe^{3+} based on any of the calibrations determined in modified seawater (Figure 2.4b, 2.5a). Calibrating the sensor to the NICA-Donnan model as shown in Figure 2.12 produces an electrode slope of 27 mV/dec (Figure 2.11a), similar but slightly higher than the calibrations in modified seawater. Again, this is likely a scenario where the optimal model lies between these two end-members. As the seawater aliquots were only left at pH for a day, we may be observing only a fraction of the “full precipitation” that this chemical equilibrium model assumes. It may be

that NICA-Donnan DOM alone cannot fully explain observed Fe activity over the full pH range, and the incorporation of stronger organic ligands is necessary to increase Fe solubility. While our model DOC concentration input was only an estimate based on recent measurements at Scripps pier, realistic differences in DOC totals only marginally affect aFe^{3+} ranges, and do not change the major features of the $\log(aFe^{3+})$/pH curve when comparing models which either include or exclude precipitation (Figure 2.13). Thus, even with differing total DOC, the titration's agreement with the features of the no-precipitation model is compelling. Although we note that the aFe^{3+} offset compared to the models of the modified seawater solutions emphasizes the difficulty in attempting to quantify these very low aFe^{3+} values rather than just their trends.

Potentiometric Titrations to Analyze Natural Seawater

While visualizing Fe activity over a range of pH has predominately been used for model-validation thus far, we now examine how these curves may be used as an analytical tool for the assessment of seawater Fe-speciation. We plot $\Delta\log[aFe^{3+}]$-vs-pH for four unmodified seawater samples in Figure 2.14. Measured voltage is converted to aFe^{3+} using a B5 modified seawater calibration (Figure 2.5a), and $\Delta\log[aFe^{3+}]$ is calculated as the difference from the lowest measured $\log[aFe^{3+}]$ point. We focus specifically on pH 5 – 10, as it represents the properties of the Fe-chelator pool most relevant to natural seawater. Although we note that these titrations did extend below this pH range, so the smoothed fit line connects to additional points where applicable. It should also be noted that these curves were not generated as part of one run, as in Figure 2.9. These were measured over the course of several months, with instances of Fe-ISE polishing and reconditioning between each titration. Thus, the standard electrical potential of the Fe-ISE likely shifted slightly from titration to titration, and we should assume some offset between these curves. But, as we will see, it is the relative shape of the curves, rather than their absolute potentials, that appear to have analytical value.

Measured Fe totals for these seawater samples are listed in Table 2.1, determined by FI-CL (see Experimental section). However, also relevant is the time a given sample sat before it was measured on the Fe-ISE, which is noted in the legend of Figure 2.14. The light green and dark green data points represent two titrations of the same bulk volume of filtered Scripps pier seawater, with one titration (dark green) immediately after water collection, and the other (light green) after the water had sat in a carboy at room temperature for 3 months. The brown data is a titration of *unfiltered* Scripps pier seawater, analyzed immediately after collection. The light blue data was a titration of offshore, low Fe seawater which had been collected over a year prior to its measurement on the Fe-ISE, also stored in a carboy at room temperature until analysis.

All titrations display very similar curves from pH 6 to 7, with Fe-ISE potential decreasing about 1 log[aFe^{3+}] unit over this single pH unit. At a pH of just about 7.3, a divergence from this slope is apparent in each sample, the magnitude of which differs from sample to sample. The unfiltered seawater shows the largest inflection, with very little change in log[aFe^{3+}] to the next titration point at pH 8.2. The two filtered pier seawater samples display comparable features, though to a lesser extent (still with decreasing log[aFe^{3+}]), and certainly distinct from one another. The aged, offshore seawater titration exhibits no inflection at all, forming one continuous curve over this entire pH range.

The magnitude of this feature, or its absence, in this pH 7.5 – 8.5 region, is likely related to the Fe-speciation of the seawater sample. The relative Fe-ISE potentials do seem to be somewhat correlated to the total Fe measured in each sample (Table 2.1). The unfiltered seawater obviously had the highest total Fe, and the offshore seawater had the lowest by far, with the filtered pier seawater samples in-between. This makes sense especially if we assume our 3-month aged filtered pier sample may have lost Fe relative to the fresh sample, perhaps due to wall loss or precipitation (all samples were stored unacidified). But this does not fully explain why the measured potential differences are most stark around pH 8, and not in lower pH regions.

Where we see these inflections, we may be observing the presence of some Fe-binding species that is limiting precipitation at higher pH points. Such natural chelators may not retain much ability for Fe complexation below environmental pH, which would explain these curves' convergence below pH 7. If these species were susceptible to photo- or bio-degradation, or formed larger colloids, it might result in a loss of Fe to precipitation as the seawater sample ages (compare the "Pier filtered" curves, Figure 2.14). The smooth titration curve of the offshore seawater indicates a sample where pH is the major control on aFe^{3+}. Either due to its age or its oligotrophic origin, there is likely very little organic matter to interact with Fe in a way that affects aFe^{3+}. In our fresher, coastal water however, we may be observing enough of an Fe-chelator to keep Fe in solution and raise the relative Fe activity at seawater pH. In terms of the chemical speciation models we have been discussing, this would be the equivalent of moving from the precipitation-inclusive model toward a precipitation-free model, at least in this pH 7.5 – 8.5 region.

In any case, this type of potentiometric titration is quite promising as an analytical technique. Unmodified seawater samples certainly have enough natural variation to be distinguished by the Fe-ISE, both in the context of a pH titration as well as at ambient seawater pH. The sensitivity to sample changes over time suggest the Fe-ISE may even be useful in studies of kinetic processes. Increasing the resolution of pH points in a titration would further elucidate the intricacies of the acidimetric curve. With an improved understanding of the time-dependence of pH-related changes to Fe-speciation, a completely automated titrator could be devised which would provide a fully continuous aFe^{3+}/pH curve, involving continual additions of small volumes of acid. A rotating disk electrode system, rather than the CFA, could be employed to minimize sample volume while still cleansing the electrode diffusion layer (De Marco and Pejcic 2000, Zirino et al. 2002).

Conclusion

Here, we have presented an improved seawater-based calibration system for the Fe-ISE. This matrix, filtered seawater spiked with 10 µM $FeCl_3$ and 100 µM EDTA, produces calibration slopes of ~25 mV/dec as related to modeled values of aFe^{3+}. Additionally, being a seawater matrix, it imparts no change to the standard electrochemical potential of the Fe-ISE as compared to natural seawater, which *has* been observed with more artificial calibration systems likely due to their inability to assimilate the $MgCl_2$ scaling phenomenon noted in surface studies of CFA seawater aged electrodes. We recommend that this modified seawater system be used for all Fe-ISE calibrations. However, if measurements of DOC are available, natural seawater aFe^{3+} appears to be well-modeled with the inclusion of NICA-Donnan Fe-binding organic matter, in which case this unmodified seawater system may be an ideal calibration system. With any calibration system, we emphasize that although aFe^{3+} does not represent any real fraction of Fe, being able to relate measured Fe-ISE potential to this value so consistently does allow for excellent quantification of the theoretical thermodynamic nature of the Fe system and Fe-binding ligand pool.

We see that the Fe-ISE is responding not simply to pH, but to the effects of pH on the Fe-system. We show that chemical speciation models are in the best agreement with Fe-ISE-measured aFe^{3+} in situations where precipitation of Fe species can be assumed to have fully occurred, or where precipitation is completely prevented by acidic pH or by high concentrations of a strong ligand. Systems that lie in between these two endmembers, likely due to kinetic effects, are more difficult to model. Natural seawater appears to fall in this category, at least when modeled with NICA-Donnan DOM as the only organic Fe-chelator, suggesting that chemical speciation models alone may not be enough to truly quantify ambient Fe activity.

We present the first Fe-ISE potentiometric pH titrations of natural seawater samples, which illustrate that the generated aFe^{3+} vs pH curves can be valuable tools for seawater

analysis. We show what appears to be a time-sensitive feature in these curves around ambient seawater pH, which likely indicates the presence of a somewhat transient organic ligand pool serving to increase Fe solubility and overall Fe activity in fresh as opposed to aged samples. A greater resolution of pH points, or a completely continuous acidimetric titration, would better reveal the details of the Fe-binding and acid-base properties of the natural ligand pool. The relative ease of these measurements in comparison to the current techniques for assessing Fe-speciation (CLE-AdCSV) would greatly facilitate studies of the effects of ocean acidification on Fe chemistry and biological uptake, especially in relation to changing ocean conditions such as temperature or solar irradiance. Additionally, there are perhaps some kinetics experiments that could be imagined which are well-suited to the Fe-ISE given its sensitivity to the dynamic nature of seawater Fe-speciation.

Importantly, these results also show that there is indeed enough variation in potentiometrically-measured Fe activity at ambient seawater pH for the Fe-ISE to be used for in-situ oceanographic analysis. Chapter 3 will discuss such measurements.

Acknowledgements

This chapter, in part, is currently being prepared for submission for publication of the material, Fenton, Maxwell; Barbeau, Katherine; Martz, Todd. The dissertation author will be the primary author. All work was supported by grant NSF OCE 1924386. We would like to thank Abigail Severance, Minerva Padilla-Villa, and the trace metal team on the Pupcycle II cruise for their help with bulk trace metal clean water collection.

Figures and Tables

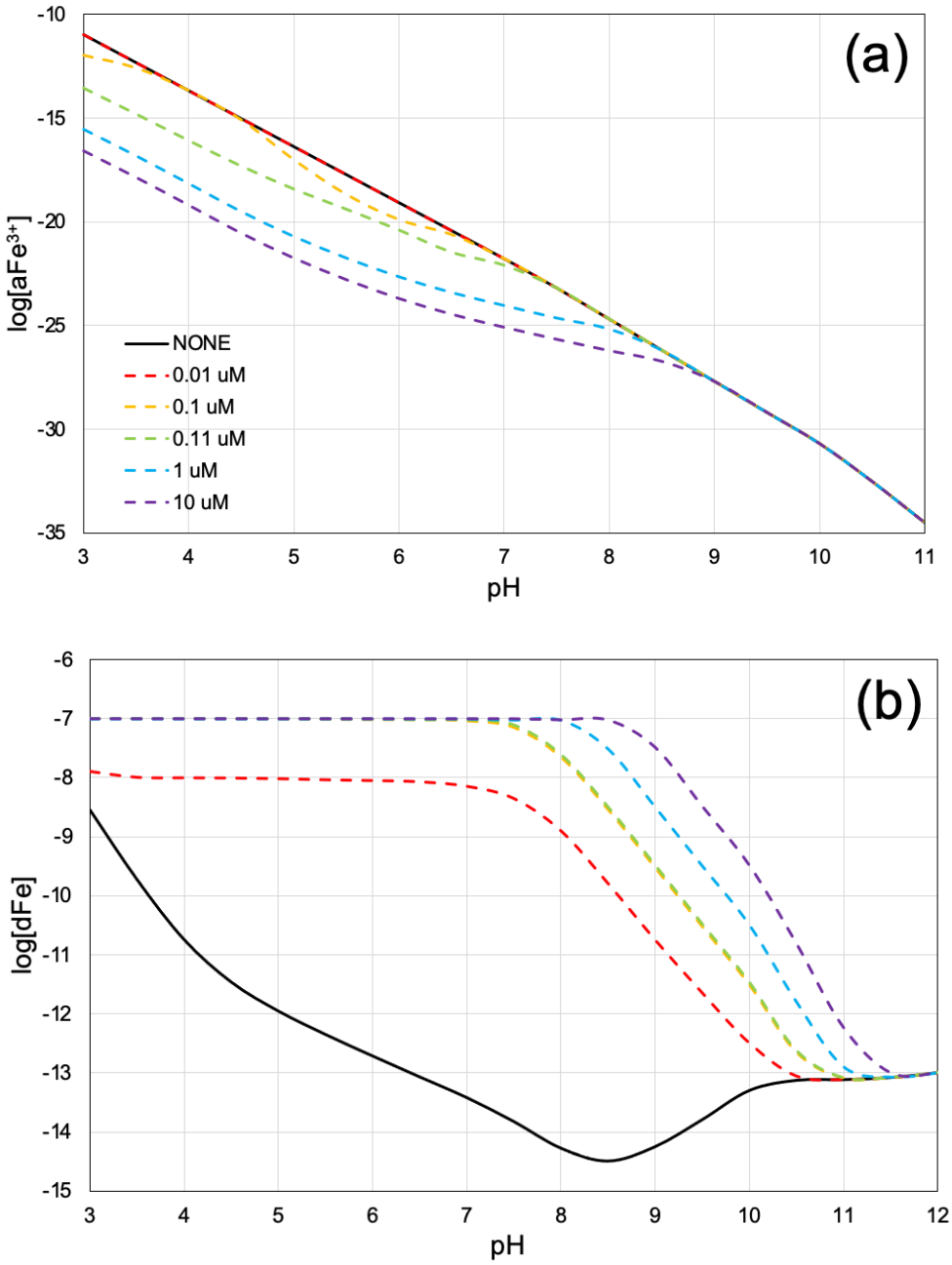

Figure 2.1: (a) Modeled aFe^{3+} in seawater over a range of pH, with varying DTPA, a strong Fe chelator (log K_{Fe} = 31.22). (b) Modeled total dissolved Fe for the same DTPA concentrations. Models made in Visual MINTEQ. Total Fe = 100 µM. For other seawater model inputs, see **Experimental**.

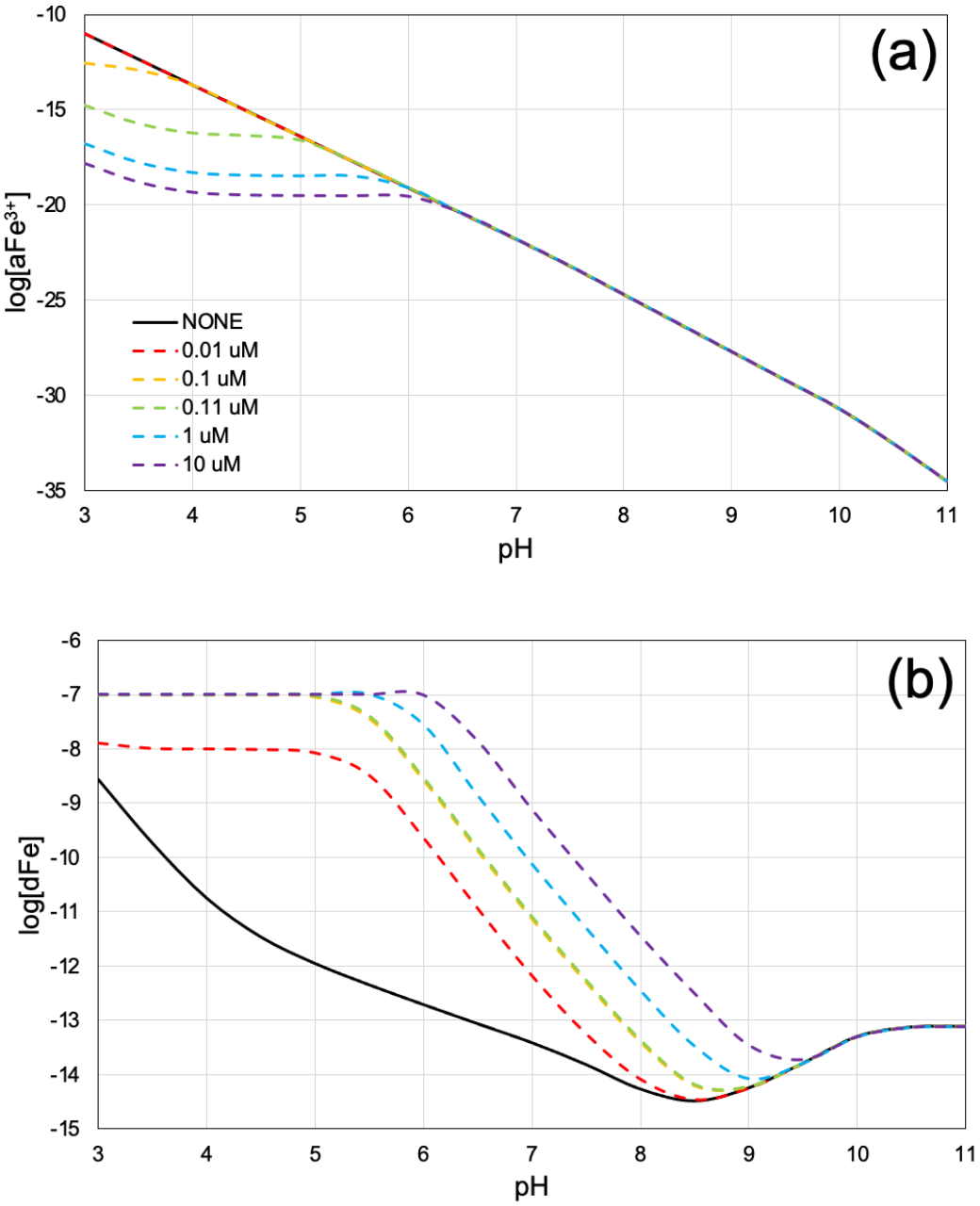

Figure 2.2: (a) Modeled aFe^{3+} in seawater over a range of pH, with varying EDTA, a strong Fe chelator (log K_{Fe} = 27.66). (b) Modeled total dissolved Fe for the same EDTA concentrations. Models made in Visual MINTEQ. Total Fe = 100 µM. For other seawater model inputs, see Experimental section.

Table 2.1: Ambient total dissolved iron (dFe) for all seawater samples used in this work, as measured with in-house FI-CL methods.
†Collected at 31.5398°N, -122.5289°W
‡Collected at 39.2479°N, -124.1610°W
Sample filtered directly **after acidification to pH 1.8, and analyzed immediately thereafter.*

Seawater Sample	dFe (nM)
Scripps Pier	6.10 ± 0.28
P2402 Offshore†	0.18 ± 0.03
Pupcycle Offshore‡	0.13 ± 0.01
Pier Unfiltered	27.95 ± 7.76*

Table 2.2: Modified seawater formulations for Fe-ISE calibrations and acidimetric titrations

Seawater Label	Added Fe	Added EDTA
A1	10^{-4} M	10^{-2} M
A2	10^{-4} M	5×10^{-3} M
B4	10^{-5} M	5×10^{-4} M
B5	10^{-5} M	10^{-4} M

Table 2.3: Input concentrations for all ionic components used in all Visual MINTEQ chemical speciation models for seawater and modified seawater.

Ion	Concentration (M)
Cl^-	0.56
Cu^{2+}	9.9×10^{-10}
Na^+	0.48
Br^-	8.4×10^{-4}
B^{3+}	4.8×10^{-4}
Ca^{2+}	0.01
CO_3^{2-}	0.00238
Co^{2+}	2.5×10^{-9}
F^-	7.1×10^{-5}
Mg^{2+}	0.0546
Mn^{2+}	2.3×10^{-8}
MoO_4^{2-}	1.5×10^{-9}
NO_3^-	1×10^{-4}
PO_4^{3-}	1×10^{-5}
K^+	0.0103
Si	1.25×10^{-5}
Sr^{2+}	6.38×10^{-5}
Zn^{2+}	4×10^{-9}
Fe^{3+}	*varying*
EDTA	*varying*

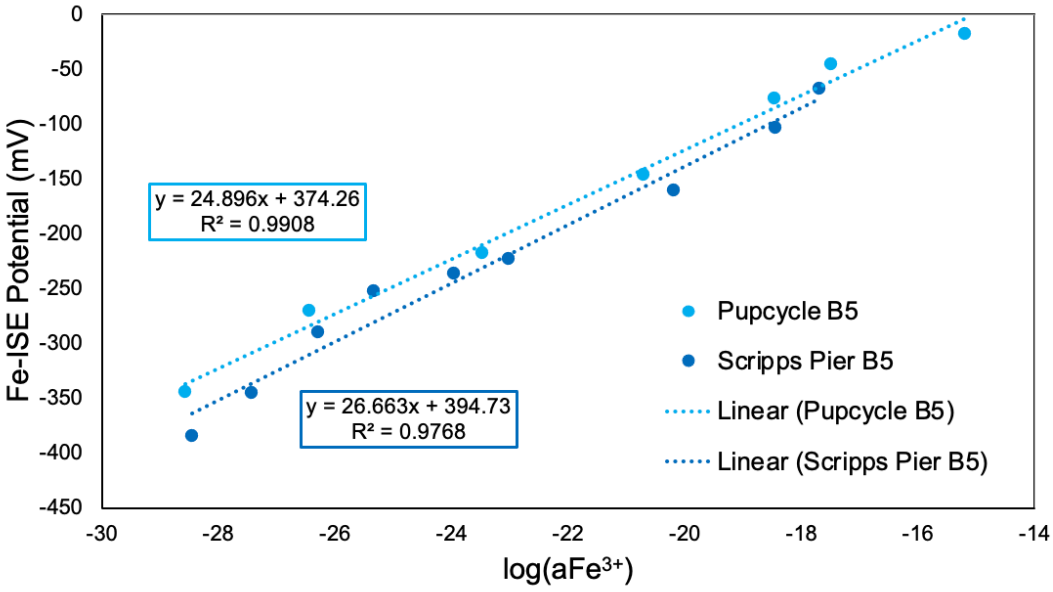

Figure 2.3: Calibration curves and linear regression data for Fe-ISE calibrations in B5 modified seawater from Pupcycle II (light blue) and Scripps pier seawater (dark blue).

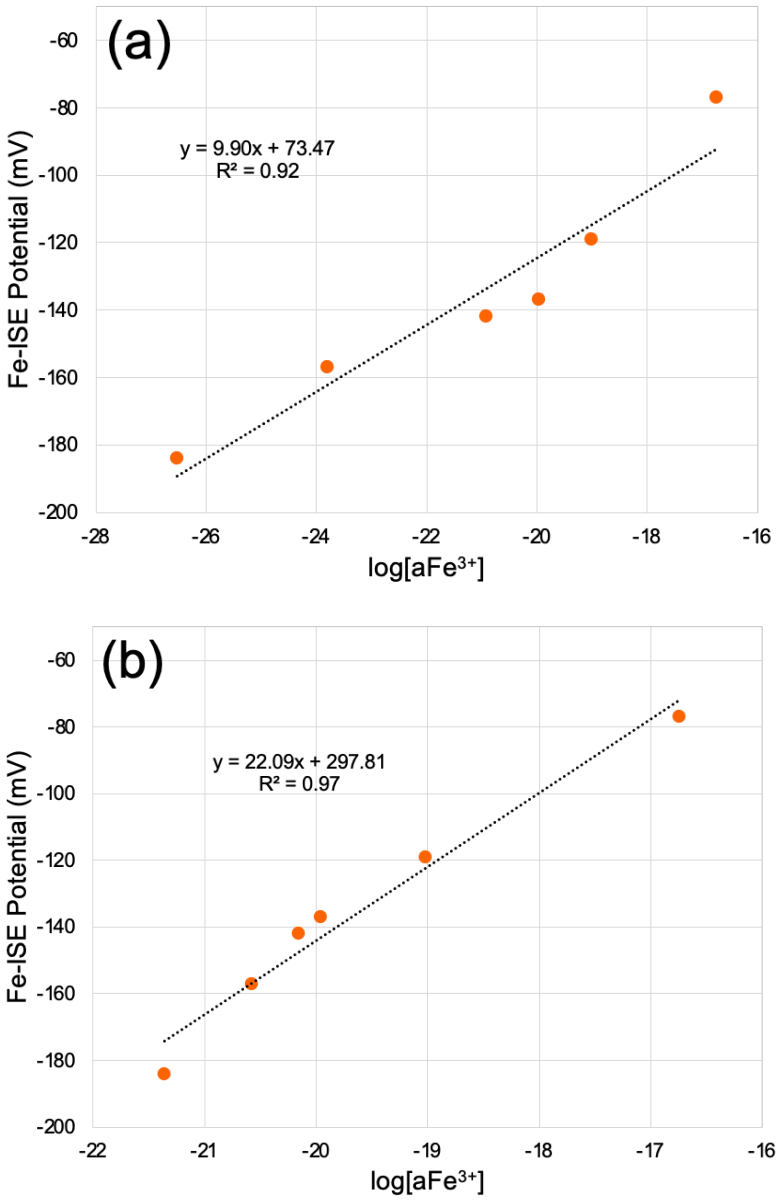

Figure 2.4: Calibration curves and linear regression data for a calibration in A1 modified seawater based in Pupcycle II seawater, with aFe^{3+} values calculated using speciation models which either assume solid precipitation (a) or assume no precipitation (b).

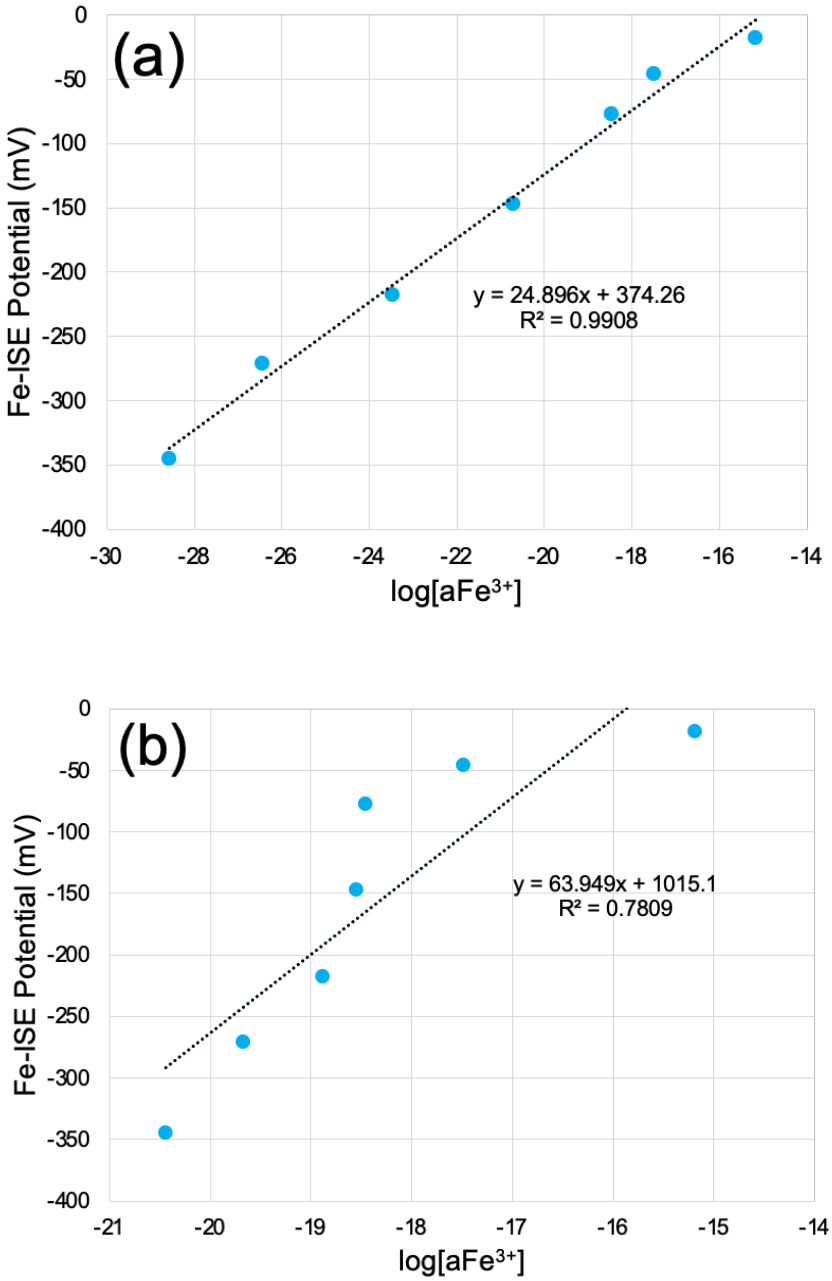

Figure 2.5: Calibration curves and linear regression data for a calibration in B5 modified seawater from Pupcycle II seawater, with aFe^{3+} values calculated using speciation models which either assume solid precipitation (a) or assume no precipitation (b).

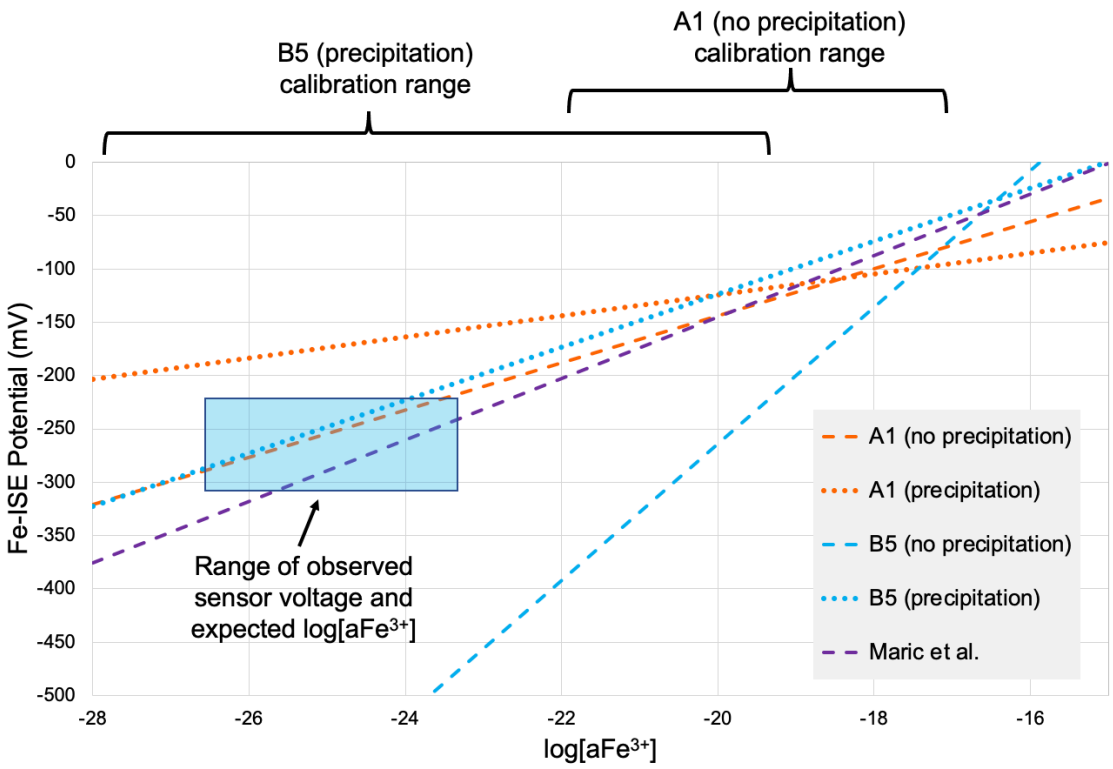

Figure 2.6: Compiled calibration trendlines for A1 and B5 modified seawater modeled both with and without the incorporation of precipitation, as well as the calibration trendline from Maric et al. 2015, the most recent study of the Fe-ISE.

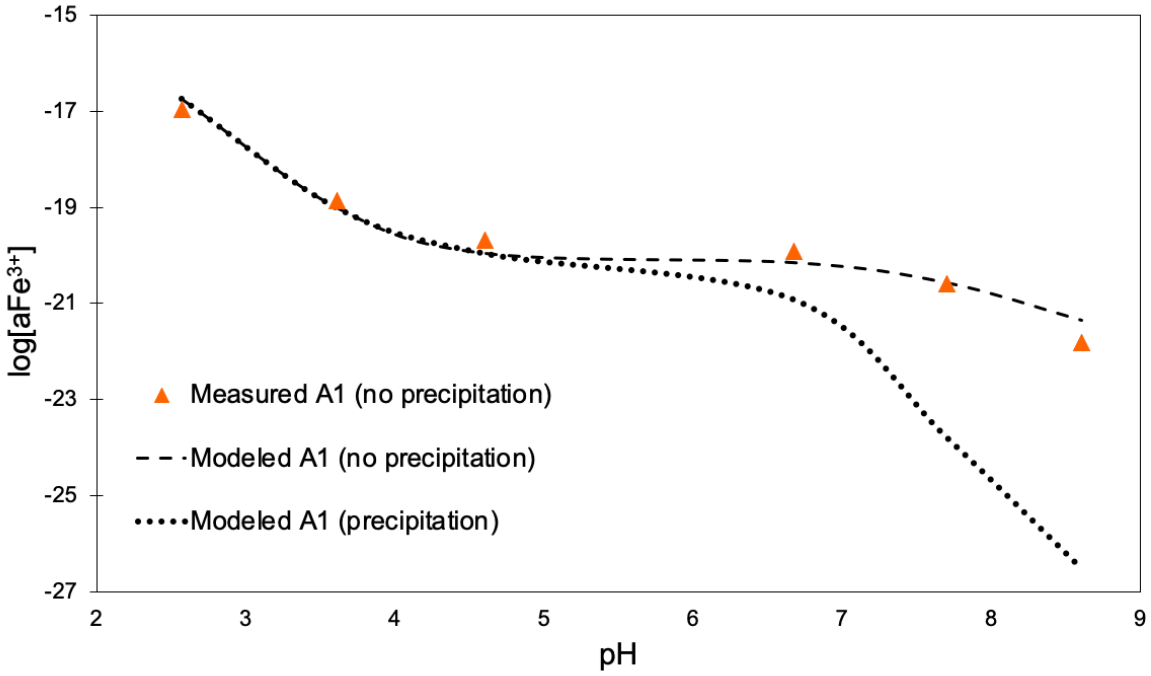

Figure 2.7: Measured log[aFe^{3+}] vs pH curve for the A1 seawater calibration based in Pupcycle II seawater shown in Figure 4 (colored data points), compared to aFe^{3+} calculated by two aqueous speciation models (dashed/dotted lines).

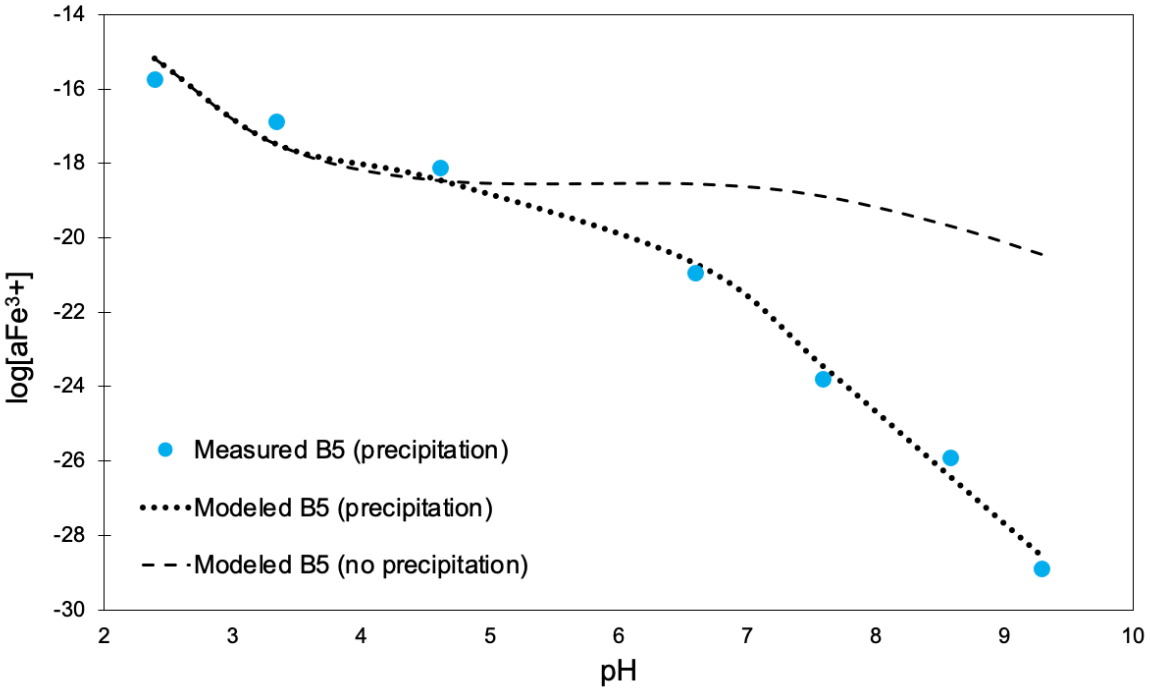

Figure 2.8: Measured log[aFe^{3+}] vs pH curve for the B5 seawater calibration based in Pupcycle II seawater shown in Figure 5 (colored data points), compared to aFe^{3+} calculated by two aqueous speciation models (dashed/dotted lines).

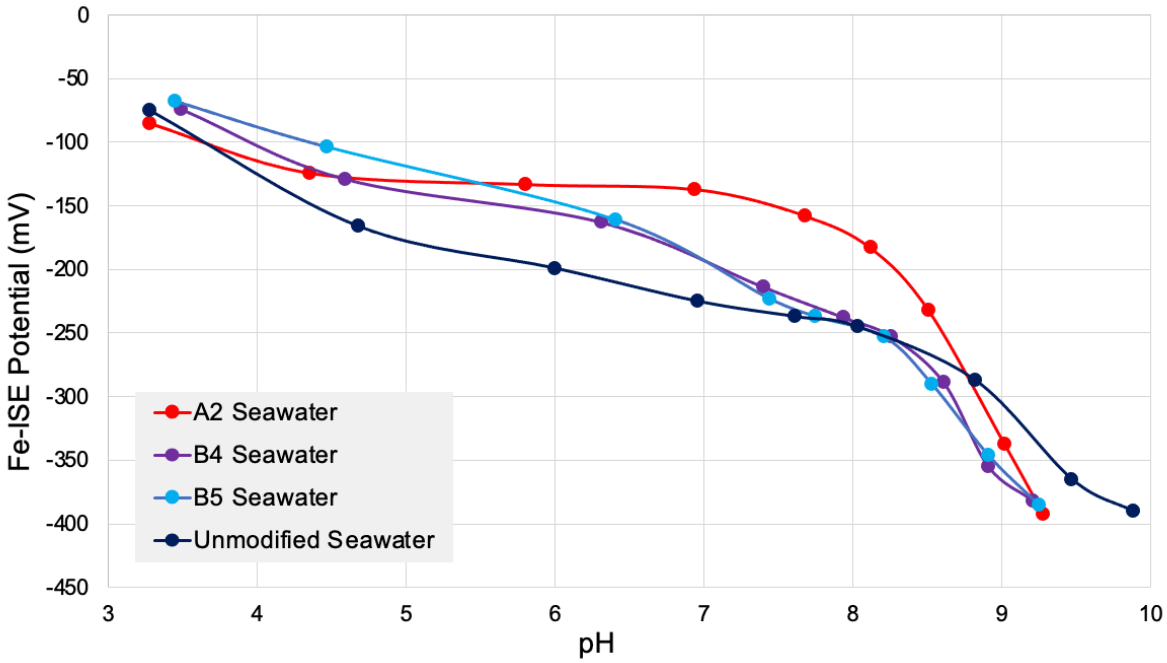

Figure 2.9: Measured Fe-ISE potential vs pH curves for titrations of filtered Scripps pier seawater with varying Fe and EDTA additions (see Table 2.2).

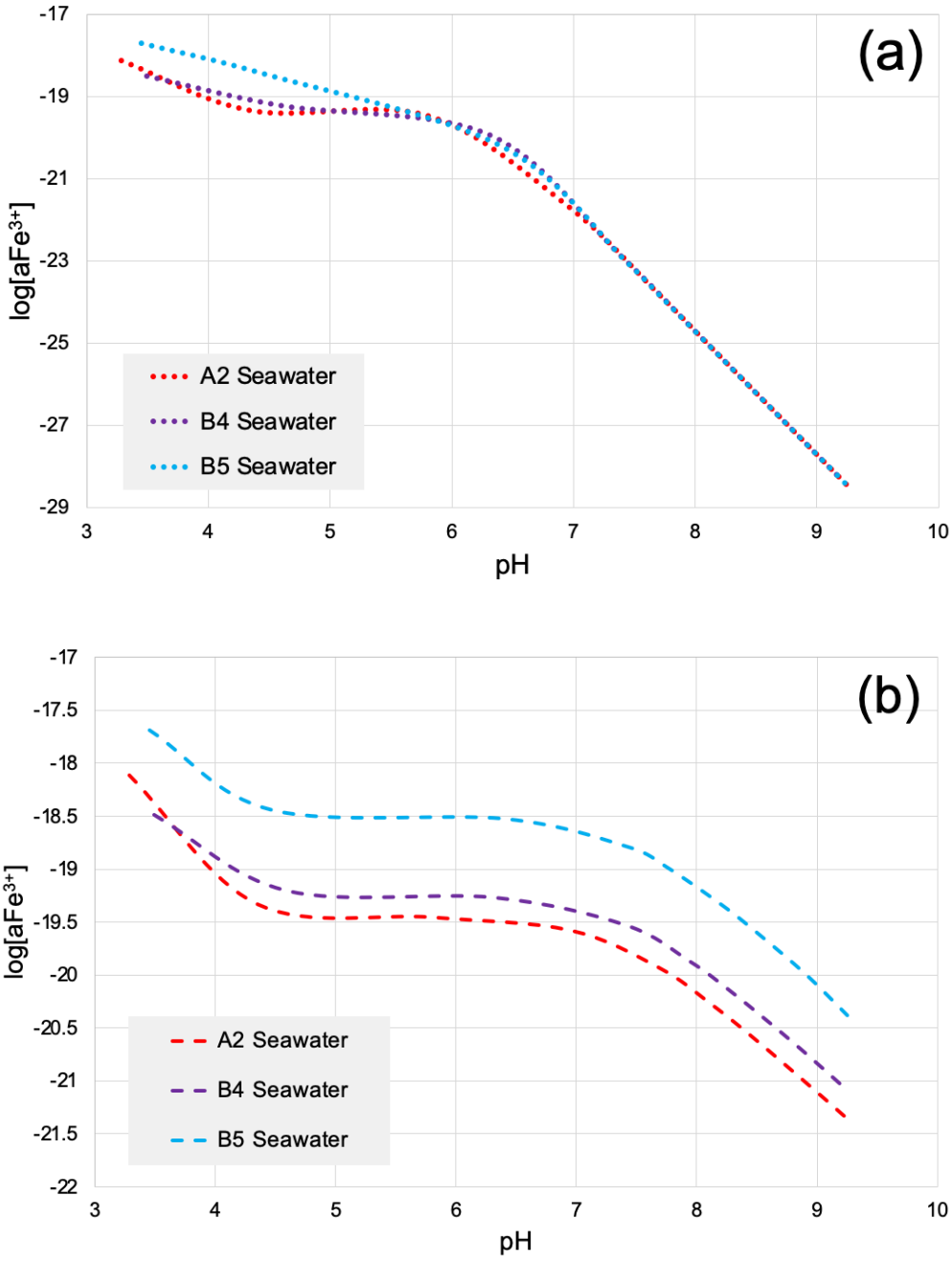

Figure 2.10: Modeled aFe^{3+} vs pH curves for three formulations of modified filtered Scripps pier seawater, utilizing speciation models which either assume precipitation (a) or no precipitation (b).

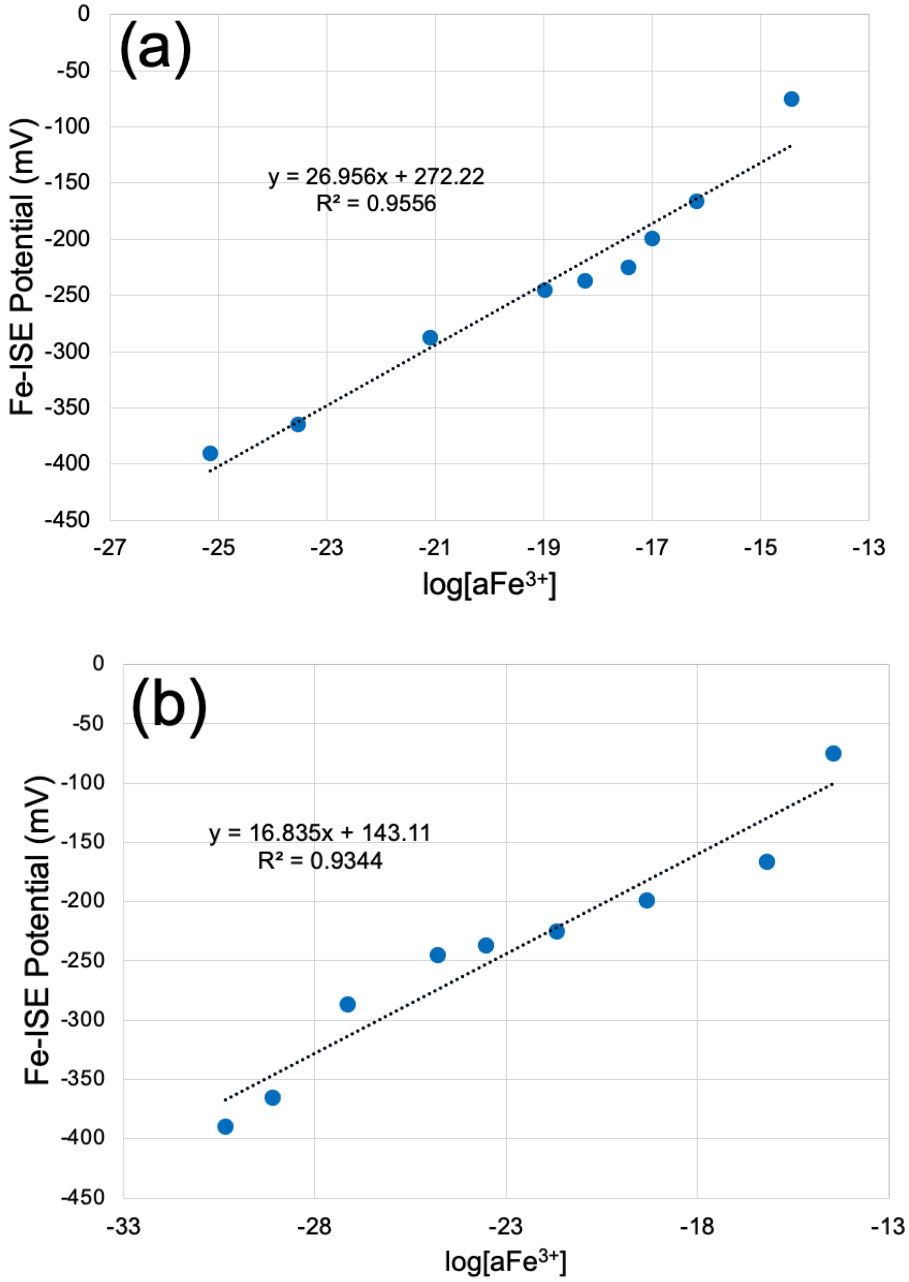

Figure 2.11: Calibration curves and linear regression data for a calibration in unmodified Scripps pier seawater, with aFe^{3+} values calculated using speciation models incorporating NICA-Donnan Fe-binding DOM, which either assume no precipitation (a) or assume precipitation (b).

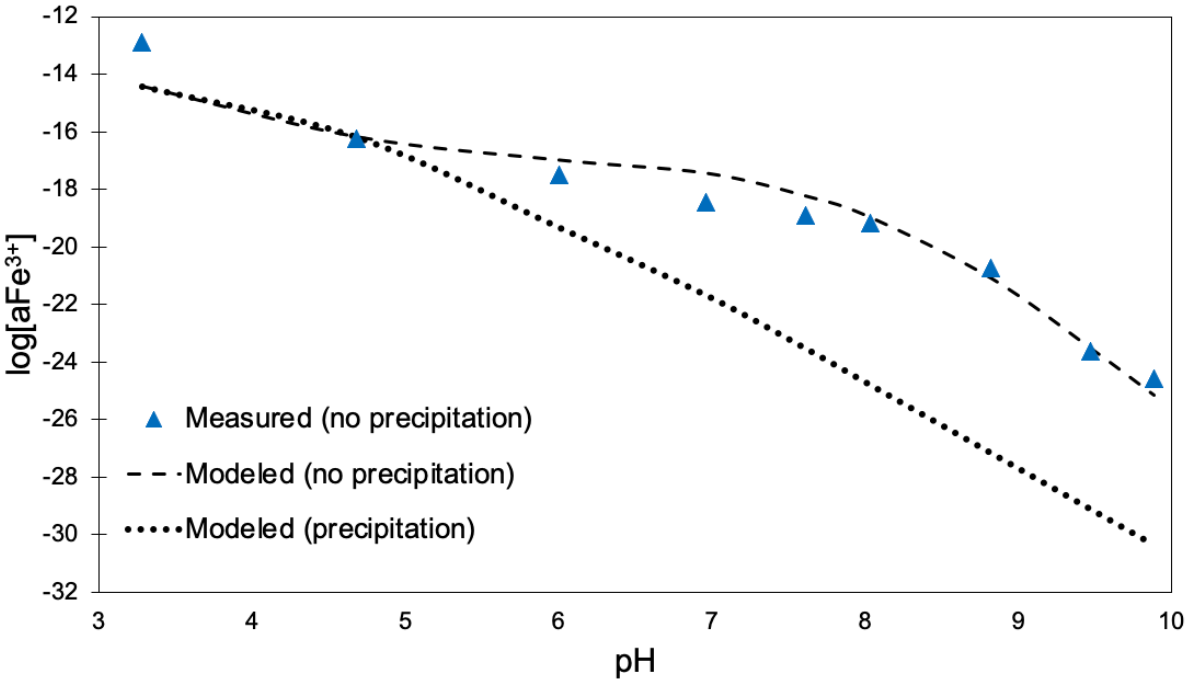

Figure 2.12: Measured log[aFe^{3+}] vs pH curve for unmodified Scripps pier filtered seawater (colored data points), compared to aFe^{3+} calculated by two aqueous speciation models (dashed/dotted lines).

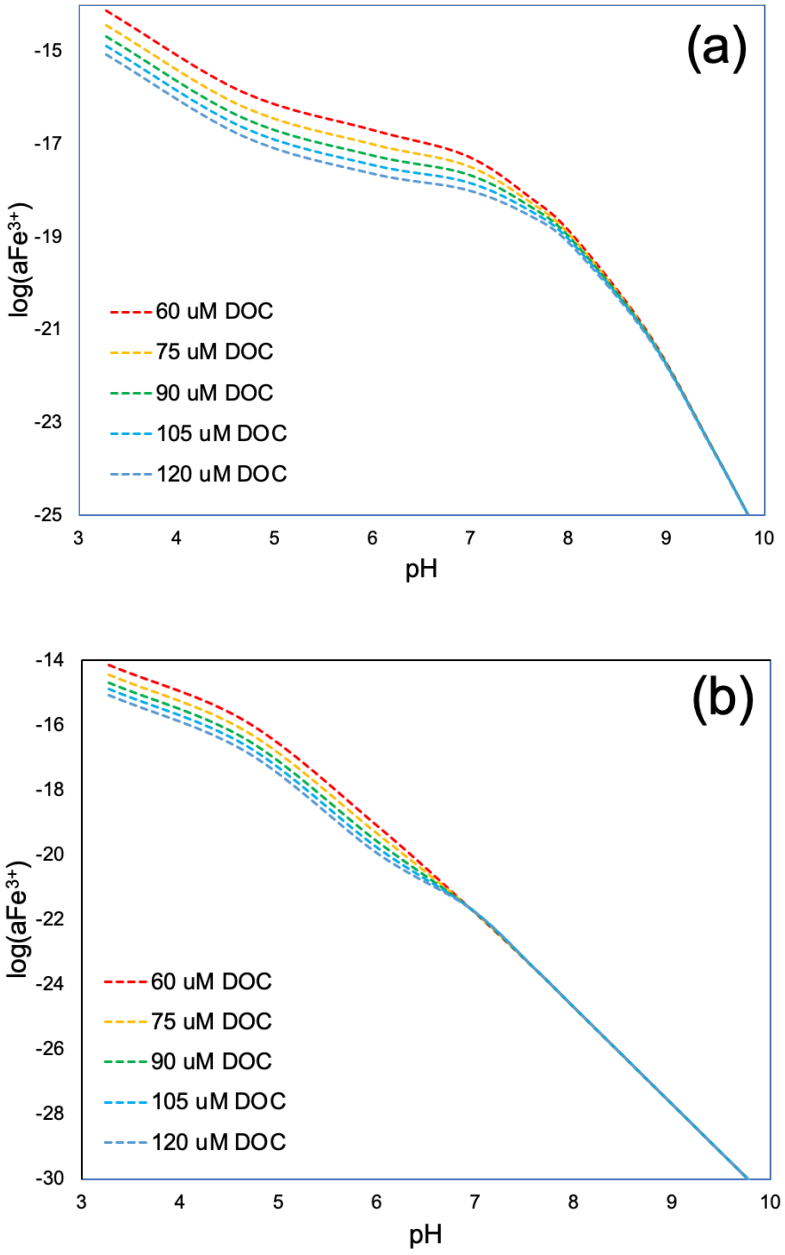

Figure 2.13: Visual MINTEQ speciation models for seawater with 6.1 nM total Fe and varying concentrations of NICA-Donnan DOC over a range of pH, assuming no precipitation of solids **(a)** or assuming precipitation of solids **(b)**. Note different y-axes ranges.

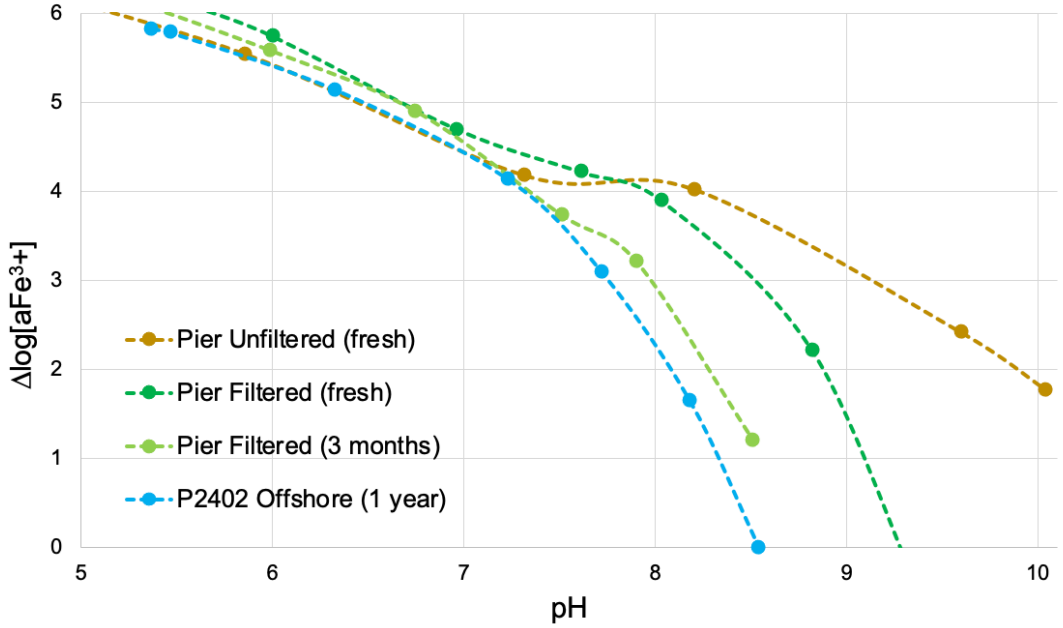

Figure 2.14: Fe-ISE potentiometric pH titrations for four different natural seawater samples. Δlog[aFe^{3+}] represents the difference from the lowest log[aFe^{3+}] measurement. All aFe^{3+} calculated using a B5 modified seawater calibration (Figure 2.5a).

Chapter 3. Fe-ISE Field Measurements of In-Situ Fe-activity in the Eastern Pacific: Surface Transects and Depth Profiles

Abstract

The chalcogenide Fe^{3+} ion-selective electrode continuous flow analyzer (Fe-ISE CFA) is incorporated into a trace-metal clean seawater flow-through system for shipboard measurements of in-situ aFe^{3+}. Surface transects and depth profiles are conducted in several sites off the California and Oregon coast, encompassing nearshore locations as well as regions of coastal upwelling and offshore oligotrophy. Trends in aFe^{3+} are observed in surface transects and depth profiles that coincide with parallel sensor measurements of other oceanographic variables (pH, temperature, salinity, chlorophyll, oxygen) which indicate changes in the water mass. Corresponding samples are analyzed for dissolved Fe and Fe-binding ligand data. Surface gradients in aFe^{3+} are predominantly driven by pH and the associated acid-base properties of the Fe-binding ligand pool, while aFe^{3+} gradients with depth appear to be more dependent on variations between ligand pools of differing Fe-complexation capacities. Fe-ISE measurements of aFe^{3+} appear sensitive to changes in total dissolved Fe only when pH and ligand Fe-complexation capacity are relatively constant. We discuss the added value of the in-situ nature of this Fe activity measurement as it compares to traditional analyses of seawater Fe chemistry. The Fe-ISE proves to be a powerful new oceanographic tool for assessing Fe activity in a way that is passive, efficient, and easy to integrate into existing analytical platforms.

Introduction

Methods for assessing seawater Fe chemistry have expanded considerably since the importance of Fe as a limiting nutrient was first demonstrated in the 1980s (Martin and Fitzwater 1988, Martin and Gordon 1988, Martin 1990, Anderson 2020). The earliest techniques treated

Fe as it would any other chemical nutrient – by measuring the concentration of the total dissolved species to gauge its availability to microorganisms (Worsfold et al. 2014). This dissolved Fe fraction, dFe, is really an operational term, referring to the Fe that passes through a 0.2 or 0.4 μm filter. The sample is then acidified to pH ~1.8 to destroy all Fe-complexation and ensure Fe ions are liberated for analysis, generally by atomic adsorption spectrometry, mass spectrometry, or standardized chemiluminescent reaction (Achterberg et al. 2001, Lohan et al. 2006). While these methods are robust and intercomparable, the total dissolved fraction may not represent in-situ Fe bioavailability as it might for a more abundant macronutrient such as nitrogen or phosphorus. By acidifying dFe samples, we lose information about the Fe-speciation at natural seawater pH, which has been shown to be paramount to the overall chemical activity and biological accessibility of Fe (Anderson and Morel 1982, Millero et al. 1995, Millero 1998).

To probe the organic ligand pool directly and gain information about its Fe-complexation properties, scientists have adopted a voltammetric technique which makes use of a hanging mercury drop electrode. In competitive ligand exchange – adsorptive cathodic stripping voltammetry (CLE-AdCSV), a known added ligand (AL) is allowed to compete with the ambient ligand pool for Fe-complexation (Gledhill and van den Berg 1994, van den Berg 1995, Rue and Bruland 1995). The Fe-AL complex is quantified using stripping voltammetry at a series of increasing dFe points, and the resulting titration curve allows for the derivation of metal complexation parameters of the natural ligand pool. These include the total ligand binding-site concentration [L], non-ligand-bound Fe concentration [Fe′], and the conditional thermodynamic binding constant $K^{cond}_{FeL(Fe')}$ (Omanovic et al. 2015, Mahieu et al. 2024). This method has been able to assess the state of Fe from a different angle than measurements of dFe, with [Fe′] data providing additional insight as to where the most available Fe might be located (Gledhill and Buck 2012, Gerringa et al. 2015, Caprara et al. 2016).

Due to observed biases in derived $K^{cond}_{FeL(Fe')}$ and [L] that seem to scale with dFe in metal complexation models, a more robust parameter appears to be $\alpha_{FeL(Fe')}$ the overall side-reaction coefficient for the natural ligand pool (Town and Filella 2000, Laglera et al. 2013, Gledhill and Gerringa 2017). This value takes into account $K^{cond}_{FeL(Fe')}$, [L], and total dFe to represent the overall excess-ligand binding capacity, or the probability that added Fe will be complexed. Still, Fe-complexation information determined by the CLE-AdCSV method is far from in-situ, with pH generally buffered to a standard value, and equilibration steps that allow time for potential shifts from the natural state of the Fe-chelator system (Gledhill and Buck 2012, Laglera and Fillela 2015, Gerringa et al. 2021).

The chalcogenide glass Fe-ISE has emerged as a promising tool to resolve information about ambient Fe-speciation given its sensitivity to the activity of the free Fe^{3+} ion (Koenig and Grabner 1995, De Marco et al. 1999, De Marco and Mackey 2000). In seawater, this Fe^{3+} activity (aFe^{3+}) is related to the overall Fe-binding capacity of the ligand pool, and has been shown to be well correlated with the accessibility of Fe to microorganisms (Anderson and Morel 1982). The Fe-ISE is capable of passive, continuous, and truly in-situ measurements of marine systems, and has potential as a shipboard instrument or integrated into autonomous sensor arrays. Utilizing the Fe-ISE in such a way would offer a novel, high-resolution perspective into the complex Fe system, and could provide new information regarding the cycling of Fe and its bioavailability to marine organisms.

While there has not yet been oceanographic implementation of the Fe-ISE for in-situ measurements of Fe activity, Zirino and colleagues have employed a Cu-ISE to explore Cu speciation in natural seawater systems. Using a jalpaite Cu-ISE plumbed into to a ship's onboard flow-through system, Zirino measured in-situ free Cu^{2+} activity during several transects through San Diego Bay in 2000 and 2001 (Blake et al. 2004; Zirino and Seligman 2002). Simultaneous onboard stripping analyses provided total and "labile" Cu concentrations for the

same area. While total Cu concentrations rose from 8 nM at the mouth of the bay to 55 nM at the innermost regions, free Cu^{2+} activity had the opposite trend. The apparent paradox was likely due to increased Cu complexation by organic and particulate matter that was more prevalent further into the bay. Zirino also set up the Cu-ISE for stationary, pier-based measurements at Scripps Pier (Zirino et al. 1998). Zirino discovered a significant temporal change in pCu that likely resulted from seasonal swings in local tidal flows, and was able to explain previously observed patterns of biological Cu toxicity. Temporal variations in total Cu concentrations were not nearly of the same magnitude and alone could not explain the toxicity patterns, emphasizing the importance of the extra information provided by an in-situ ISE measurement.

Here, we present the first oceanographic field data collected by an Fe-ISE. Using a trace-metal clean shipboard pumping technique combined with the Fe-ISE continuous flow analyzer (CFA) system, we examine spatial gradients in in-situ aFe^{3+} at several study sites off the coast of California and Oregon. Surface transects are carried out in the northern California Current, a well-studied area where deep water upwelling stimulates seasonal primary productivity. Previous dFe and Fe-ligand studies of this region note significant benthic sources of Fe supplied to coastal surface waters through upwelling, with Fe limitation occurring quickly following a bloom with the sinking of biogenic particles as waters are advected offshore (King and Barbeau 2011; 2007; Hogle et al. 2018, Forsch et al. 2023). Fe ligands vary spatially, generally decreasing in strength further from the shore, yet exhibiting log K minima in the benthic boundary layer (Buck et al. 2007, Bundy et al. 2014, Mellet et al. 2018). We also survey changes in aFe^{3+} with depth by conducting pumped depth profiles in the Southern California Bight. We target the San Pedro Ocean Time-Series (SPOT) site, a well-monitored station in the San Pedro Basin between Catalina Island and the port of Los Angeles, which exhibits seasonal anoxia at depth and associated gradients in pH, salinity, and temperature in the upper water

column (Lie et al. 2013, Haskell et al. 2017). This station is compared to profiles of surrounding coastal waters.

Fe-ISE depth profiles and surface transects are supplemented by parallel sensor measurements of pH, temperature, salinity, chlorophyll, and oxygen. Additionally, dFe and CLE-AdCSV Fe-speciation analyses are carried out on discrete bottle samples to provide further comparison to the trends of aFe^{3+} as determined by the Fe-ISE. Thus, we interpret our novel aFe^{3+} data in the context of a suite of additional oceanographic variables to elucidate the major drivers of Fe activity in different marine systems.

Experimental

In-Situ Fe-ISE and Hydrographic Measurements

The field data discussed in this work were obtained as part of two research expeditions: the Pupcycle II (phytoplankton upwelling cycles) cruise in May/June of 2023 on the R/V Sally Ride, and the P2507 in-situ profiling cruise in March of 2025 on the R/V Robert Gordon Sproul. Both cruises entailed the continuous pumping of seawater through a trace metal clean system (acid-cleaned plastic tubing, Teflon diaphragm pump), for rapid measurement on the Fe-ISE.

The Pupcycle II cruise involved a series of transects over the course of two weeks in the northern California Current, seeking surface gradients in Fe chemistry related to sites of deep-water upwelling and subsequent algal blooms. Locations of each transect site are shown in Figure 3.1. Transects ranged from 15 km to over 100 km in length, the longer transects being carried out overnight. A trace metal clean towed-fish surface sampling system, in conjunction with a high-flow (50 L/min) Teflon diaphragm pump, was used to continuously pump seawater on deck and into a trace-metal van (HEPA-filtered air, metal-free). In the van, the seawater stream was diverted directly into the Fe-ISE CFA system for immediate potentiometric

measurement, and then expelled to a drain as waste. As such, surface water reached the sensor in less than 45 seconds.

In-situ hydrographic data for each transect was obtained simultaneously using the R/V Sally Ride's seawater flow through system, equipped with a thermosalinograph (Seabird SBE-45), fluorometer (Seapoint SCF), and oxygen sensor (Seabird SBE-43). Sea surface temperature was measured using a hull-mounted sensor (STS SEG-14).

The P2507 cruise sought to measure changes in in-situ seawater Fe chemistry with depth. Over the course of the four-day cruise, shallow depth profiles were carried out at four stations in the Southern California Bight (Figure 3.2). Total water column depth at each station ranged from ~1000 m (SPOT) to 400 m (Test Cast, Scripps Canyon) to 80 m (LA Nearshore), but vertical profiles only extended to 80 m at most, given pumping limitations. Similar to Pupcycle II, an on-deck Teflon diaphragm pump was used for continuous pumping of seawater. Plastic tubing was affixed to a weighted, coated wire (Amsteel II) and lowered to depth. Seawater was pumped from each depth into a trace-metal "bubble" in the ship's lab space, where it was plumbed directly into the Fe-ISE CFA system. Given the length of tubing, it took roughly 4 minutes for a given aliquot of seawater at depth to reach the Fe-ISE, and the inlet was held at each depth for an additional 5 to 10 minutes to allow ample time for discrete sampling (detailed below). Thus, while pumping was continuous, plotted data points for Fe-ISE and pH vertical profiles represent sensor measurements when voltage had stabilized for each depth. Pumped profiles rarely continued shallower than 20 m in order to avoid sampling or measuring seawater potentially contaminated by the ship.

Immediately prior to all pumped profiles, hydrographic data were determined for the station with a standard depth profile using the ship's rosette and CTD (conductivity-temperature-depth) system. The rosette was also equipped with a fluorometer (Seapoint SCF) and oxygen sensor (Aanderaa, 3830).

Profiles were conducted at a different station each day. At both the test cast station and Scripps canyon station, only one profile was conducted (at 1000 and 0800 respectively), consisting of a CTD cast followed by a pumped profile which included Fe-ISE analysis as well as discrete sampling for dFe and FeL speciation. At both SPOT and the LA Nearshore station, two profiles were conducted to assess variability throughout the day. The first cast at each station took place at 0800 in the morning, and consisted of a CTD cast followed by a pumped profile with both Fe-ISE analysis and discrete dFe and FeL bottle sampling. The second profile at these two stations took place at 1800 each day, and consisted of a CTD cast and pumped profile for Fe-ISE analysis, but discrete samples were not collected.

To determine if Fe-ISE analyses of bottle samples are comparable to the direct measurement of pumped seawater, additional discrete samples were collected from the morning casts at SPOT and the LA Nearshore station for subsequent analysis on the Fe-ISE. Unfiltered seawater from each depth was collected from the pumped stream in acid-clean 500 mL fluorinated high-density polyethylene (FLPE) bottles, and stored at room temperature for 4 – 5 hours. At the time of analysis, each sample was circulated through the Fe-ISE CFA system until a stable Fe-ISE potential was reached (<0.15 mV/min). The flow-cell containing the thermistor probe was disconnected from the CFA path to prevent contamination of the recirculated sample until an Fe-ISE signal had been obtained, at which point the thermistor cell was reconnected for a temperature reading. Given the multi-hour equilibration time prior to the analysis of each sample, temperature changes were expected to be minimal by that point.

Fe-ISE CFA System and Data Processing

The chalcogenide glass electrode used in all measurements was of the formulation $Fe_{2.5}(Se_{60}Ge_{28}Sb_{12})_{97.5}$ as described in Chapter 1 (Baker and Trachtenberg, 1971). Similarly, all potentiometric electric circuits, as well as the Fe-ISE CFA system itself, were identical to those detailed in Chapter 1. Briefly, the continuously flowing sample stream is exposed to the Fe-ISE,

the Ag/AgCl reference electrode, the glass combination pH electrode, and the thermistor in that order before being expelled to waste. Tubing, connectors, and the flow cells which housed the sensors were all acid-cleaned before use.

Prior to analyses, the Fe-ISE was polished on nylon and micro-cloth pads using an alumina slurry of decreasing particle size (Buehler), and subsequently rinsed with 18.2 MΩ cm^{-1} water. The Fe-ISE was then conditioned in its flow-cell for at least 48 hours with flowing, unfiltered seawater recirculated from a 20 L carboy, which was refilled from the ship's clean seawater system every 4 to 5 hours. A stability criterion of 0.5 mV/hour was used to deem the Fe-ISE conditioned for analysis. This continually replenished seawater was also used to keep the Fe-ISE conditioned between measurements over the course of each cruise.

Fe-ISE potential drift was quantified during Pupcycle II by comparative reference seawater measurements before and after each transect. We do not account for potential drift over the course of the entire Pupcycle II cruise, given an instance of re-polishing and reconditioning mid-cruise. Thus, while *trends* in the Fe-ISE surface transect data as they relate to other oceanographic parameters may be compared between transects, absolute potentials (and associated Fe-activity) will only be interpreted within the context of a given transect. During P2507, drift was assessed throughout the four-day cruise period with daily measurements of a 1 L aliquot of reference seawater recirculated until a stable voltage was reached (generally less than 5 minutes), allowing for intercomparison between depth profiles.

The Fe-ISE was calibrated as described in Chapter 2, utilizing B5 modified Scripps' pier filtered seawater (10^{-5} M Fe, 10^{-4} M EDTA). Values of aFe^{3+} for each calibration standard were calculated using Visual MINTEQ aqueous speciation modelling software. The glass pH electrode was calibrated to Orion pH buffer solutions traceable to NIST standards. Temperature corrections to the Fe-ISE standard potential utilized the temperature coefficient determined in Chapter 1 (-0.82 mV/°C), and corrected measured voltage according to the following equation:

$$E_{corr} = E_{meas} - \frac{0.82mV}{°C} * (\bar{T} - T_{meas}) \quad (1)$$

where E_{corr} is the temperature-corrected potential, E_{meas} is the measured potential, $\bar{T}$ is the mean temperature of the sample set, and T_{meas} is the flow cell temperature at the time E_{meas} was measured. For Pupcycle, $\bar{T}$ represented the mean temperature for each transect. For P2507, $\bar{T}$ represented the mean temperature for the entire cruise dataset.

Final calculation of log(aFe^{3+}) utilized temperature corrections to the Nernstian calibration slope according to the following equation:

$$\log(aFe^{3+}) = \frac{E_{corr} - E°}{\frac{S}{T_{cal,K}} * T_{meas,K}} \quad (2)$$

where $E°$ and S represent the standard potential and slope determined from the Fe-ISE calibration, $T_{cal,K}$ is the temperature in Kelvin at which the calibration took place, and $T_{meas,K}$ is the measured temperature in Kelvin.

For surface transects of the Pupcycle II cruise, Fe-ISE measurements are reported as Δlog(aFe^{3+}); i.e., the difference in log(aFe^{3+}) from the first measurement of each transect. For P2507, because all depth profiles over the four-day period are intercomparable, the reported Δlog(aFe^{3+}) values are referenced to the lowest log(aFe^{3+}) measurement of the entire cruise dataset.

Trace-Metal Clean Seawater Collection

All sampling efforts adhered to the trace-metal clean sampling and bottle-cleaning protocols detailed in the GEOTRACES cookbook (https://www.geotraces.org/methods-cookbook/). On both Pupcycle II and P2507, discrete dFe and Fe-speciation samples were collected from the pumped seawater line for comparison to Fe-ISE measurements. For Pupcycle II, this sampling occurred at various time points throughout most surface transects. For P2507, samples were collected at each depth throughout pumped profiles. In each case,

pumped seawater was diverted from a Teflon manifold/valve system in the trace metal lab space, through an in-line 0.2 µm filter (Acropak 200 capsule, VWR) into acid-clean bottles. Samples for dFe were collected in 30 mL low-density polyethylene (LDPE) bottles, and acidified to pH 1.8 using optima HCl. Samples for Fe-speciation were collected in 500 mL fluorinated high-density polyethylene (FLPE) bottles, and stored frozen at -20°C until analysis.

Laboratory Determination of dFe and Fe-L Parameters of Seawater

All seawater samples were analyzed at Scripps Institution of Oceanography using in-house methods for determination of total dissolved Fe (dFe) and Fe-binding ligand (Fe-L) parameters. Measurements of dFe were made using a flow-injection with chemiluminescence (FI-CL) system based on the manifold by Lohan et al. (2006). Briefly, dissolved Fe is oxidized to Fe^{3+} with 10 mM Q-H_2O_2 (Suprapur grade). An ammonium acetate solution buffers the sample to pH 3.5 in-line, where it is preconcentrated on a chelating resin column (Toyopearl AF-Chelate-650M). The salt matrix is removed, and the Fe is eluted from the column using 0.14 M HCl (Optima grade, Fisher Scientific). The Fe catalyzes a chemiluminescent reaction between H_2O_2 and luminol (Sigma Aldrich), and this luminescence is recorded by a photomultiplier tube (Hamamatsu Photonics). A full description of this method is available in Forsch et al. (2021).

Fe standards were made with an ICP spectrometry standard (TraceCERT, ultra-high purity, in 2% HNO_3) added to Pacific ocean surface seawater to match the sample matrix, to final concentrations of 0, 0.4, 0.8, 3.2, and 10 nM Fe. Standards were measured at the beginning and end of each analytical run, and precision and drift were assessed with replicate analyses of aliquots of a large volume of reference seawater measured throughout each run.

Seawater was analyzed for Fe-binding ligands using single analytical window competitive ligand exchange – adsorptive cathodic stripping voltammetry (CLE-AdCSV), a technique described in depth by Buck et al. (2018), adhering to the best practices outlined in Mahieu et al. (2024). Seawater samples were partitioned into 20 clean and seawater-

conditioned polypropylene vials (50 mL Metal-free, Labcon) and buffered to pH 8.2 using boric acid (Alfa Aesar, 99.99%). Additions of dissolved Fe from 0 to 20 nM were made to the vial set, and allowed to equilibrate with the natural ligands for two hours. After equilibration, salicylaldoxime (SA, Fluka >98% Assay) was added to each titration point at a concentration of 25 µM, for an SA side reaction coefficient of $\alpha_{Fe(SA)_x}$= 115. For each Fe-addition, the electroactive Fe-SA complex was quantified by differential pulse stripping voltammetry using a hanging mercury drop electrode (BioAnalytical Systems Inc.). Sensitivity (S) was determined by the linear portion of the higher-Fe additions of each titration, where natural ligands are assumed to be saturated. A final 5 nM Fe spike was made directly into the analytical cell to assess titration linearity and assure complete ligand saturation (Mahieu et al. 2024).

Resulting peak heights were quantified using ECDSOFT software. Metal complexation parameters including ligand concentration [L], conditional Fe′-ligand thermodynamic binding constants ($K^{cond}_{FeL(Fe')}$), and the concentration of soluble inorganic Fe species [Fe′], were determined using ProMCC software (Omanovic et al. 2015). All samples were fitted to Fe-binding by a single organic ligand to simplify trends among and between datasets.

For a given cruise dataset, we report parameters calculated using a single metal complexation fitting model for consistency, chosen based on minimized uncertainty values. We also report $\alpha_{FeL(Fe')}$, the side reaction coefficient of the excess ligand pool, which is calculated according to equation 1 below:

$$\alpha_{FeL(Fe')} = [L'] * K^{cond}_{FeL(Fe')} \quad (3)$$

where [L′], the concentration of non Fe-bound ligands, is taken as the difference between [L] and dFe (Gledhill and Gerringa 2017).

Results and Discussion

Pupcycle II Surface Transects

We begin by examining data from two shorter (~15km) transects off the coast of Point Blanco, Oregon on the afternoons of May 31st and June 2nd. Figures 3.3a,b and 3.4a,b show the transect paths in red overlayed on sea surface temperature and chlorophyll plots (NOAA Coast Watch), with numbers indicating transect timepoints. Local temperature minima and chlorophyll maxima indicate a productive region of recently upwelled waters; expected given offshore wind events. Figures 3.3c and 3.4c display aFe^{3+} and pH as measured by the Fe-ISE CFA system, as well as temperature, salinity, fluorescence, and oxygen sensor data from the ship's flow-through system, over the course of each transect. Numbers at the top of the time series (Figures 3.3c and 3.4c) correspond to the transect locations labeled in Figures 3.3a,b and 3.4a,b, with point 2 corresponding to a turnaround point with high chlorophyll-a fluorescence, and points 1 and 3 to the beginning and end points of the transect with lower fluorescence

These shorter transects provide good evidence for the basic functionality of the Fe-ISE CFA system coupled with the towed-fish surface water pump. We observe symmetry about point 2 in in-situ $\Delta\log(aFe^{3+})$, which is similarly displayed by all other sensor signals (Figures 3.3c, 3.4c); expected given the path of both transects to and from their respective point 2.

Salinity and temperature remain relatively constant in the May 31st and June 2nd transects. The pH spans 0.15 – 0.2 units in both transects, reaching maxima at locations where the ship's fluorometer as well as chlorophyll satellite data indicate chlorophyll maxima and coincide with aFe^{3+} minima. The May 31st transect displays a decrease in $\log(aFe^{3+})$ of 0.3 units from its starting Point to the minimum at Point 2 (Figure 3.3c), which mirrors a pH increase of just over 0.2 units. The June 2nd $\log(aFe^{3+})$ decrease from the initial location to the chlorophyll-a fluorescence maxima at location 2 is close to 0.15 units, while the pH increases about 0.15 units over this section (Figure 3.4c). The measured trends in $\Delta\log(aFe^{3+})$ may be explained by these

almost perfectly mirrored features in pH, given the inverse relationship between pH and aFe^{3+} stemming from the acid-base properties of the Fe-binding ligand pool discussed at length in Chapter 2. The differences in relative $\Delta\log(aFe^{3+})$/pH changes between transects and transect sections is examined further below (see Section "**Comparing Surface and Depth Gradients in aFe^{3+}**).

The coincidence of $\log(aFe^{3+})$ minima and fluorescence maxima may also be related to stronger Fe-binding by organic matter. Figure 3.3d shows the Fe and Fe-ligand data from the bottle samples taken during the May 31st transect (no bottle samples were collected during the June 2nd transect). The highest $\log(\alpha)$ values are seen at point 2, which would suggest a site of increased Fe-binding capacity of the natural ligand pool. Though this also happens to be a maximum in dFe, which is known to skew CSV-derived binding strengths (log K) toward higher values (Gledhill and Gerringa 2017). While the use of $\alpha_{FeL(Fe')}$ to quantify overall binding capacity theoretically accounts for the effect of dFe (equation 1), the closely matching trends of $\Delta\log(aFe^{3+})$ and pH make it difficult to establish if $\Delta\log(aFe^{3+})$ was more affected by changes in pH or organic Fe-binding on this short transect.

Next, we examine data from a longer, 12-hour transect which took place over the night of May 31st to June 1st (Figure 3.5). The ship started in the Point Blanco upwelling region and steamed offshore for about 40 km into warmer, less productive waters, before turning around and returning to its initial station. A general symmetry about point 2 is observed in all traces which is again characteristic of this out-and-back path, although the features in the most coastal waters appear to have shifted slightly by the time the ship returns to its starting station. Similar to the shorter transects discussed above, $\Delta\log(aFe^{3+})$ mirrors pH especially on a more resolved scale, again suggesting an Fe-system where pH is a major control on Fe activity. Over the course of the entire transect, however, $\Delta\log(aFe^{3+})$ exhibits a noticeable decrease that is not accompanied by a concomitant increase in pH (Figure 3.5c).

The dFe and FeL bottle samples (Figure 3.5d) help explain the trend observed in the sensor data (Figure 3.5c). Ligand Fe-binding capacity, as represented by $\alpha_{FeL(Fe')}$ shows a broad increase throughout the transect, with marked differences between points 1 and 3 which support the notion that Fe-binding properties have changed in the more coastal, upwelled site over the course of the night. The increase in $\alpha_{FeL(Fe')}$, driven largely by a strengthening of the ligand pool as characterized by the conditional binding constant data (Figure 3.5d, log K), may explain the overall trend in $\Delta\log(aFe^{3+})$ observed by the Fe-ISE. The drop in [Fe′] further supports that overall Fe activity was decreased by ligand binding despite the lack of an observed trend in dFe.

The overnight shift in the ligand pool may be due to a mixing event in the more coastal, upwelled region. Or, a lack of photochemical degradation at night may lead to a gradual increase in the Fe-binding strength and capacity, as biologically-produced ligands continually generated in the surface ocean are allowed to accumulate in the absence of photodegradation (Powell and Wilson-Finelli 2003, Barbeau et al. 2006).

Figure 3.6a and 3.6b show the path of a transect conducted over the night of June 2nd to June 3rd in which three distinct ocean environments were observed (Figure 3.6c): Point 1, is a productive site of aged, upwelled water characterized by lower temperatures (~10°C) and a relative maximum in chlorophyll; point 2, is a higher temperature (3°C greater than point 1) oligotrophic, (low chlorophyll) setting with high and stable pH (~8.05). Points 3 and 4, are shoreward and exhibited temperatures more than 1°C colder than Point 1. Unlike Point 1, Points 2 and 3 exhibited low pH (7.8) and oxygen concentrations. Combined with the very low chlorophyll-a fluorescence levels, this suggests recently-upwelled water, likely containing un-utilized nutrients.

Fe activity as measured by the Fe-ISE was highest in the aged/upwelled waters, low throughout the oligotrophic conditions, and increased slightly when entering the freshly upwelled

region (Figure 3.6c). While the $\Delta\log(aFe^{3+})$ increase at the end of the transect could be partially attributed to the drop in pH, the pronounced change from points 1 to 2 occurred when pH was largely constant. Figure 3.6d shows that overall Fe-binding capacity ($\alpha_{FeL(Fe')}$) changed little (or only marginally decreased) over this span of the transect. Therefore, this may have been a situation where the total Fe was the dominant driver of aFe^{3+}. A relatively stable $\alpha_{FeL(Fe')}$ indicates that dFe is the primary driver of [Fe′]. Further, a stable pH from Point 1 to 3 leads to correlation between [Fe′] and aFe^{3+}. We note that the highest in-situ aFe^{3+} is not seen in the most freshly upwelled water (point 4), but the water showing the most recent productivity (point 1).

Our final overnight transect, from June 7th to June 8th, is shown in Figure 3.7. Higher pH (8.0 - 8.1) low chlorophyll, low salinity, and warmer temperatures (Figure 3.7c) throughout the transect, as well as consistently sub-nanomolar dFe (Figure 3.7d), all point to an aged water mass of low productivity. We once again observe in-situ Fe activity which is highly (inversely) coupled to pH. The only exception occurs near point 4, where we pass through what is clearly a different water mass as evidenced by excursions in all hydrographic data (Figure 3.7c). In this water mass, the Fe-ISE also detects a stark decrease in Fe activity, which is *positively correlated* with pH, chlorophyll, and oxygen. This correlation is not observed in any of the other transects and is opposite what is implied by the pH-dependence of aqueous Fe^{3+} chemistry (Chapter 2). The same feature persists upon returning to the same general region at the end of the transect (point 7).

The total Fe and Fe-speciation data (Figure 3.7d) do not seem to resolve this anomaly. Therefore, what the Fe-ISE is detecting here may be truly in-situ; time-dependent in a way that equilibrated laboratory samples cannot well distinguish. We should also emphasize that while all dFe and Fe-L samples were filtered, the Fe-ISE CFA system is exposed to raw, unfiltered

seawater, and may be sensitive to the influence of a particulate species present on only one side of the front.

P2507 Depth Profiles

Figures 3.8 through 3.13 show the depth profiles from the six casts from the P2507 cruise. For each cast, $\Delta\log(aFe^{3+})$ and pH measured by the Fe-ISE CFA system are shown in panel a, representing stabilized sensor measurements from each depth (see **Experimental**). Temperature, salinity, fluorescence, and oxygen from the CTD rosette are shown in panel b. Sporadic issues with the CTD's fluorometer led to what are likely erroneous signals for some casts, which are denoted by dashed green fluorescence traces. Casts where bottle samples were collected include dFe and Fe-L speciation data shown in panels c through g.

In general, $\Delta\log(aFe^{3+})$ and pH align with the other common features observed in the hydrographic data. The largest changes in $\Delta\log(aFe^{3+})$ and pH in most profiles appear along the thermocline (aligning also with the oxycline and halocline). Depth profiles at the test cast station (Figure 3.8), at SPOT (Figures 3.9 and 3.10), and at the Scripps Canyon station (Figure 3.13) display notable depth gradients in all hydrographic data, as do associated $\Delta\log(aFe^{3+})$ and pH. At the LA Nearshore station (Figures 3.11 and 3.12), CTD profiles indicate a shallow (<20 m) pycnocline, such that pumping took place deeper than any significant hydrographic changes. As such, it is at this station that we measured the weakest depth gradients in $\Delta\log(aFe^{3+})$ and pH.

For the profiles with pronounced gradients, $\Delta\log(aFe^{3+})$ and pH are positively correlated, similar to the rarely observed surface anomaly discussed above (Figure 3.7, point 4), indicating a system not controlled by pH alone. In these depth profiles, high pH appears to be associated with a low $\alpha_{FeL(Fe')}$ and a maximum in aFe^{3+}. Evidently, the aFe^{3+} observed in these profiles is not governed by a single ligand pool. The Fe-ligand bottle data appear to support this. Figures 3.8d, 3.9d, and 3.13d, show that $\alpha_{FeL(Fe')}$ increases with depth at these three stations. As the

CLE-AdCSV technique is carried out at a buffered pH, the method is not sensitive to any pH-related changes in Fe-speciation. Thus, the log(α) trends displayed here suggest that the chemical composition of the natural ligand pool changes with depth. This appears to be the dominant control on aFe^{3+} at these stations. Total dFe increases with depth, and should theoretically have the opposite effect on aFe^{3+} if it were the only factor (Figures 3.8c, 3.9c, 3.13c).

At the LA Nearshore station (Figures 3.11, 3.12), a shallow pycnocline led to a narrow observed range of pH and $\Delta\log(aFe^{3+})$. Under these conditions, pH and $\Delta\log(aFe^{3+})$ inversely correlate (Figure 3.11a, 3.12a), suggesting pH as the dominant control. The FeL bottle data are somewhat supportive of this (Figure 3.11c-g), although this was a shallow station located on the continental shelf in only ~70 m of water, and the benthic source of Fe resulted in very high dFe (>10 nM). This makes Fe-speciation parameters difficult to derive with our standard single analytical window CSV procedure (Bundy et al. 2014, Gledhill and Gerringa 2017, Laglera et al. 2013), and thus perhaps less reliable than at other stations.

Temperature in the Fe-ISE CFA flow cell (data not displayed here) generally remained between 15 to 16°C, meaning that water pumped from depth warmed by about 5°C on average by the time it reached the Fe-ISE. We note that this temperature change is unlikely to contribute to major aFe^{3+} changes based on temperature effects to the Fe-binding properties of the ligand pool. MINTEQ speciation models for seawater with NICA-Donnan Fe-binding DOC, or specific Fe-chelators such as EDTA or citrate, indicate that temperature affects log(aFe^{3+}) on the order of 0.01 log unit/°C, with the direction of the effect dependent on the specific chelator. That said, a temperature-controlled analytical regime, or a pressure-tolerant Fe-ISE system capable of measurement at depth, would mitigate even the minute aFe^{3+} changes that might be observed due to temperature differences.

At SPOT and at the LA Nearshore station, two pumped profiles were carried out to examine potential variability throughout the day. The first cast took place in the morning at 0800

(Figures 3.9, 3.11), the second at 1800 in the evening (Figures 3.10, 3.12). While pH and CTD-measured hydrographic properties remained largely unchanged throughout the day (Figures 3.9a,b vs 3.10a,b, Figures 3.11a,b vs 3.12a,b), aFe^{3+} appears to exhibit an increase from morning to evening that is similar at both stations (Figure 3.14). At both stations, $\Delta\log(aFe^{3+})$ measured in the evening is more than 0.1 log unit higher than that of the morning cast, with certain depths showing an increase closer to 0.3 $\Delta\log(aFe^{3+})$ units throughout the day. Although Fe-speciation data were not collected for the evening casts, the observations suggest that Fe activity may increase throughout the day, perhaps due to photodegradation of Fe-binding organic matter (Powell and Wilson-Finelli 2003, Barbeau et el. 2006).

During the morning casts of these two stations, unfiltered bottle samples were also collected from pumped water to examine the potential variability between Fe-ISE analyses of bottle samples and the direct measurement of pumped seawater. Figure 3.15 and Figure 3.16 show Fe-ISE measurements of these bottle samples, collected from the SPOT and LA Nearshore morning casts respectively (compare to Figures 3.9 and 3.11). For both casts, pH is 0.1 unit lower in the bottle samples as compared to the pumped measurements. While headspace in the bottles was minimized, this pH decrease may be due to the dissolution of carbon dioxide in the seawater prior to or during recirculated Fe-ISE CFA analysis. Values of $\Delta\log(aFe^{3+})$ are considerably higher in the bottle samples. The SPOT bottle samples (Figure 3.15) appear to have increased by 0.7 – 1 $\log(aFe^{3+})$ units in relation to the corresponding depths of the pumped measurements (Figure 3.9). This increase was more pronounced in deeper samples, serving to significantly reduce the $\Delta\log(aFe^{3+})$ vertical gradient that was observed in the pumped samples. The bottle samples collected at the LA Nearshore station (Figure 3.16) were over 1 $\log(aFe^{3+})$ unit higher than the pumped measurements (Figure 3.11), in some cases displaying an increase of over 1.5 $\log(aFe^{3+})$ units. The pH decrease is not nearly of the correct magnitude to fully explain these marked aFe^{3+} increases, at least based on the equilibrium acid-base properties of expected seawater Fe-binding species, meaning other

factors must be involved. There may be aFe^{3+} variation associated with changes in pressure (Moore and Millward 1982) or dissolved gas concentrations (Rapp et al. 2020, Zhu and Hopwood et al. 2021) from depth which have previously been immeasurable due the ex-situ nature of most Fe-speciation analyses. In any case, we recommend that Fe-ISE measurements always be carried out as close to sample collection as possible, employing direct pumping techniques whenever feasible to minimize changes from in-situ conditions.

Comparing Surface and Depth Gradients in aFe^{3+}

Comparing trends in surface transects and depth-resolved aFe^{3+}, several broad characteristics emerge. In both surface transects and profile data, $\log(aFe^{3+})$ rarely spans more than 0.5 units. This range would likely increase with deeper profiles or further-reaching transects. In most cases, surface transects display aFe^{3+} that is inversely correlated with pH, while depth profiles display the opposite. This would seem to suggest that the depth-related gradients in aFe^{3+} are more attributable to chemical changes in the Fe-binding ligand pool. Surface-related gradients on the other hand usually reflect aFe^{3+} controlled by the acid-base properties of a ligand pool that otherwise remains relatively constant. Where surface data differ from this trend (Figure 3.7c, point 4), it may imply the detection of a new ligand pool. It is only when both pH and overall Fe-complexation capacity ($\alpha_{FeL(Fe')}$) are stable that the total dFe appears to have noticeable correlation with aFe^{3+} (Figure 3.6c).

To further examine the coupling between $\log(aFe^{3+})$ and pH, several brief periods were selected from the May 31st to June 1st surface transect (Figure 3.5) during clear inverse correlation between the two signals. During these periods, the ratio of the change in $\Delta\log(aFe^{3+})$ to change in pH, $d\Delta\log(aFe^{3+})/dpH$, is calculated (Figure 3.17). This transect in particular is selected due to the large pH range over which these well-mirrored features appear. Figure 3.17 shows a clear correlation in $d\Delta\log(aFe^{3+})/dpH$ with pH. At higher pH, Fe activity is more affected by changes in pH given the increased lability and Fe-binding capacity of hydroxy species. This

agrees with the chemical speciation models and measured Fe-ISE pH titrations discussed in Chapter 2, though it is compelling to observe this predicted relationship in field data under natural variations in pH.

To visualize how this phenomenon varies in differing environments, $\Delta\log(aFe^{3+})$ vs pH is plotted in Figure 3.18 for three instances of tight inverse coupling which were observed at the start of separate surface transects off Point Blanco (May 31st, May 31st - June 1st, and June 2nd transects). Each feature displays a clear curvature in $\Delta\log(aFe^{3+})$ vs pH which indicates this increased sensitivity to pH variations in seawater of higher pH. The differences between transects are perhaps related to distinct Fe-binding ligand pools with varying acid-base properties.

In our analyses of the upper water column from the P2507 cruise, aFe^{3+} is consistently higher toward the surface (i.e. above the thermocline) where pH exhibits maxima. This is also interesting given the observed opposite trend of dFe. Total Fe minima in the surface ocean reflect the effects of biological uptake and particle scavenging, but Fe activity represents the lability and exchangeability of extant Fe, as it cycles from one form to another. Fe-ISE measurements suggest that this lability is greatest in the dynamic surface ocean. While aFe^{3+} is usually quite sensitive to pH, it appears these effects are overcome in the sub-mixed layer by what presumably must be more significant variations in the chemical nature of the dominant Fe-chelators with depth.

Our CLE-AdCSV data support the notion that the ligand pool is changing with depth. The strongest trends in our data emerge when ligand concentration, ligand strength, and total Fe are all incorporated into the $\alpha_{FeL(Fe')}$ term. As a measurement of aFe^{3+} should theoretically depend on the same factors, it makes sense that we find good correlations between the trends of these "master variables". We note that our observations of increasing complexation capacity with depth below the mixed layer agree well with previous studies off coast of California (Bundy et al. 2014, 2016, Boiteau et al. 2019). Bundy's comprehensive multiple analytical window

CLE-AdCSV study highlighted a notable increase in the concentrations of multiple ligand classes (strengths) with depth in the upper <200 m water column, especially in more productive coastal and frontal stations (Bundy et al. 2016).

That said, it is difficult to truly quantify the relationship between in-situ aFe^{3+} and CSV-derived $\alpha_{FeL(Fe')}$ especially given the confounding influence of pH and operational differences between the measurement protocols. For example, $\log(\alpha)$ at the test cast station (Figure 3.8d) increased by about 1.4 units from 20 to 80 meters, while $\log(aFe^{3+})$ decreased a bit more than 0.1 unit (Figure 3.8a). At SPOT, (Figure 9a, 9d), $\log(\alpha)$ only increases about 0.3 units for a comparatively larger decrease in $\log(aFe^{3+})$ of almost 0.4 units. The relative pH and dFe changes were almost identical from station to station. The CSV data would suggest that the Fe-chelators dispersed throughout the water column at the test station have a greater range in Fe-binding capacity, but this only necessarily applies at the pH of 8.2 at which the CLE titration was carried out. This assortment of ligands may be more susceptible to pH-related reductions to their Fe-binding capacities; i.e. protonation of their binding sites. The SPOT ligand pool on the other hand may primarily comprise Fe-binding sites with lower pKa's which would be less prone to protonation in the same pH range. This would reconcile the fact that the $\log(aFe^{3+})$ decrease with depth is larger at the site of the apparently smaller change in CSV-derived Fe-binding capacity.

Thus, aFe^{3+} measured by the Fe-ISE tells a different story than the parameters derived from the CLE-AdCSV technique. Unlike standard analytical techniques, the Fe-ISE is uniquely capable of analyses at ambient states of physico-chemical properties such as pH, temperature, solar irradiance, and dissolved oxygen concentrations. In fact, while we observe aFe^{3+} maxima in the uppermost portion of the water column, much of our evidence seems to indicate that a parcel of water requires time in the surface ocean for aFe^{3+} to increase. Pupcycle II transects which spanned marine environments in different stages of upwelling and production (Figures 3.5

and 3.6) showed that sites of very recent upwelling characterized by pH < 7.9, low oxygen, low temperature, and low fluorescence (Figure 3.5 location 3, Figure 3.6 location 4) did not exhibit aFe^{3+} maxima, but only marginally higher aFe^{3+} than that of aged oligotrophic water masses (Figure 3.5 location 2, Figure 3.6 location 2). This agrees with aFe^{3+} trends of our vertical profiles, which point to deeper water as sites of lower aFe^{3+}. Comparing morning SPOT or LA Nearshore vertical profiles (Figure 3.9, 3.11) to those measured in the evening (Figure 3.14) or to our discrete samples equilibrated at room temperature and ambient light (Figures 3.15, 3.16), also suggests a notable aFe^{3+} increase with time at the surface. It is difficult to pinpoint the exact reason for this increase, but complex dynamics associated with the effects of changing temperature, solar irradiance, and dissolved gas concentrations on Fe speciation are likely involved (Sunda and Huntsman 2003, Miao et al. 2006, Spacken et al. 2018, Zhu et al. 2023). This again emphasizes the importance of as in-situ a measurement as possible for assessing seawater Fe chemistry.

The Fe-ISE also allows for an analytical system that is particularly sensitive to the influence of pH, which has been consistently shown to be a crucial factor in the marine Fe system (Millero et al. 2009, Gledhill et al. 2015, Zhu, Birchill et al. 2021, Zhu, Hopwood et al. 2021) determining Fe availability to biota on a microscale (Liu et al. 2022), as well as functioning as a dominant driver of global Fe distributions (Zhu et al. 2023). Due to the significant pH dependence of aFe^{3+}, we stress the importance of coupled pH measurements with all Fe-ISE analyses.

Given the uniquely complex chemistry of Fe in aqueous solutions, time itself is a variable which plays a defining role in Fe speciation (Croot and Heller 2012, Laglera and Filella 2015, Sukekava et al. 2024), and which historically has been challenging to assess. Values of log(K), log(α), the various fractions of total dissolved Fe (dFe) or soluble inorganic Fe (Fe′), and even speciation model-derived values of aFe^{3+}, all stem from *equilibrium* assumptions. The Fe-ISE, in contrast, sees a real-time image of the Fe system in the midst of myriad competing kinetic

processes. The activity it measures represents the instantaneous lability of Fe as it is exchanged between various chelators, both organic and inorganic, and is therefore a master variable perhaps more relevant to the time-sensitive dynamics of microbial Fe uptake.

Conclusions and Considerations for Future Work

This work has demonstrated the value of the chalcogenide Fe-ISE as an oceanographic tool for in-situ measurements of Fe activity. At our study sites off the California and Oregon coasts, we found that surface gradients in aFe^{3+} are predominately driven by pH and the associated acid-base properties of the Fe-binding ligand pool, while aFe^{3+} gradients with depth appear to be more dependent on variations between ligand pools of differing Fe-complexation capacities. A maximum range of $\log(aFe^{3+})$ of about 0.7 across a cruise dataset indicates that there might be a consistently observed window of Fe activity due to competing effects of pH and ligand complexation capacity. Future transects spanning a greater range of marine environments, or deeper profiles, would elucidate whether certain regions exhibit even larger swings in in-situ aFe^{3+}. The Fe-ISE is well suited to continuous measurement in a shipboard flowthrough system, and could potentially be integrated into more autonomous sensing platforms. Mounted on a dock or mooring, the Fe-ISE would offer information about temporal trends in aFe^{3+}, which appear to relate to sunlight-induced photodegradation of the Fe-binding ligand pool. Such a tool would also be of great use in assessing changes in seawater Fe dynamics related to processes such as ocean warming and ocean acidification.

While the trends in our CLE-AdCSV data are informative, a larger dataset with a more in-depth multiple analytical window analysis alongside Fe-ISE measurements may allow for a more quantifiable relationship between in-situ aFe^{3+} and CSV-derived parameters. Additionally, measuring particulate Fe species through total dissolvable Fe (strong acid-leached pre-filtration) analyses would help assess the total amounts of labile Fe pools that may help parameterize Fe

activity. In this way, it may be possible to define an “Fe system” analogous to the carbonate system, where measurement of certain variables (dFe, pH, aFe^{3+}) allows for the calculation of others ($\log(\alpha)$, [Fe′]). Although, the value of in-situ measurement is clear, and the Fe-ISE signal may be responding to a parameter that is difficult to relate to traditional metrics of Fe chemistry.

Used on its own, the Fe-ISE provides a snapshot of an overall Fe activity dependent on pH, total Fe, temperature, the complexation tendencies of the Fe-chelators, and any sort of kinetic processes that may be in effect – an activity believed to be related to the ability of marine microorganisms to access Fe. Used in conjunction with complementary measurements of these factors, the Fe-ISE offers valuable information regarding the relative contributions of these parameters to Fe accessibility and how these contributions may vary in different environments.

Acknowledgements

Chapter 3 is being prepared for submission for publication of the material. Fenton, Maxwell; Barbeau, Katherine; Martz, Todd. The dissertation author was the primary researcher and author of this material. Much of this work was supported by grant NSF OCE 1924386. The UC Ship Funds program supported cruise P2507 on the R/V Robert Gordon Sproul. We thank the captains and crew of the R/V Sally Ride, the R/V Robert Gordon Sproul, and the R/V Roger Revelle. We thank Claire Till and Adrian Marchetti, chief scientists for the Pupcycle II cruise, as well as the rest of the trace metal team for their help. We thank the members of the Barbeau Lab for their help with sensor deployment and sample collection on both P2507 and P2402 research cruises.

Figures and Tables

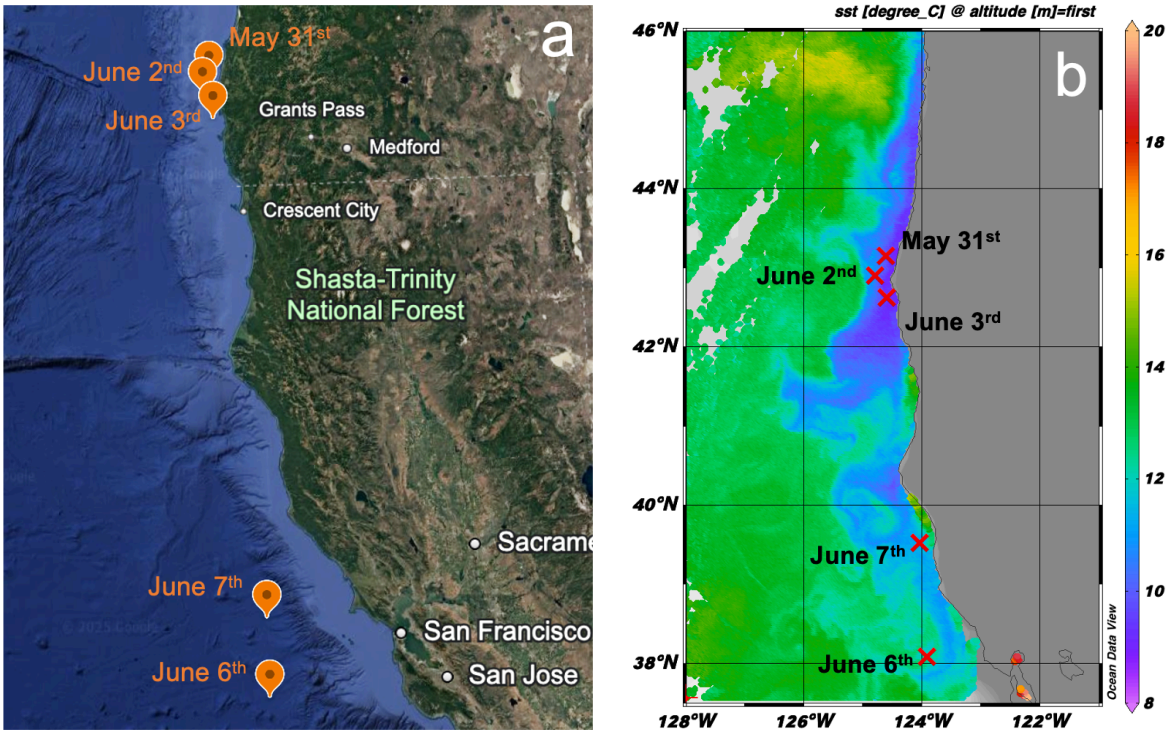

Figure 3.1: Locations of transects during the Pupcycle II cruise on the R/V Sally Ride on Google Earth **(a)** and overlayed on NOAA Coast Watch sea surface temperature satellite data from June 3rd **(b)**.

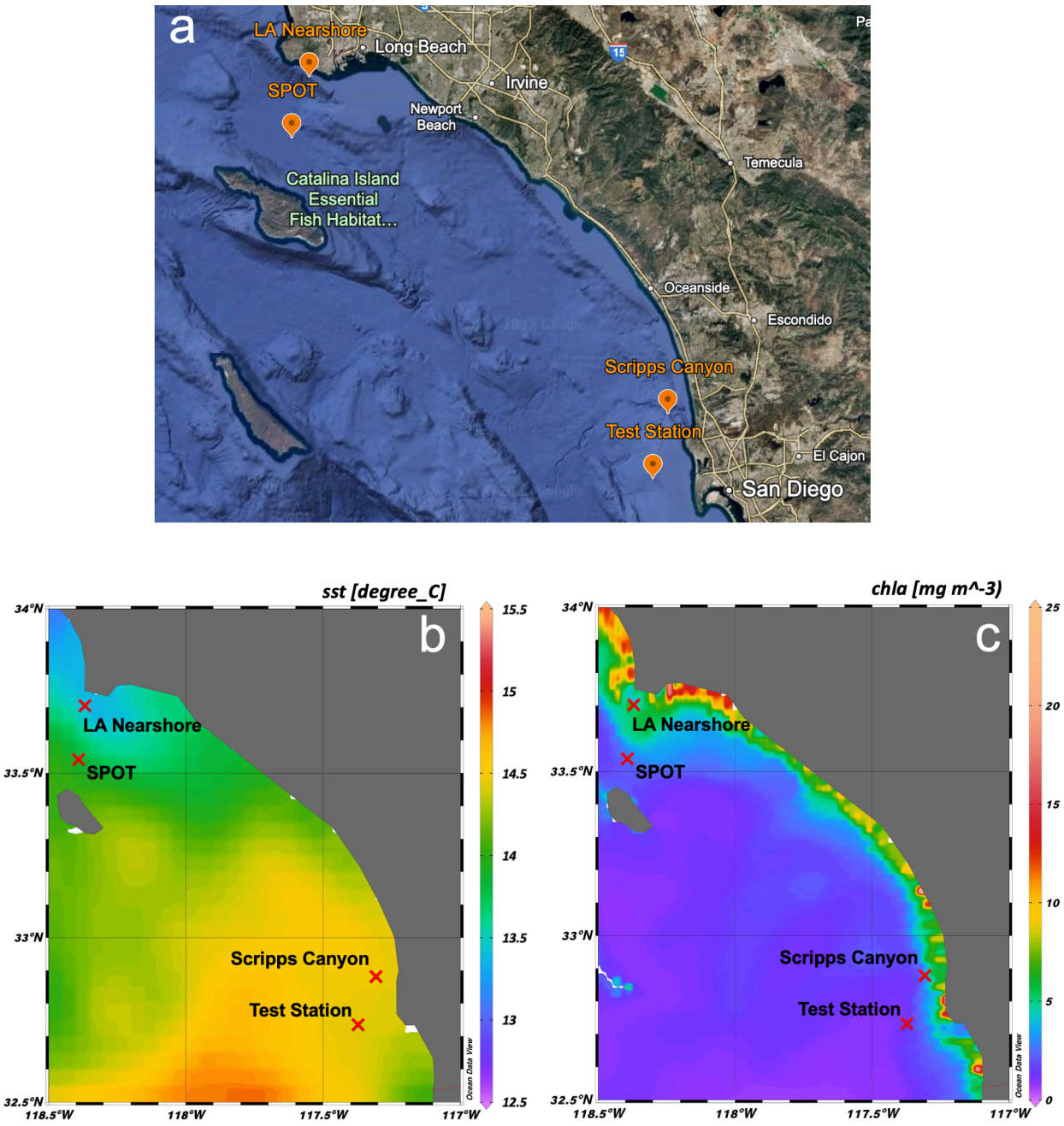

Figure 3.2: Station locations for depth profiles conducted during P2507 on the R/V Robert Gordon Sproul from Google Earth **(a)** and overlayed on NOAA Coast Watch satellite data of sea surface temperature **(b)** and chlorophyll a **(c).**

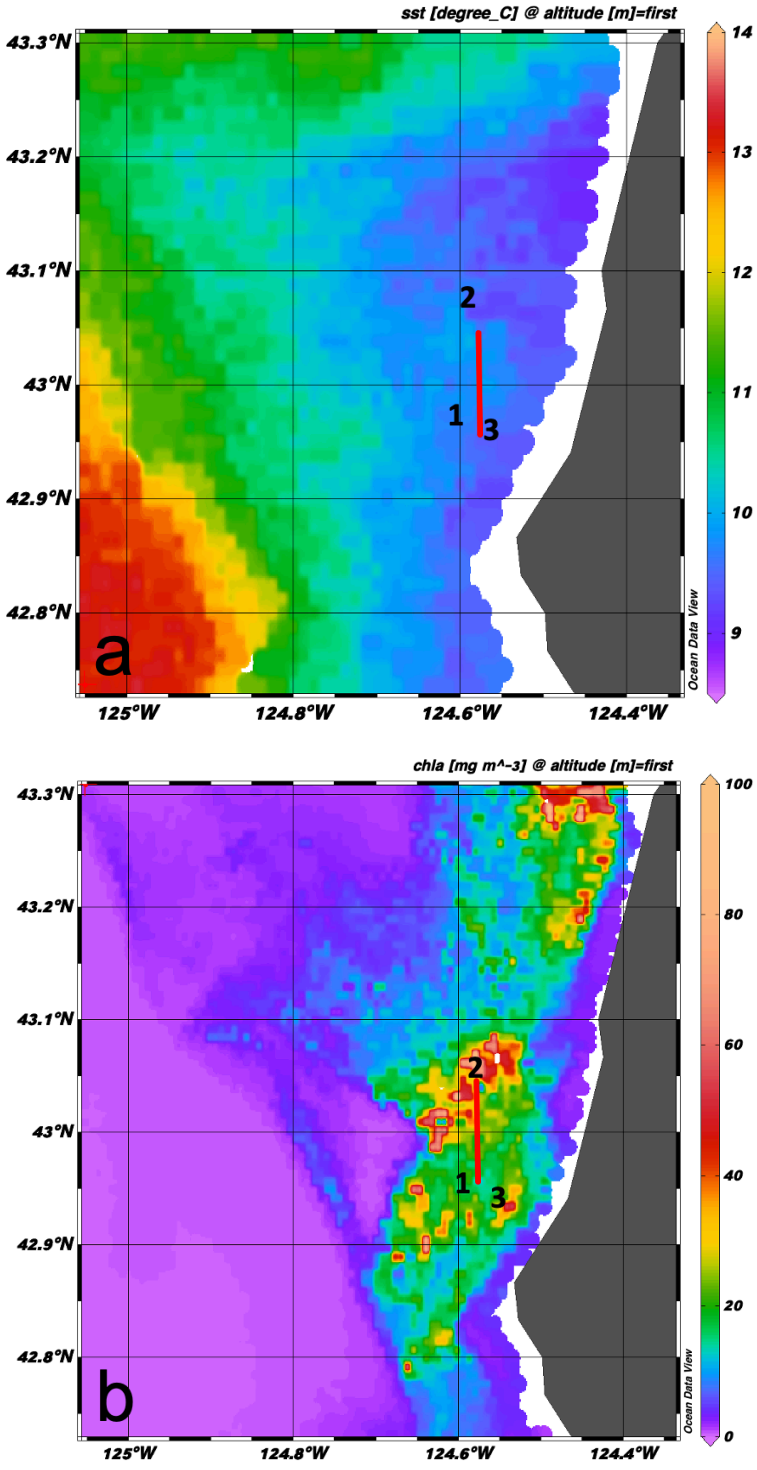

Figure 3.3: Path for Pupcycle II transect taking place May 31st, overlayed on NOAA Coast Watch satellite imagery of sea surface temperature **(a)** and chlorophyll a **(b)**.

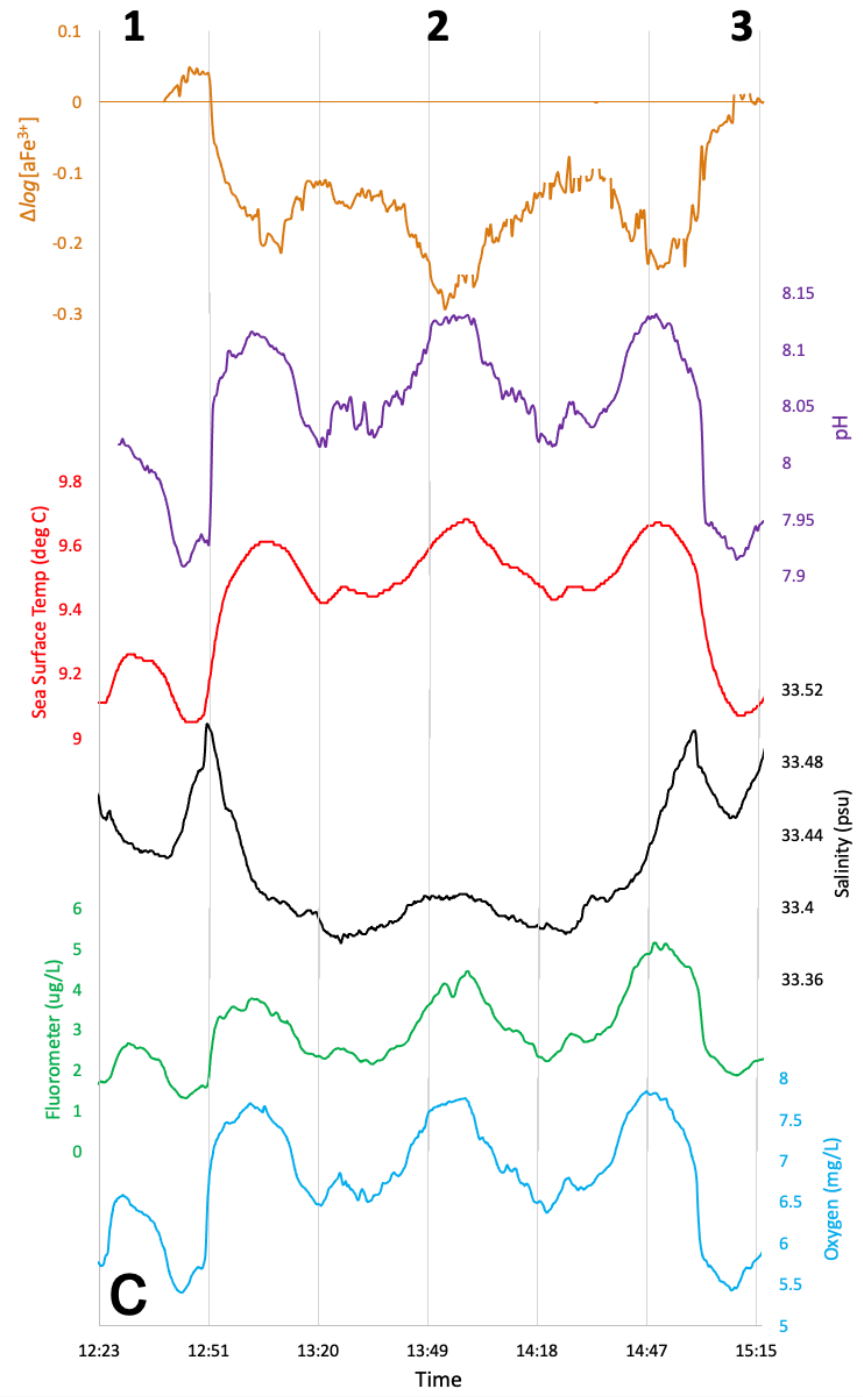

Figure 3.3, continued: c) Fe-ISE CFA and R/V Sally Ride seawater flow-through sensor measurements over the course of the transect, with numbered time points corresponding to numbered locations in **a**, **b**.

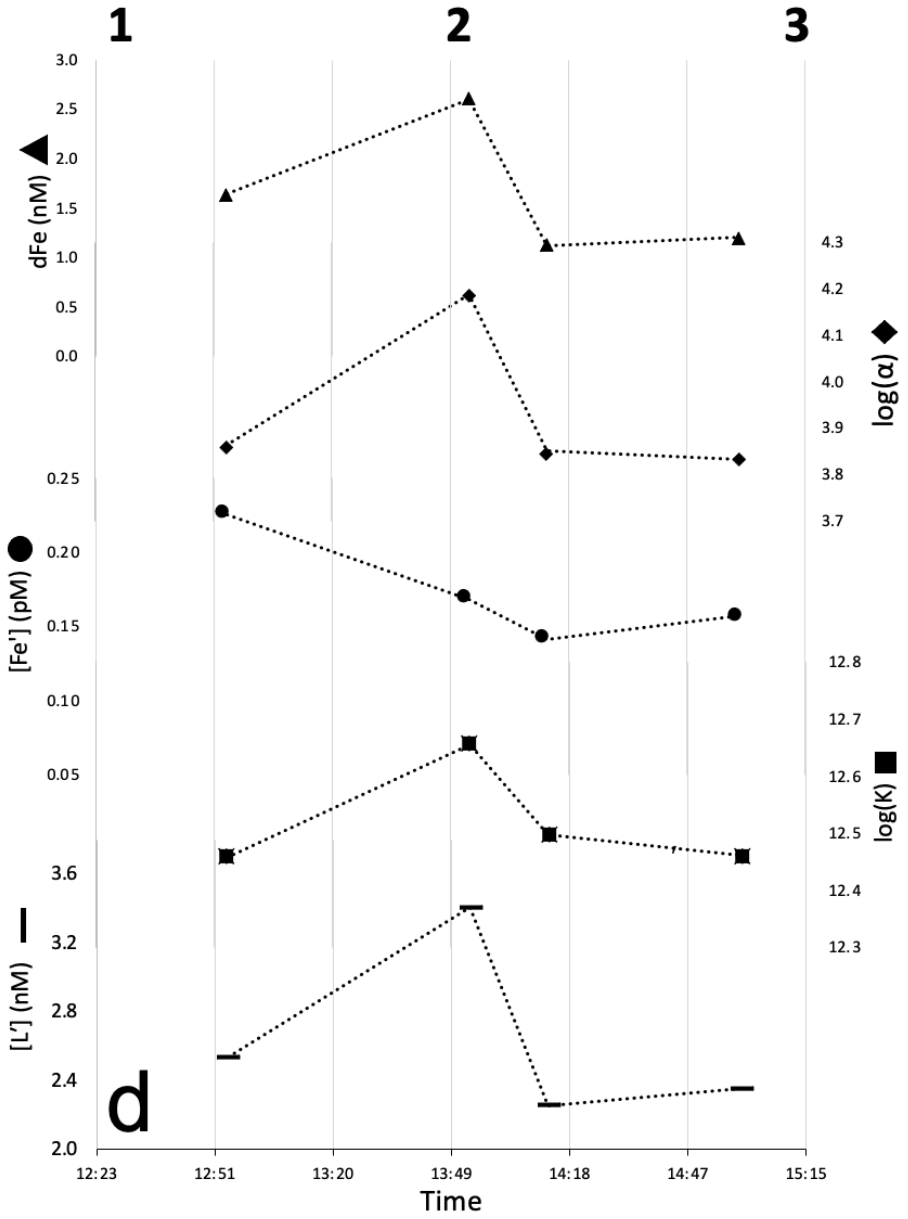

Figure 3.3: continued: d) Dissolved Fe and Fe-ligand speciation data for bottle samples taken throughout the transect, with numbered time points corresponding to numbered locations in **a, b**. K and α refer to conditional constants $K^{cond}_{FeL(Fe')}$ and $\alpha_{FeL(Fe')}$ respectively. [L′] = [L_{total}] – dFe, and refers to the concentration of excess (unbound) ligands.

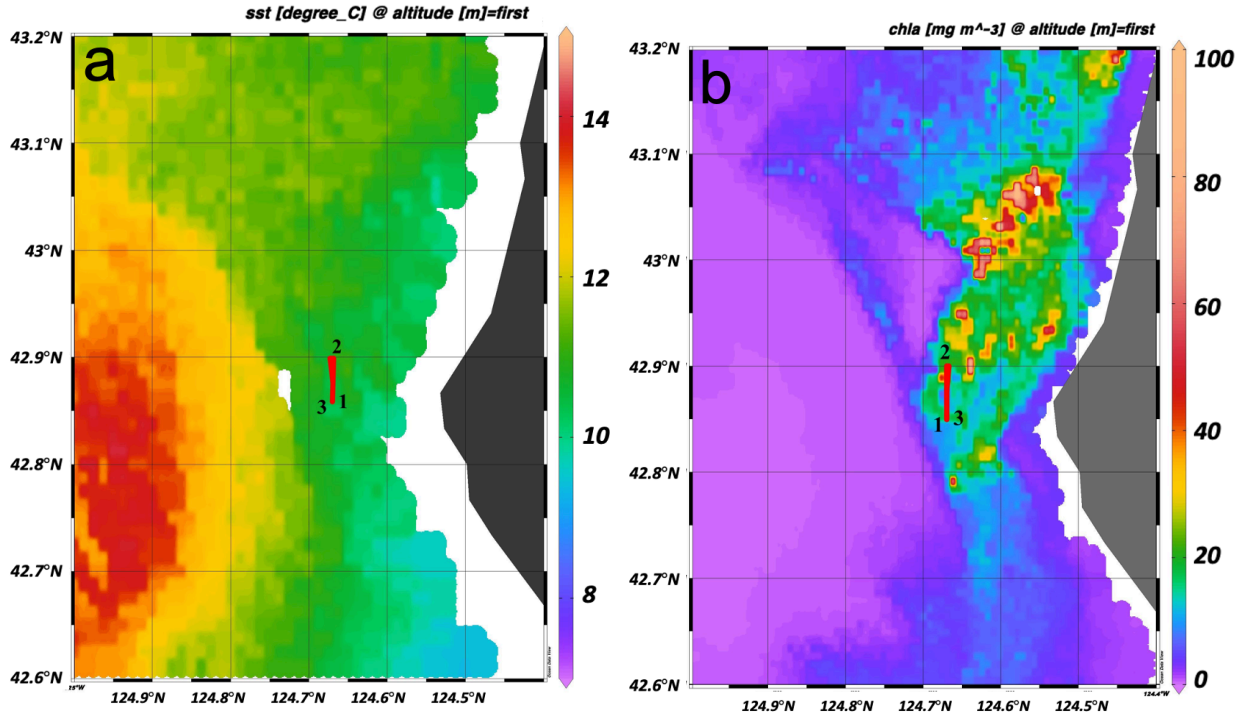

Figure 3.4: Path for Pupcycle II transect taking place June 2nd, overlayed on NOAA Coast Watch satellite imagery of sea surface temperature **(a)** and chlorophyll a **(b)**.

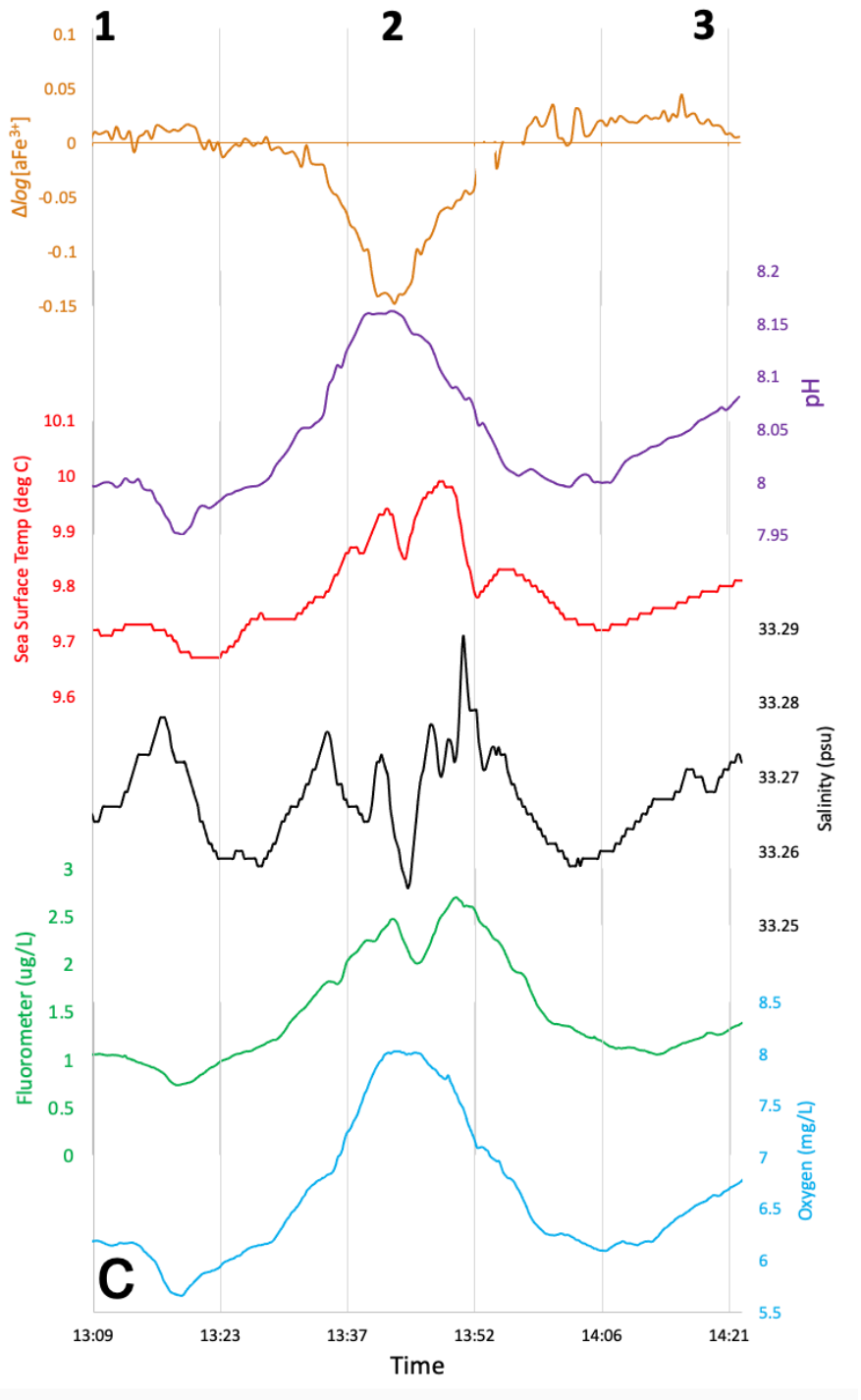

Figure 3.4: continued: c) Fe-ISE CFA and R/V Sally Ride seawater flow-through sensor measurements over the course of the transect, with numbered time points corresponding to numbered locations in **a**, **b**.

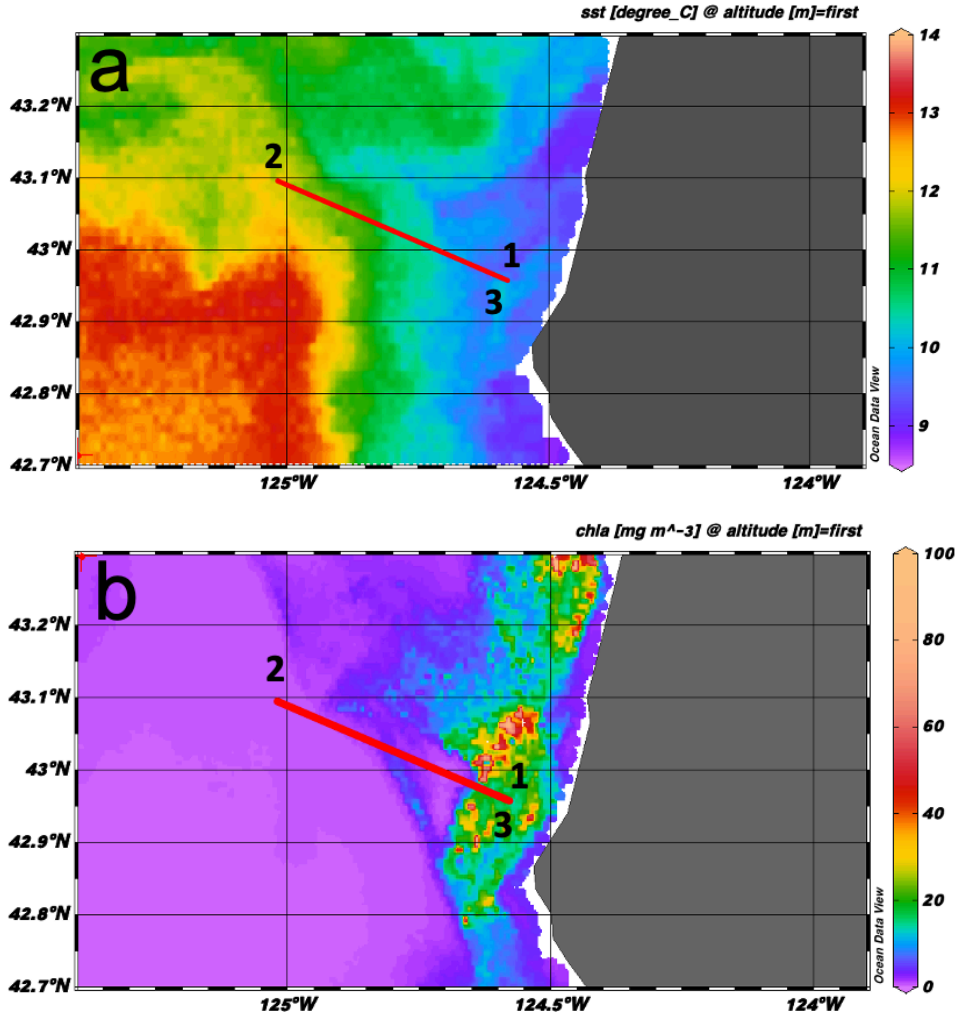

Figure 3.5: Path for Pupcycle II transect taking place overnight from May 31st to June 1st overlayed on NOAA Coast Watch satellite imagery of sea surface temperature **(a)** and chlorophyll a **(b)**.

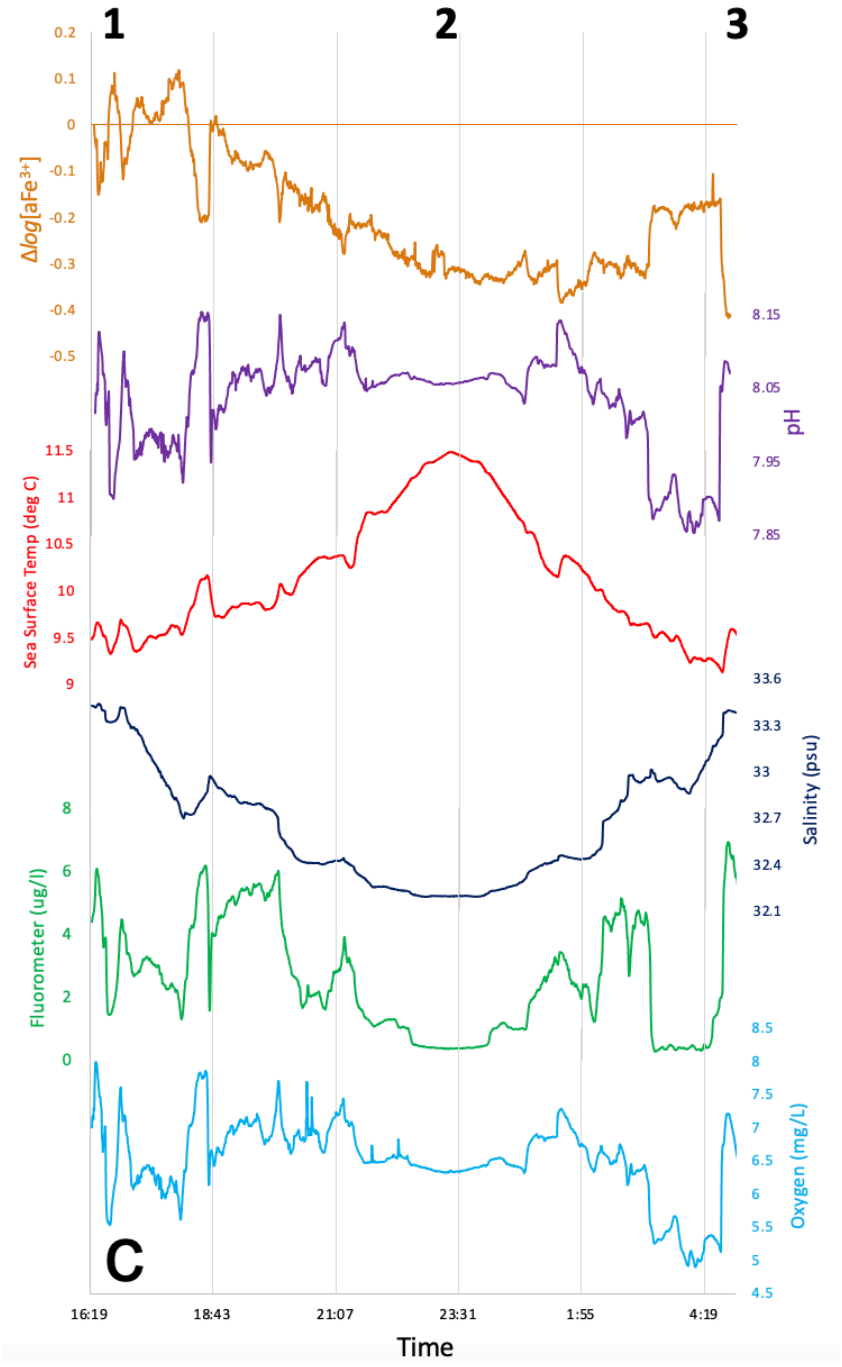

Figure 3.5, continued: c) Fe-ISE CFA and R/V Sally Ride seawater flow-through sensor measurements over the course of the transect, with numbered time points corresponding to numbered locations in **a**, **b**.

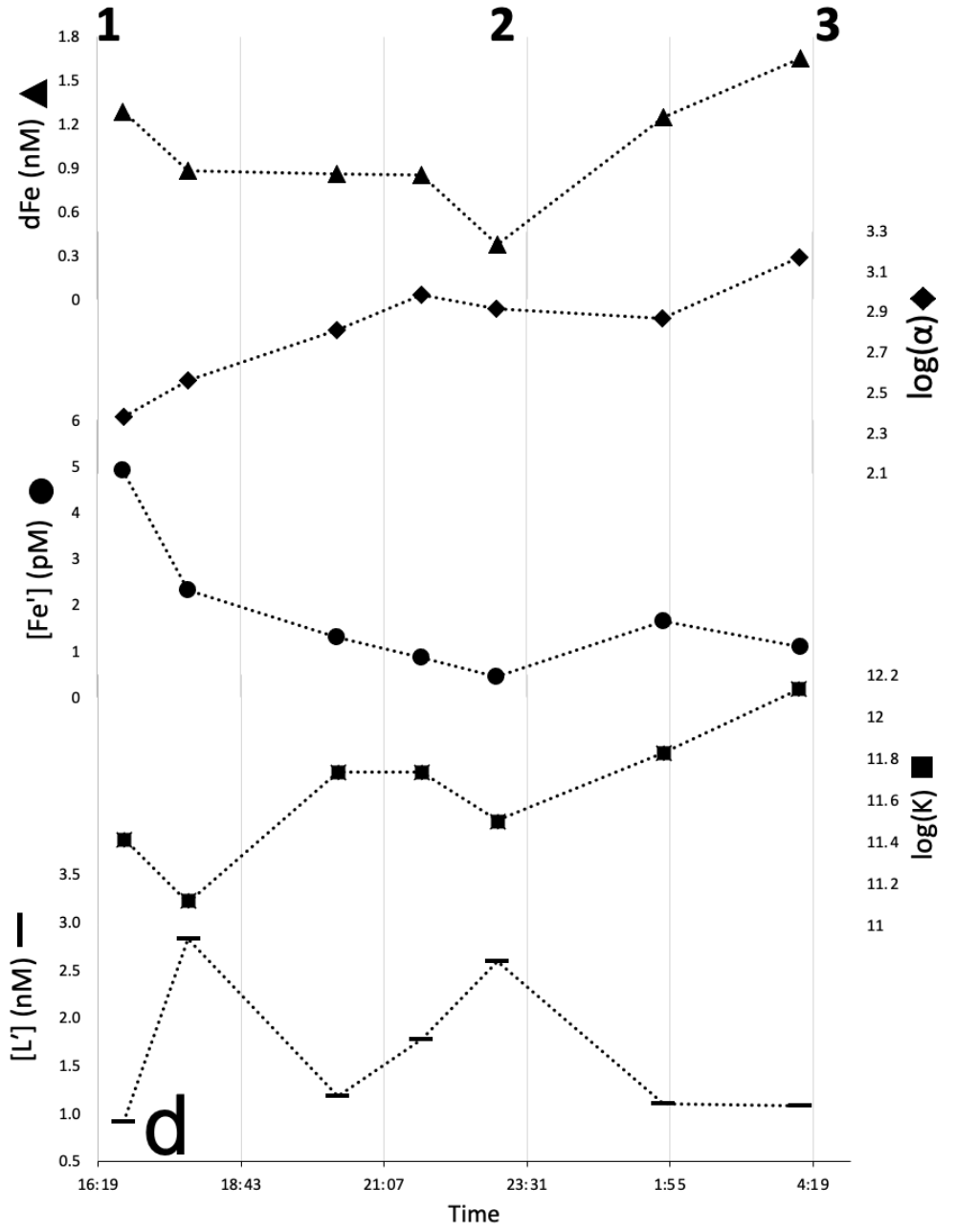

Figure 3.5, continued: d) Dissolved Fe and Fe-ligand speciation data for bottle samples taken throughout the transect, with numbered time points corresponding to numbered locations in a, b.

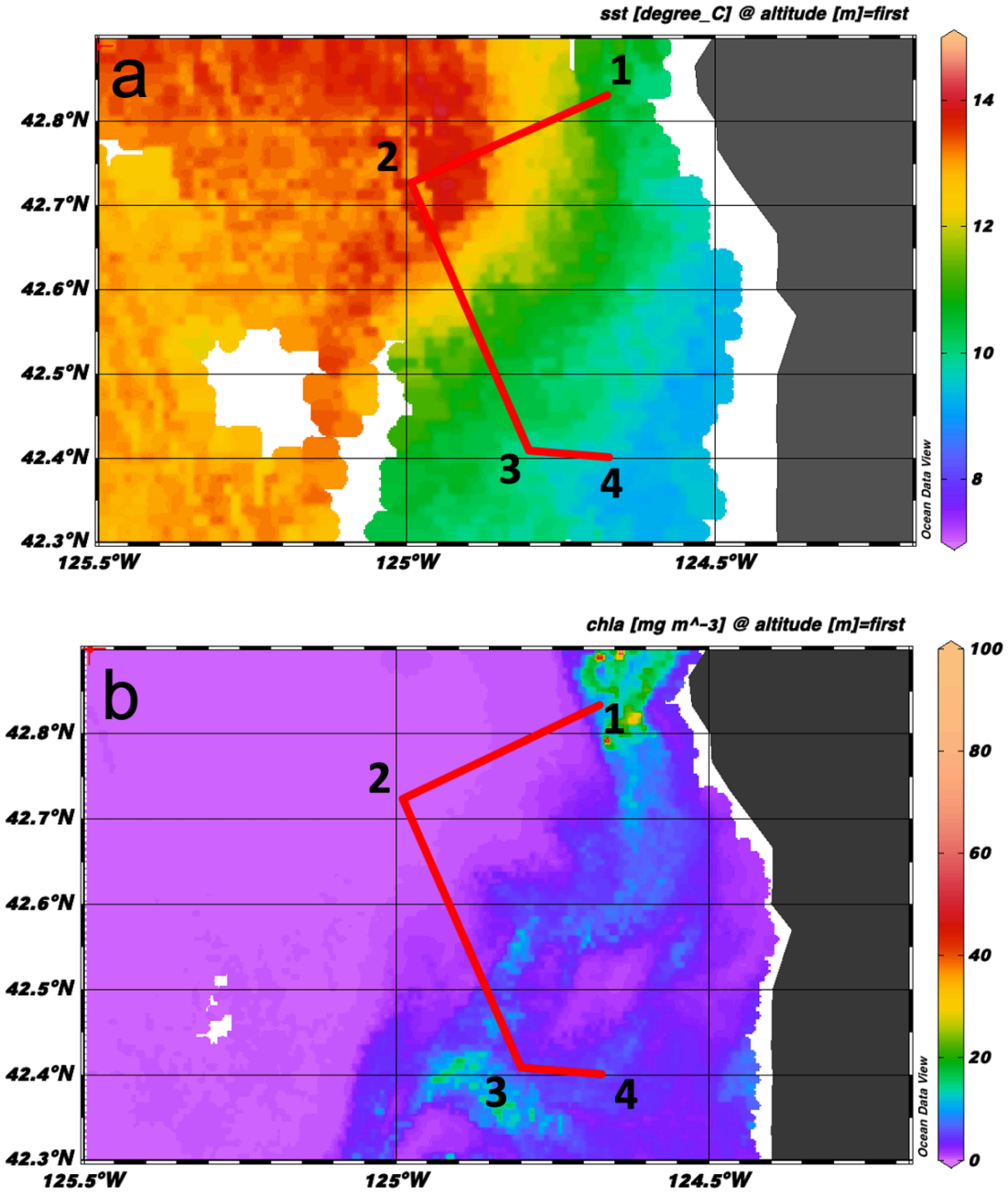

Figure 3.6: Path for Pupcycle II transect taking place overnight from June 2nd to June 3rd overlayed on NOAA Coast Watch satellite imagery of sea surface temperature **(a)** and chlorophyll a **(b)**.

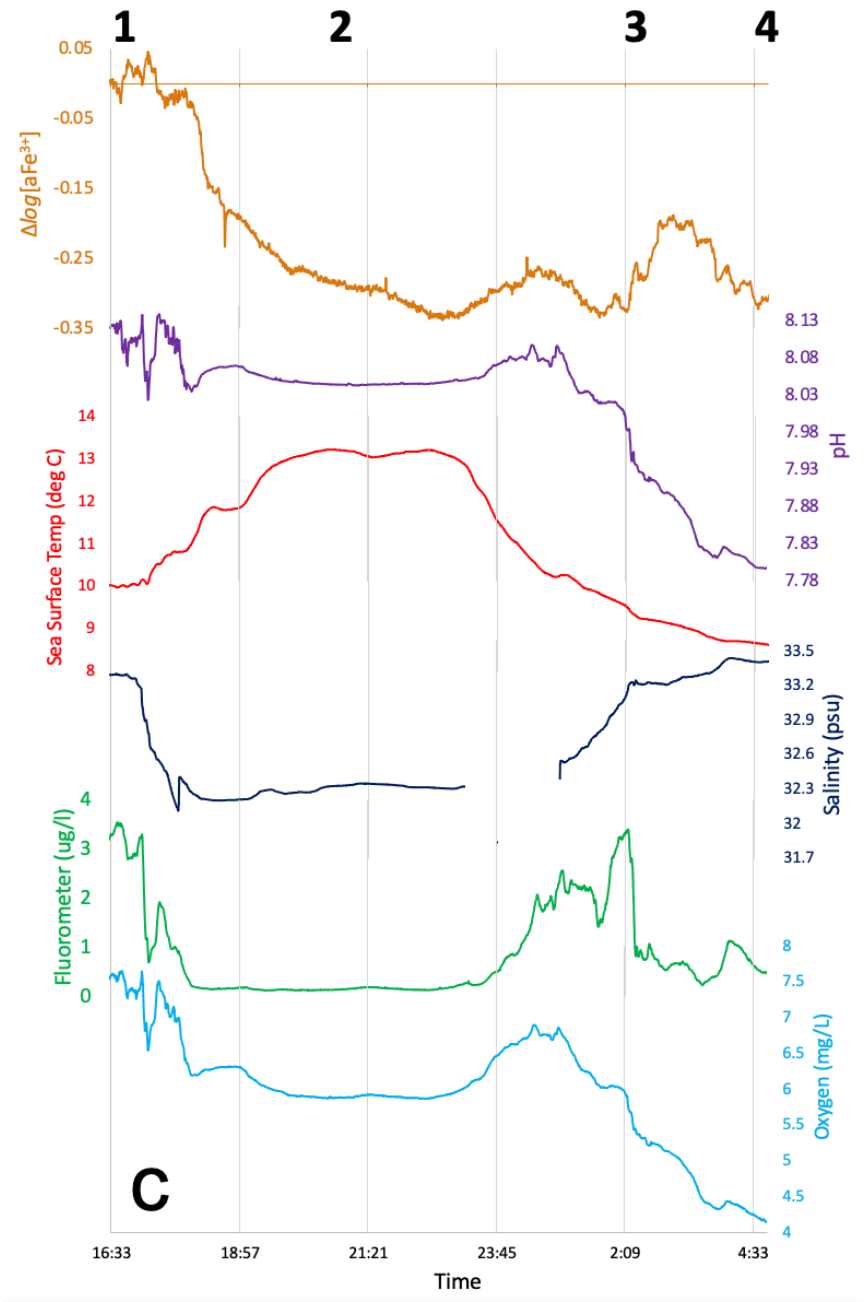

Figure 3.6, continued: c) Fe-ISE CFA and R/V Sally Ride seawater flow-through sensor measurements over the course of the transect, with numbered time points corresponding to numbered locations in **a**, **b**.

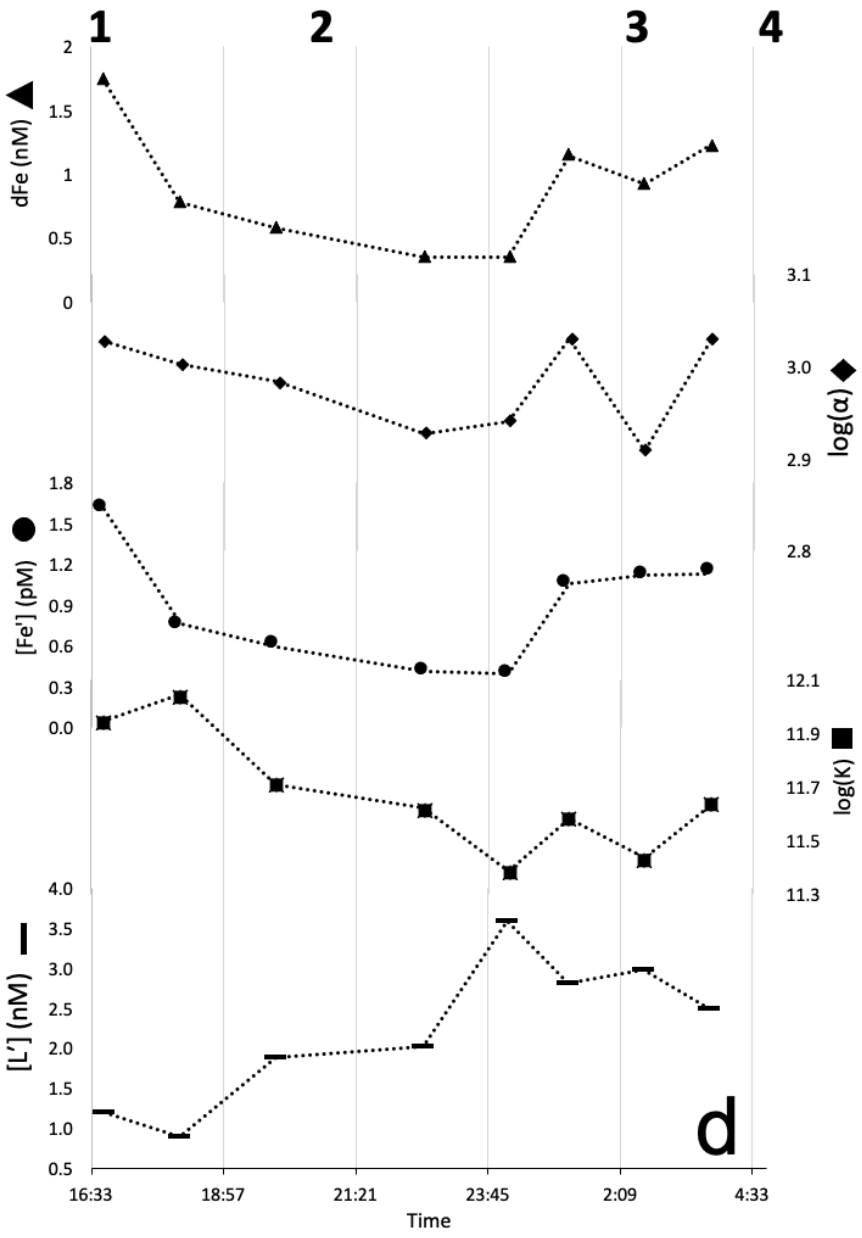

Figure 3.6, continued: d) Dissolved Fe and Fe-ligand speciation data for bottle samples taken throughout the transect, with numbered time points corresponding to numbered locations in **a, b**.

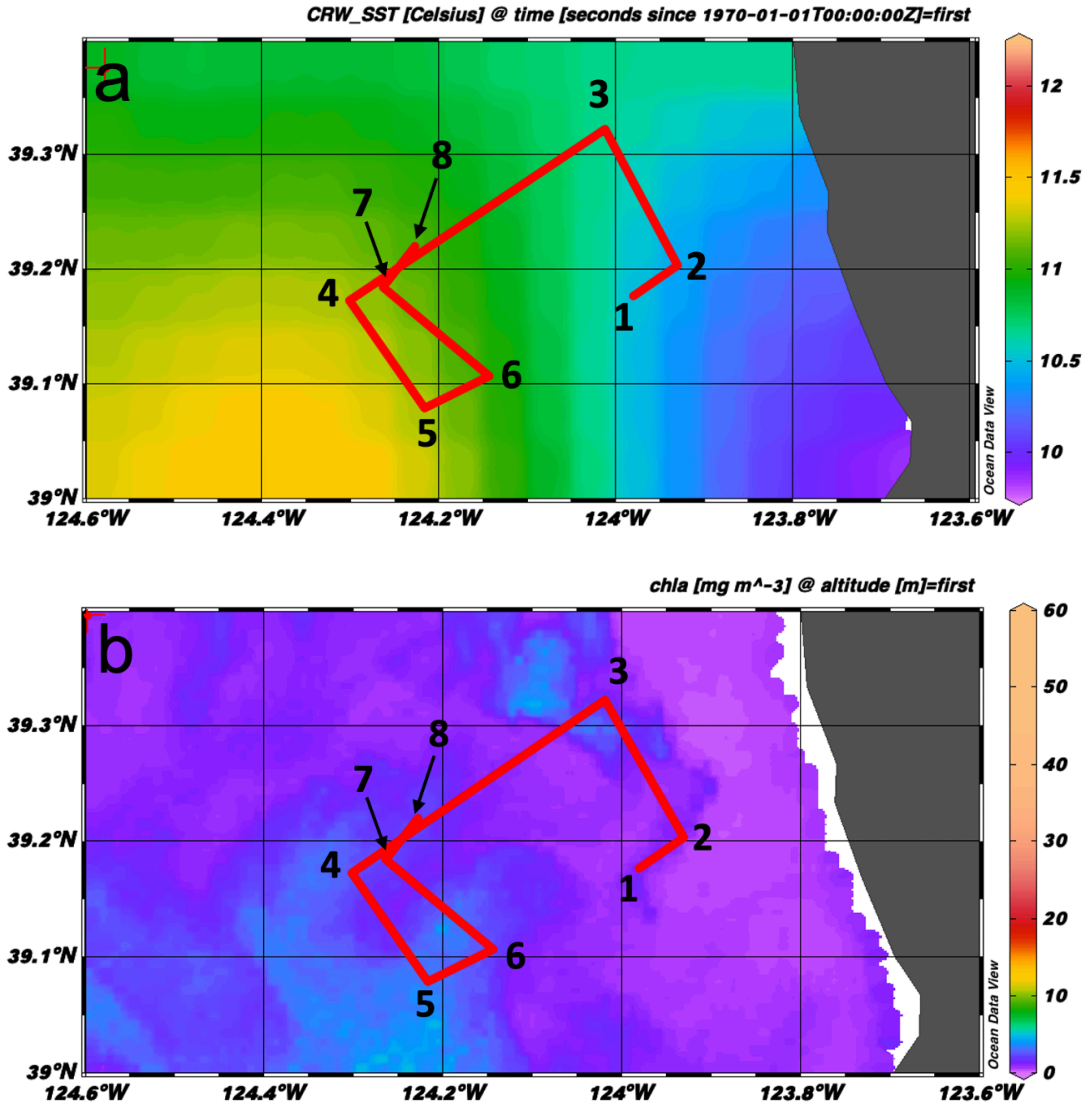

Figure 3.7: Path for Pupcycle II transect taking place overnight from June 7th to June 8th overlayed on NOAA Coast Watch satellite imagery of sea surface temperature **(a)** and chlorophyll a **(b)**.

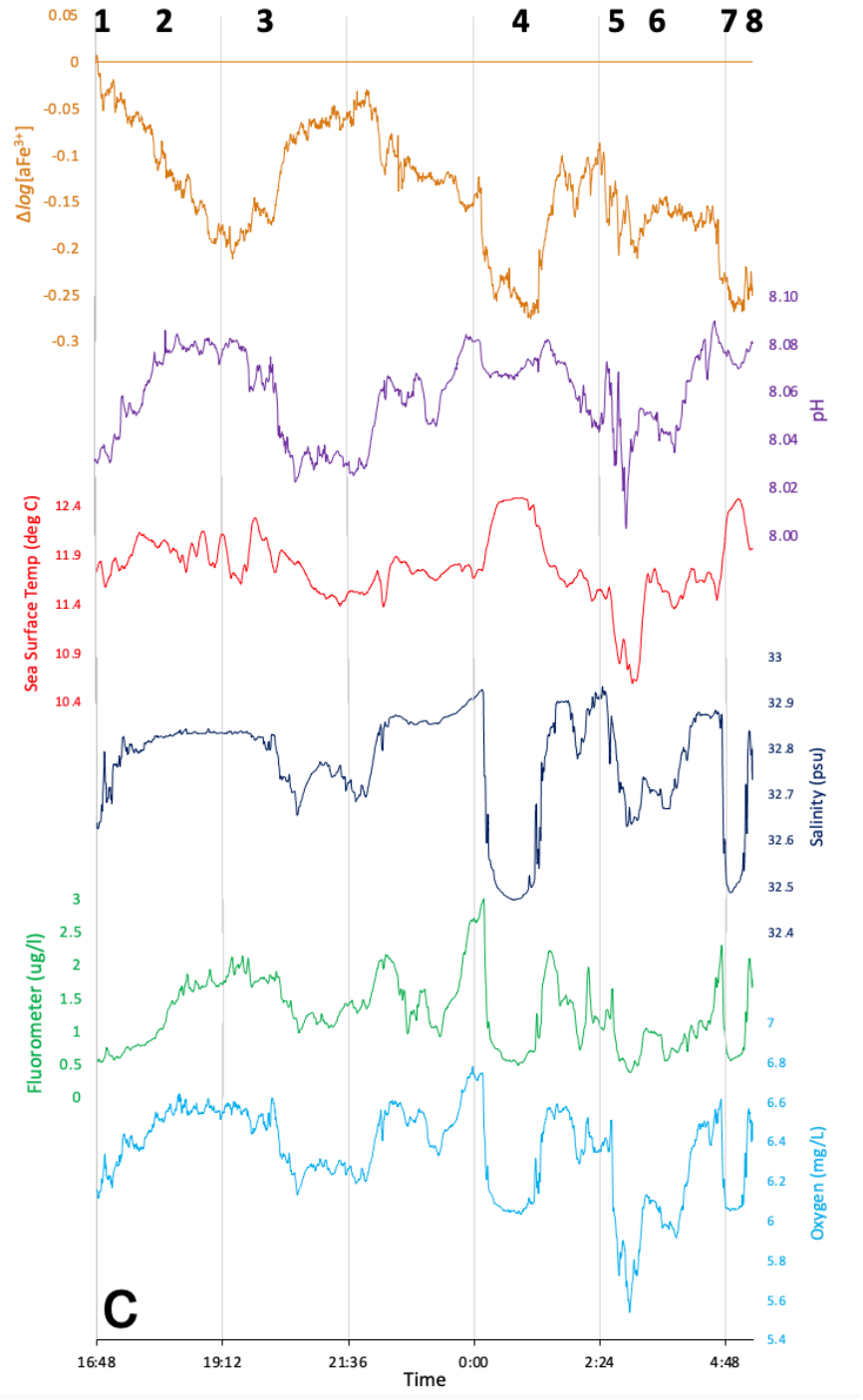

Figure 3.7, continued: c) Fe-ISE CFA and R/V Sally Ride seawater flow-through sensor measurements over the course of the transect, with numbered time points corresponding to numbered locations in **a**, **b**.

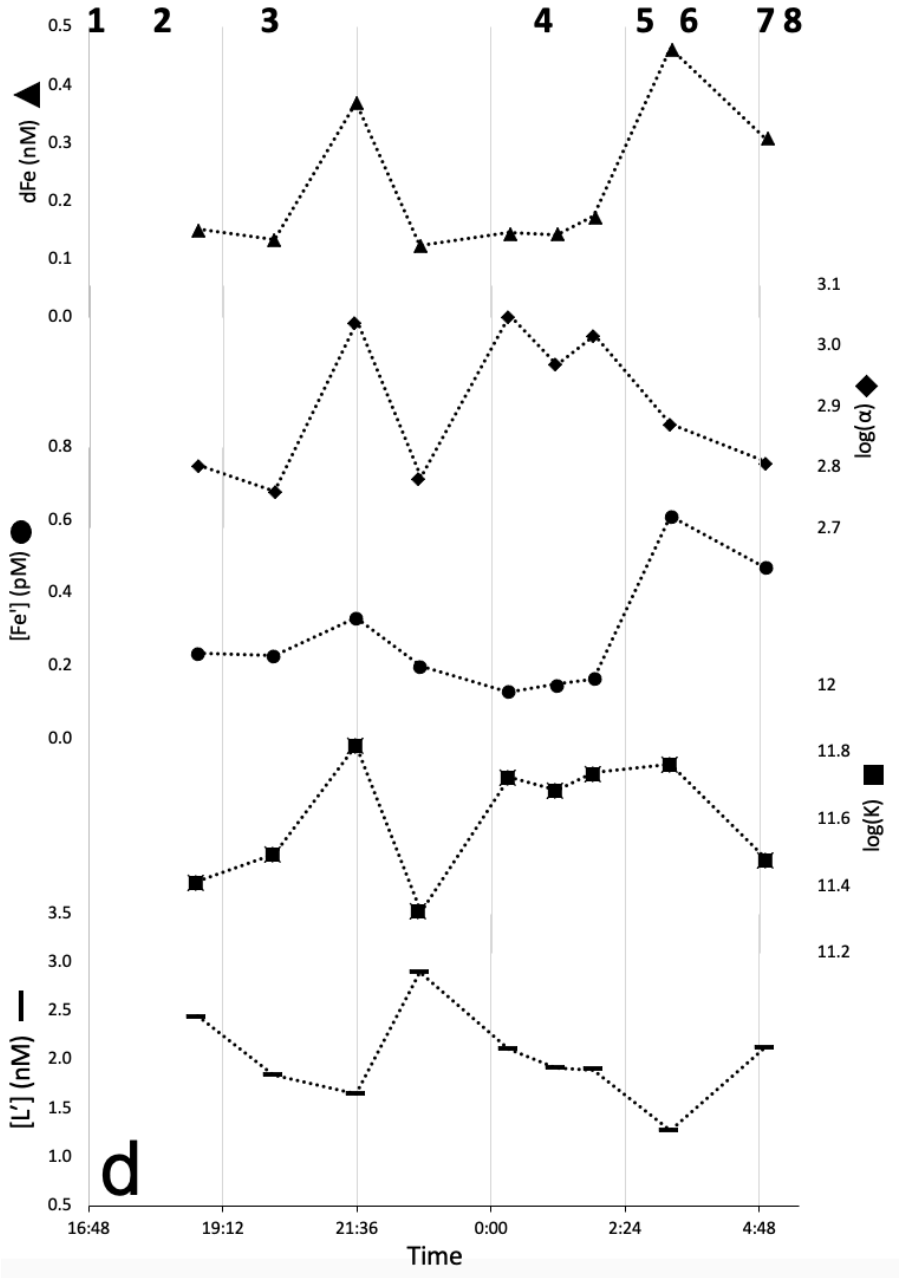

Figure 3.7, continued: d) Dissolved Fe and Fe-ligand speciation data for bottle samples taken throughout the transect, with numbered time points corresponding to numbered locations in **a, b**.

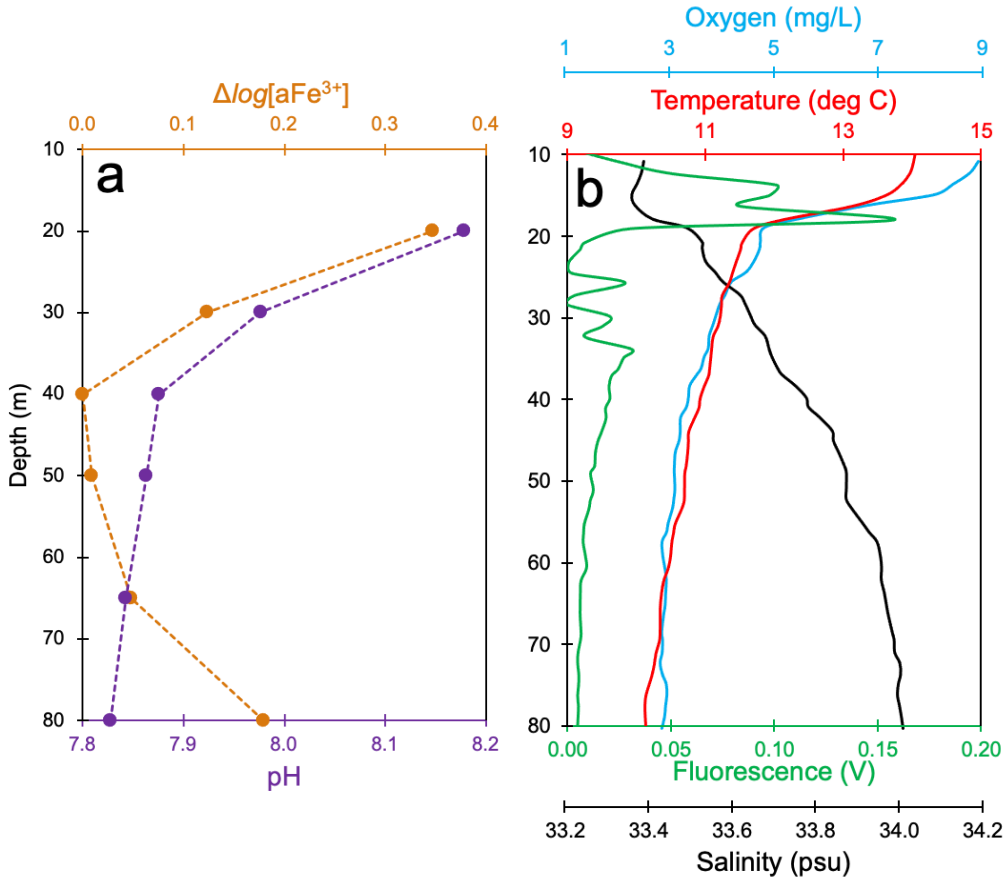

Figure 3.8: a) Fe-ISE CFA measurements from pumped depth profile and **b)** CTD rosette sensor data at the Test Cast station (see Figure 3) during cruise P2507.

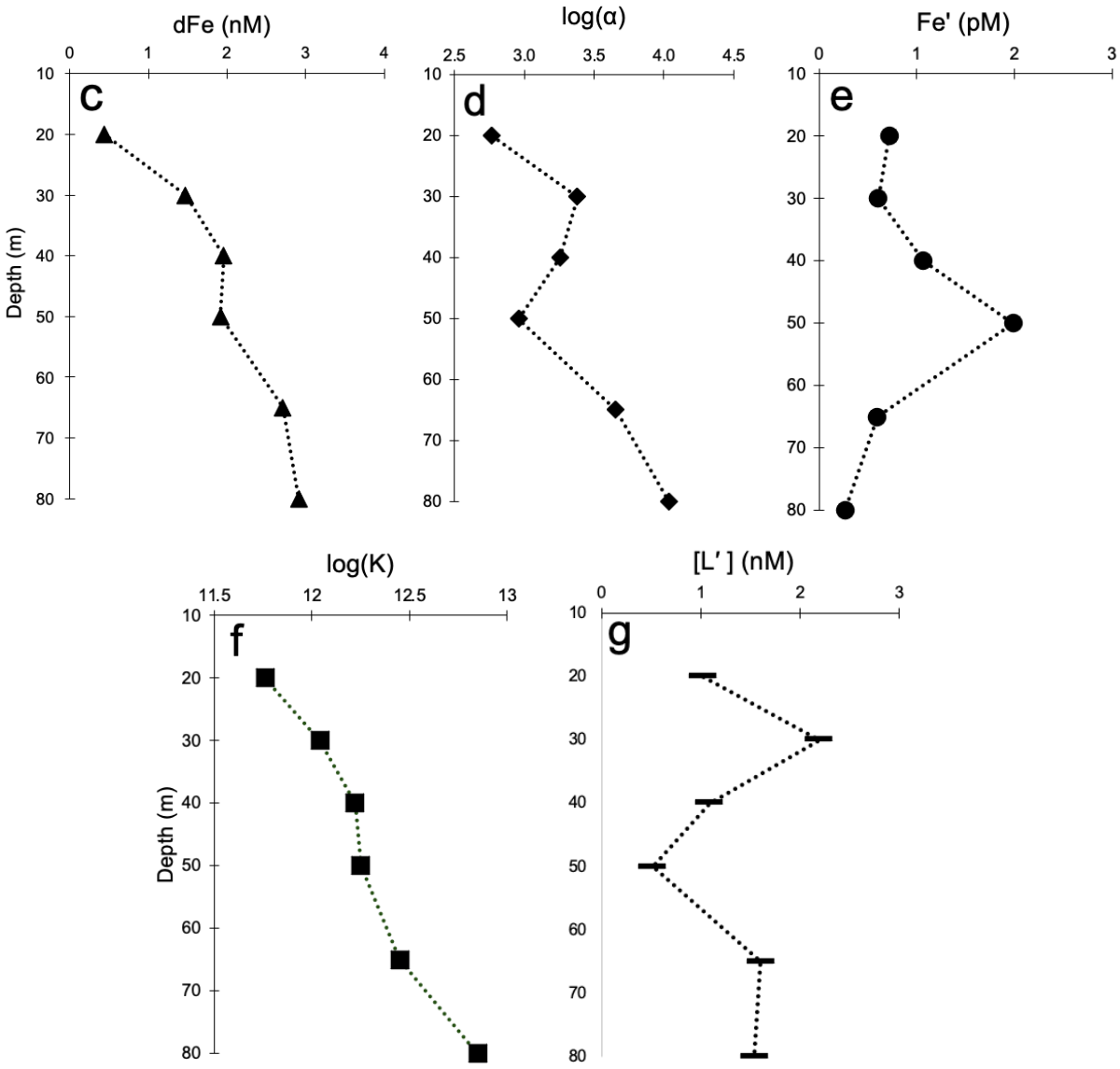

Figure 3.8, continued: Depth profiles of total dissolved Fe concentration **(c)**, excess ligand complexation capacity **(d)**, soluble inorganic Fe concentration **(e),** thermodynamic binding constant **(f)**, and excess ligand binding site concentration **(g)** collected from the pumped seawater profile at the Test Cast station during cruise P2507. K and α refer to conditional constants $K^{cond}_{FeL(Fe')}$ and $\alpha_{FeL(Fe')}$ respectively. [L′] = [L_{total}] – dFe, and refers to the concentration of excess (unbound) ligands.

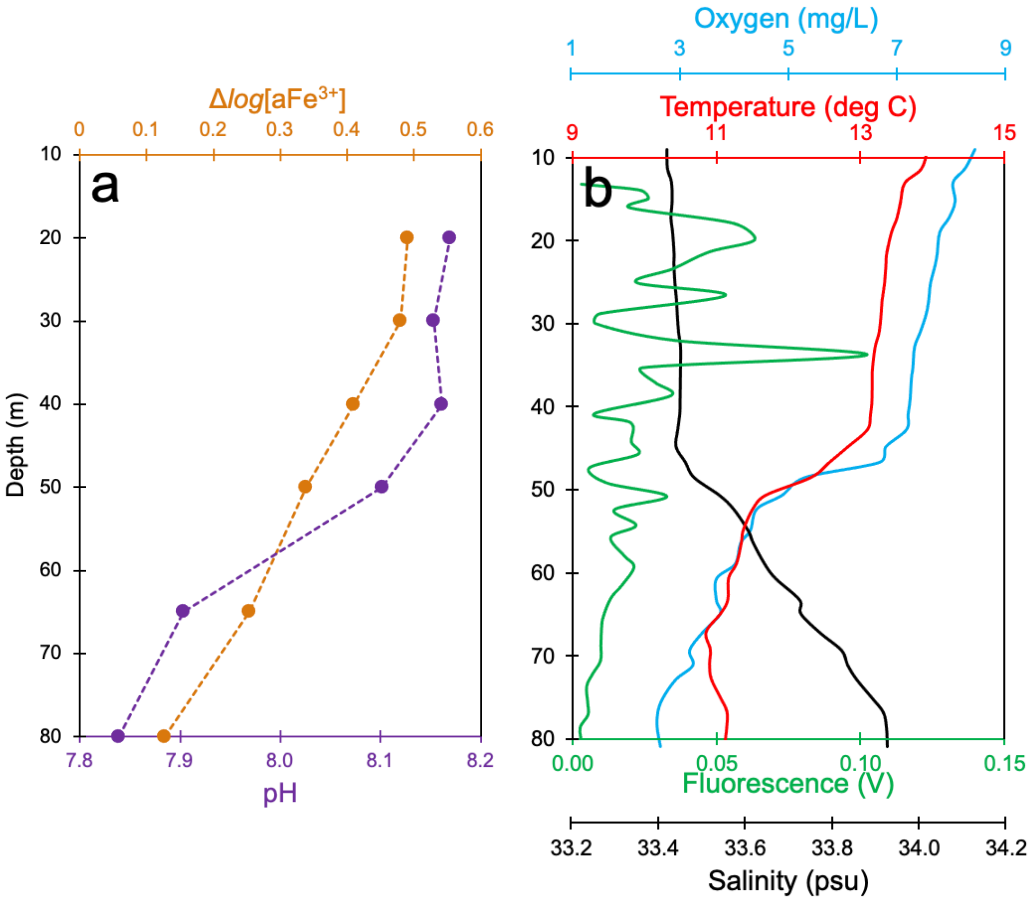

Figure 3.9: a) Fe-ISE CFA measurements from pumped depth profile and **b)** CTD rosette sensor data at the SPOT 0800 cast during cruise P2507.

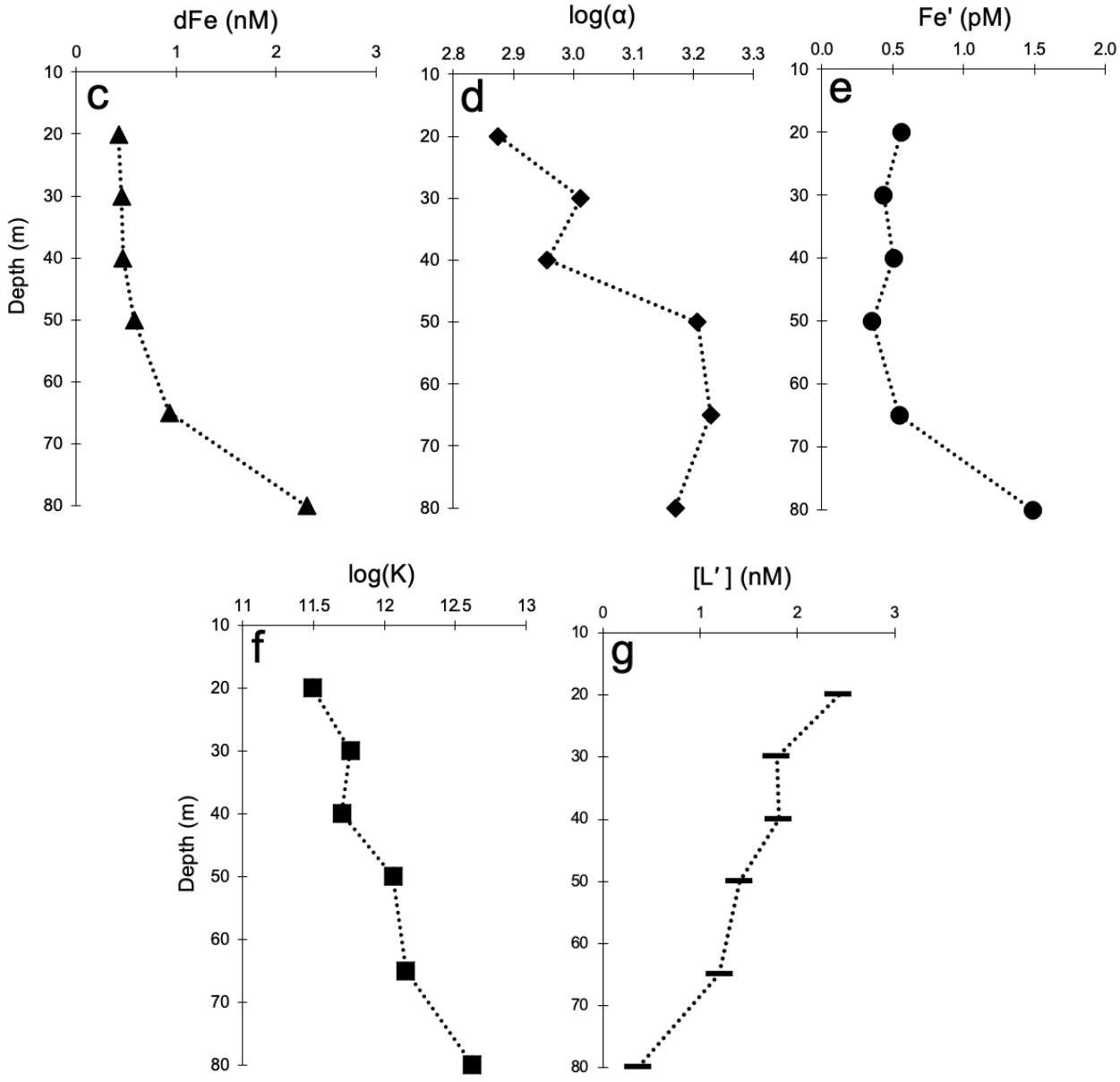

Figure 3.9, continued: Depth profiles of total dissolved Fe concentration **(c)**, excess ligand complexation capacity **(d)**, soluble inorganic Fe concentration **(e),** thermodynamic binding constant **(f)**, and excess ligand binding site concentration **(g)** collected from the pumped seawater profile at SPOT at 0800 during cruise P2507.

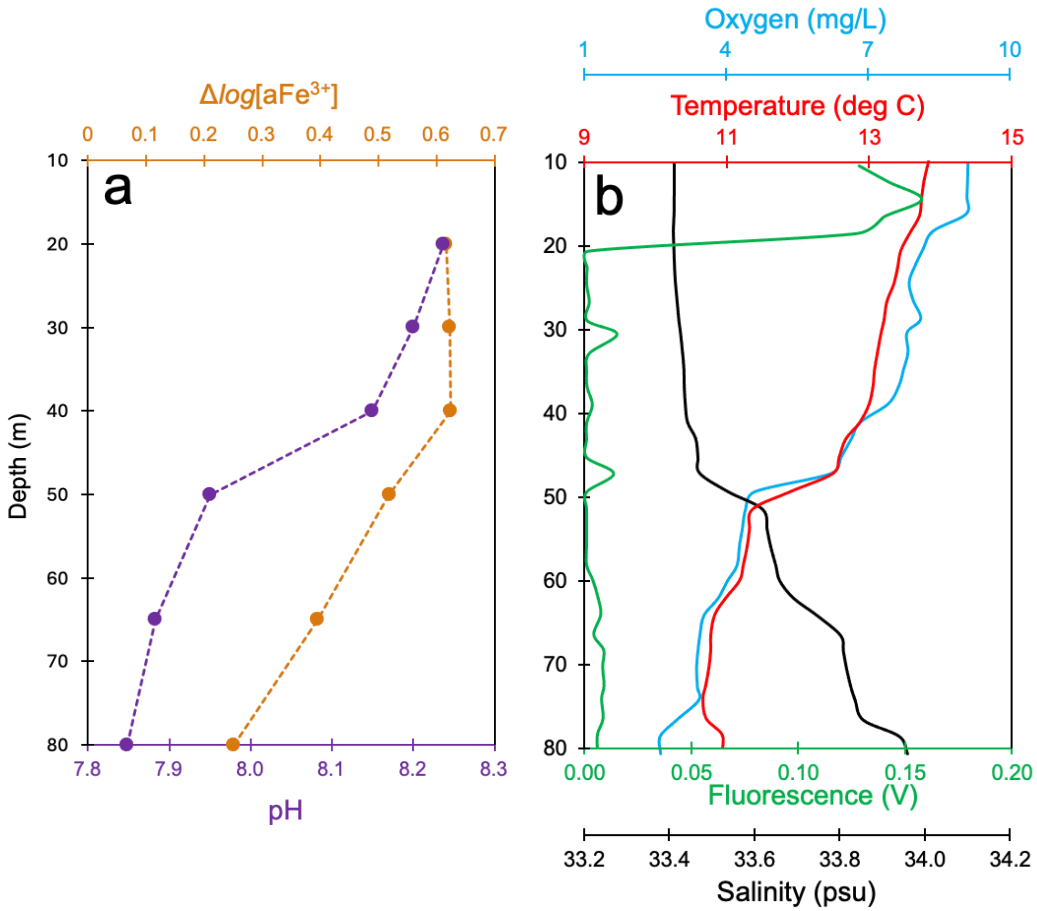

Figure 3.10: a) Fe-ISE CFA measurements from pumped depth profile and **b)** CTD rosette sensor data at the SPOT 1700 cast during cruise P2507.

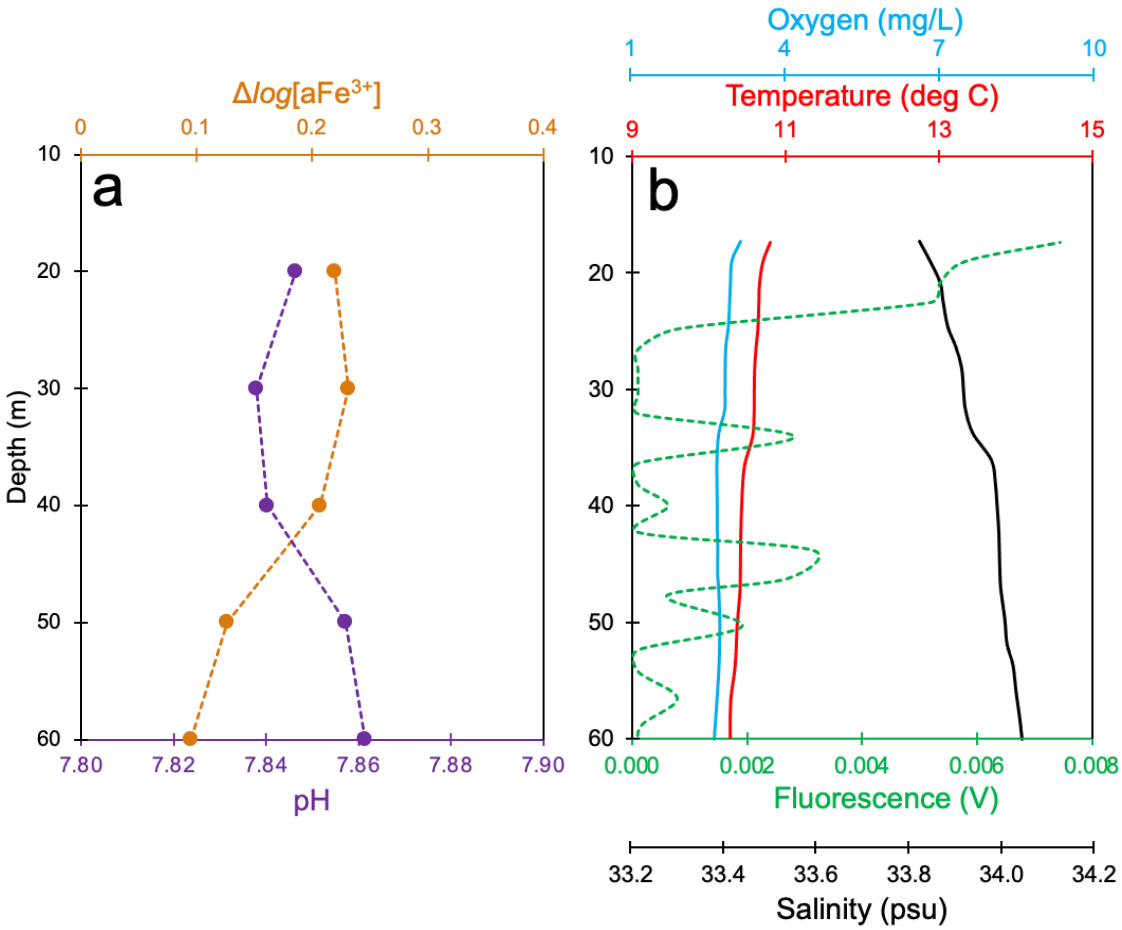

Figure 3.11: a) Fe-ISE CFA measurements from pumped depth profile and **b)** CTD rosette sensor data at the LA Nearshore 0800 cast during cruise P2507.

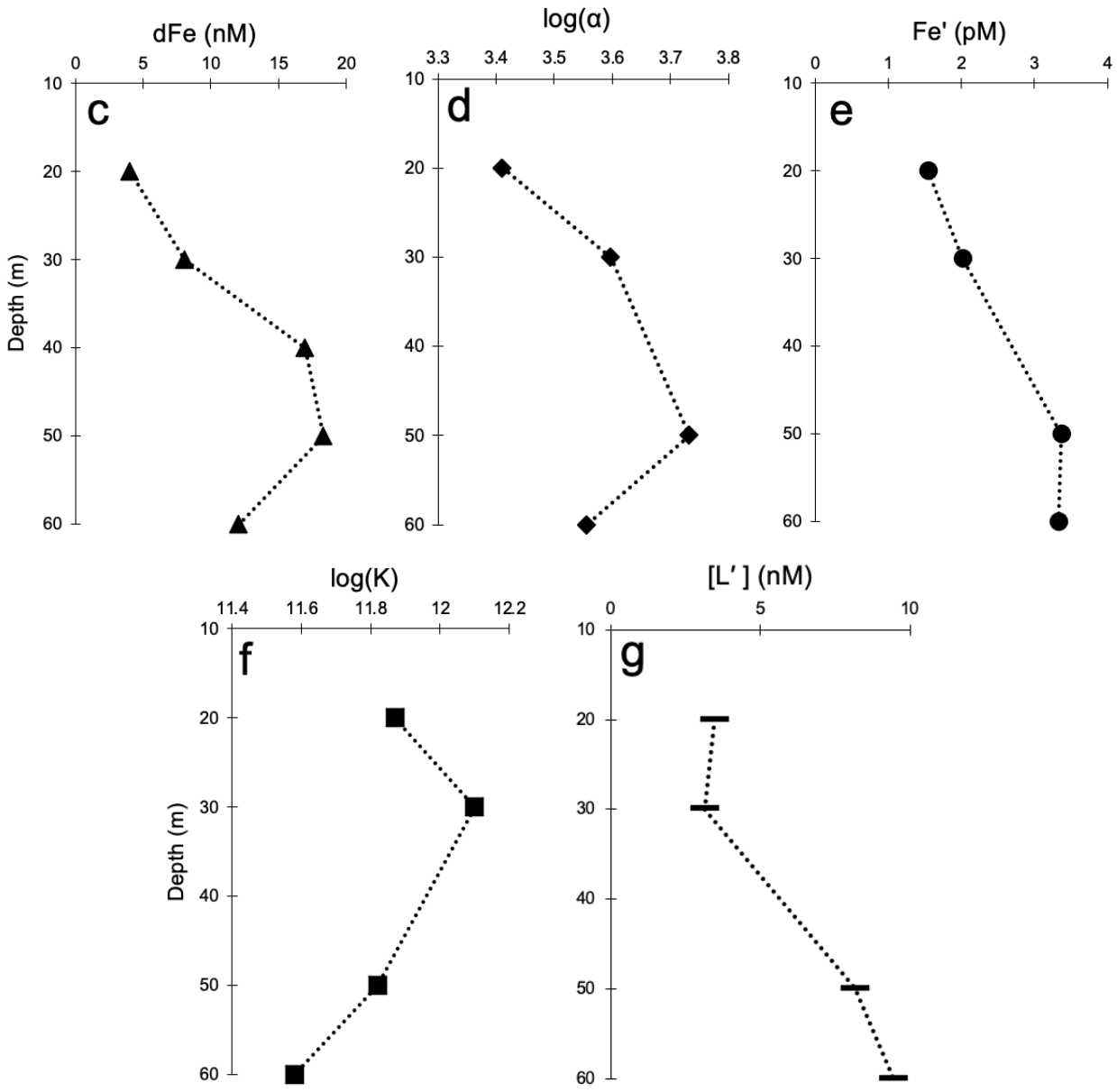

Figure 3.11, continued: Depth profiles of total dissolved Fe concentration **(c)**, excess ligand complexation capacity **(d)**, soluble inorganic Fe concentration **(e),** thermodynamic binding constant **(f)**, and excess ligand binding site concentration **(g)** collected from the pumped seawater profile at the LA Nearshore station at 0800 during cruise P2507.

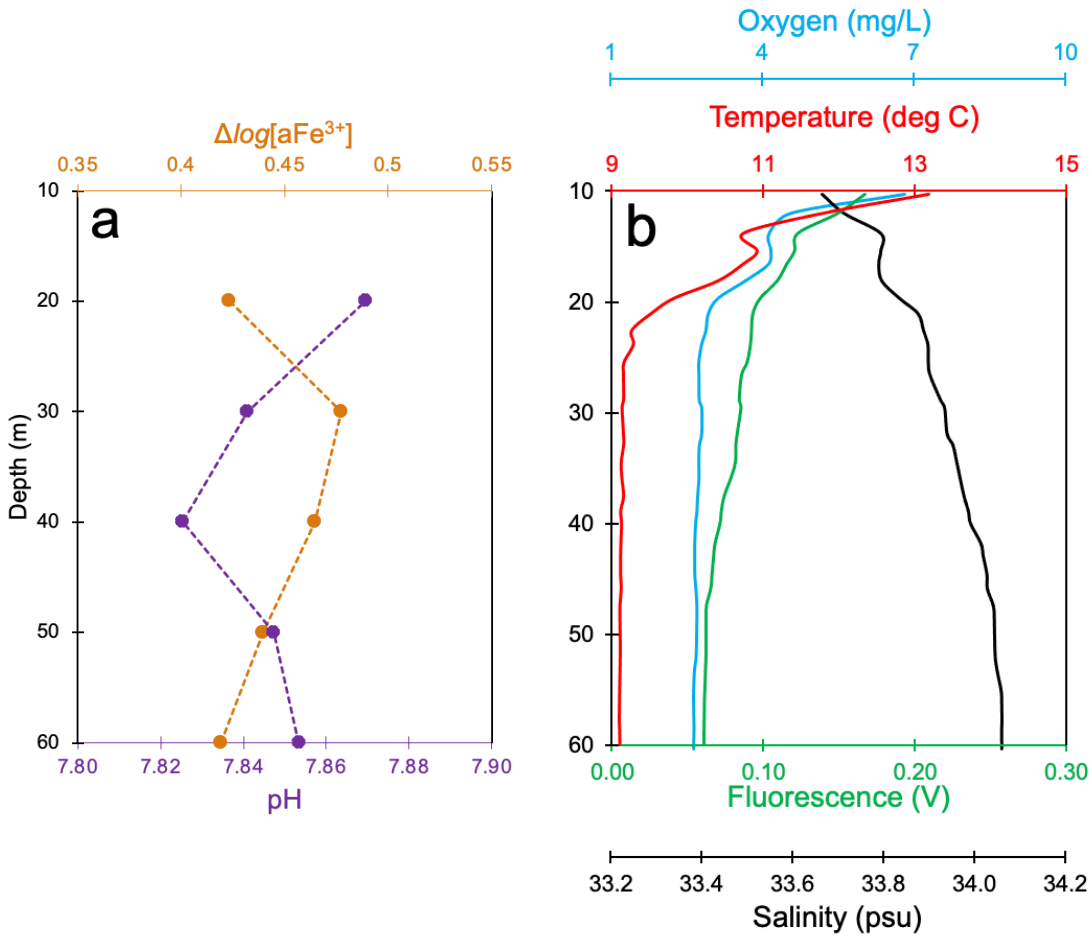

Figure 3.12: a) Fe-ISE CFA measurements from pumped depth profile and **b)** CTD rosette sensor data at the LA Nearshore 1700 cast during cruise P2507.

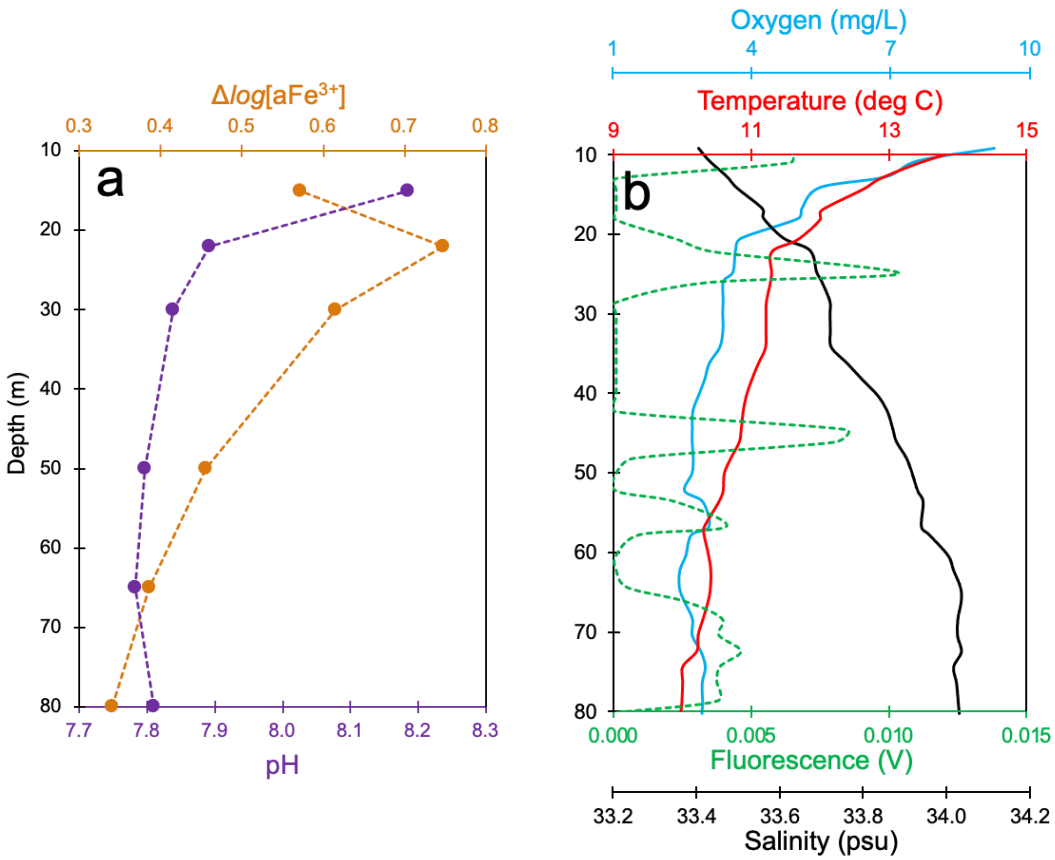

Figure 3.13: a) Fe-ISE CFA measurements from pumped depth profile and **b)** CTD rosette sensor data at the Scripps Canyon cast during cruise P2507.

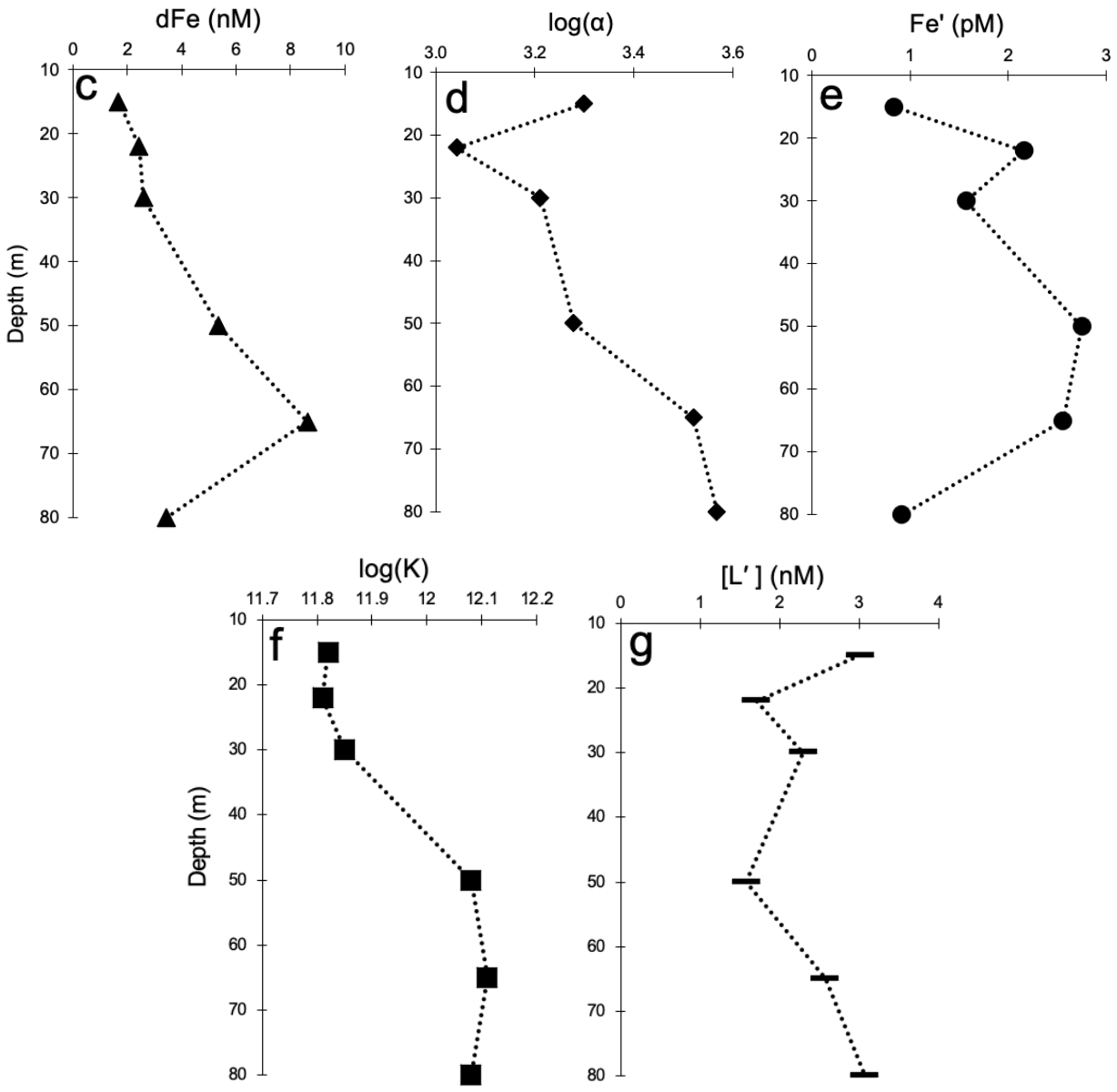

Figure 3.13, continued: Depth profiles of total dissolved Fe concentration **(c)**, excess ligand complexation capacity **(d)**, soluble inorganic Fe concentration **(e),** thermodynamic binding constant **(f)**, and excess ligand binding site concentration **(g)** collected from the pumped seawater profile at Scripps Canyon during cruise P2507.

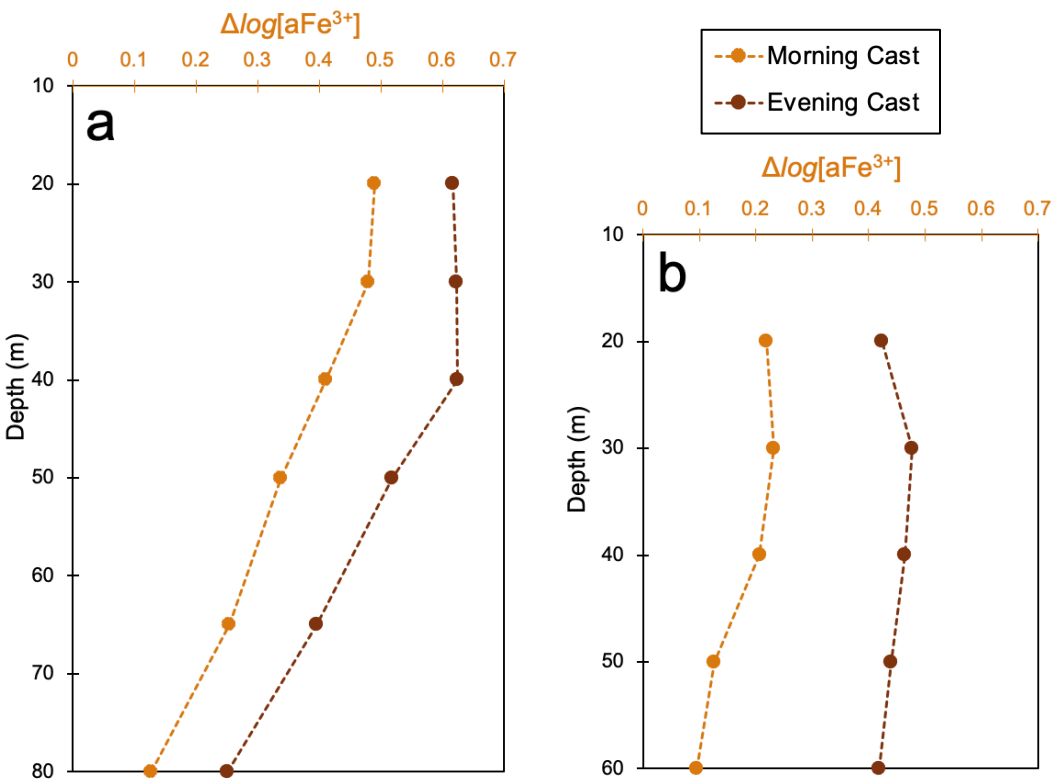

Figure 3.14: Δlog(aFe^{3+}) depth profiles at SPOT **(a)** and the LA Nearshore station **(b)** measured in the morning (0800, orange) and in the evening (1700, brown).

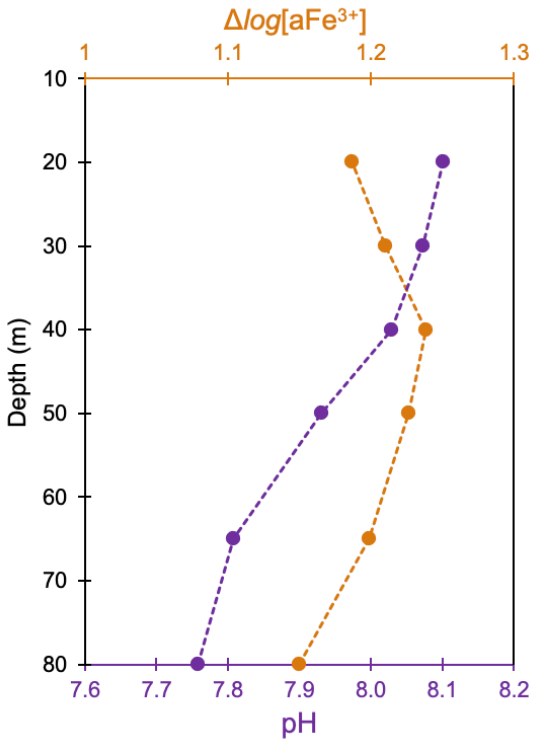

Figure 3.15: Fe-ISE CFA measurements of bottle samples from SPOT 0800 cast (compare to Figure 3.10), samples stored at room temperature and ambient light for 5 hours and measured at 1400.

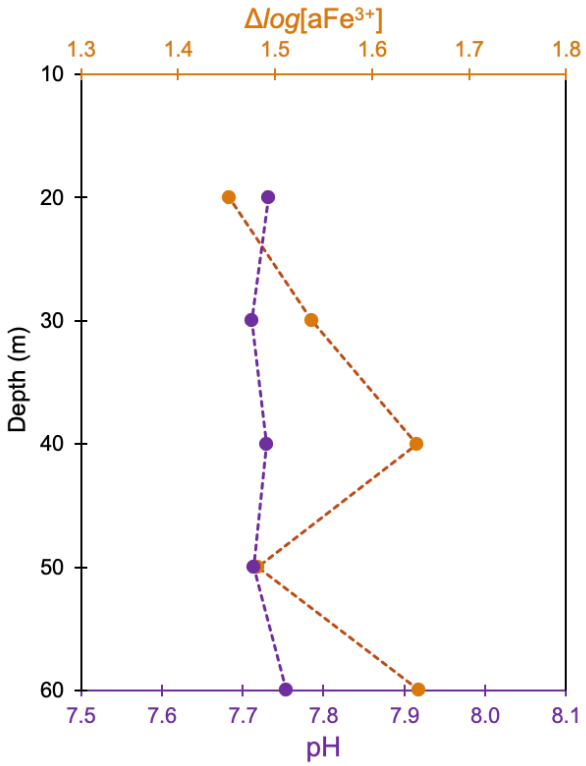

Figure 3.16: Fe-ISE CFA measurements of bottle samples from LA Nearshore 0800 cast (compare to Figure 3.12), samples stored at room temperature and ambient light for 5 hours and measured at 1400.

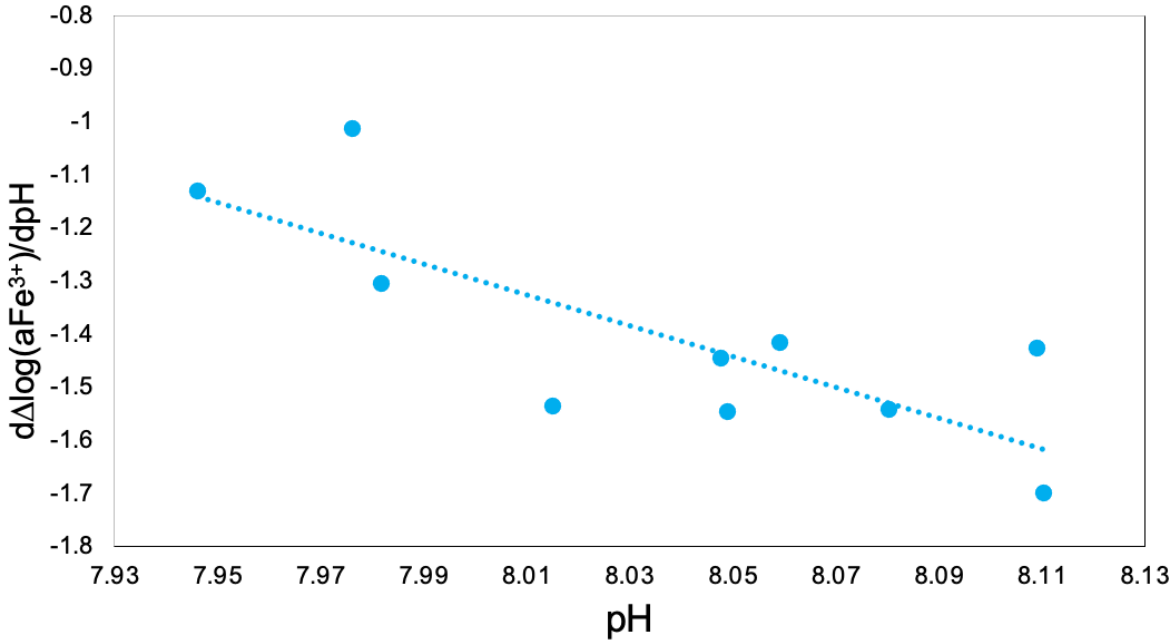

Figure 3.17: Ratio of change in $\Delta\log(aFe^{3+})$ to change in pH plotted vs mean pH for ten features throughout the Pupcycle II May 31st – June 1st overnight transect where $\Delta\log(aFe^{3+})$ and pH appeared tightly coupled.

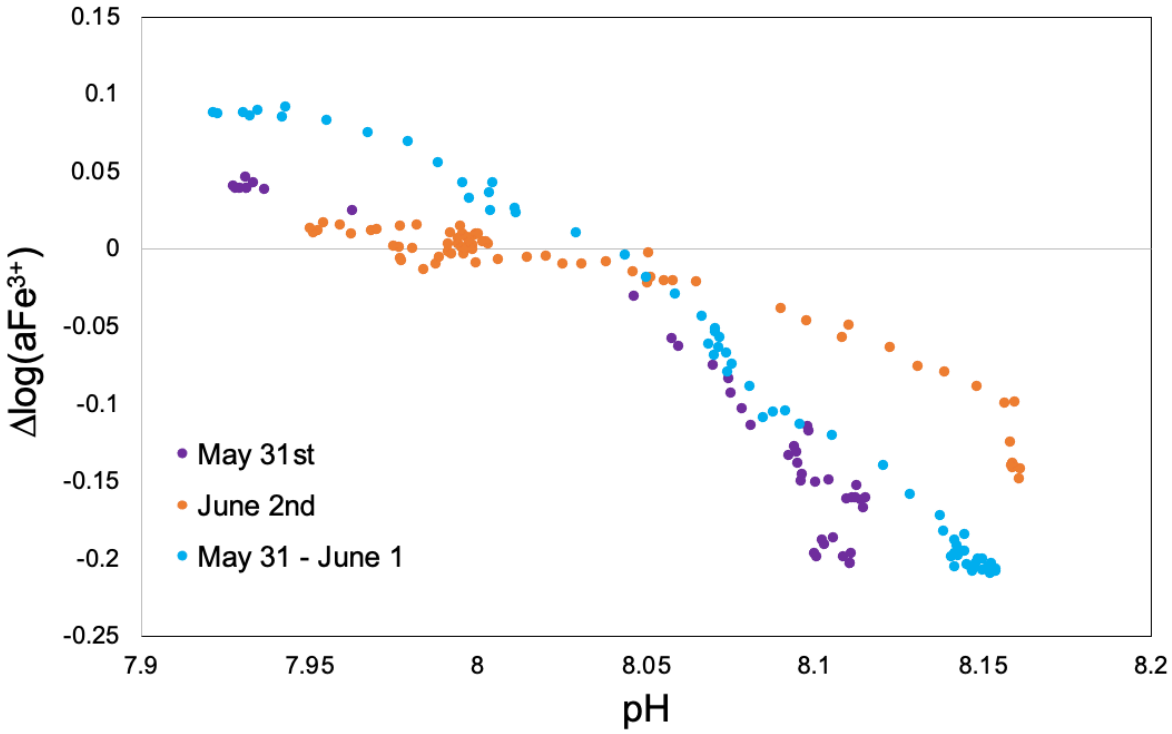

Figure 3.18: $\Delta\log(aFe^{3+})$ plotted against pH for specific features where pH appeared to be the dominant driver of changes in $\Delta\log(aFe^{3+})$, during three different transects during the Pupcycle II cruise.

Appendix

Supplemental Pupcycle Transect Figures

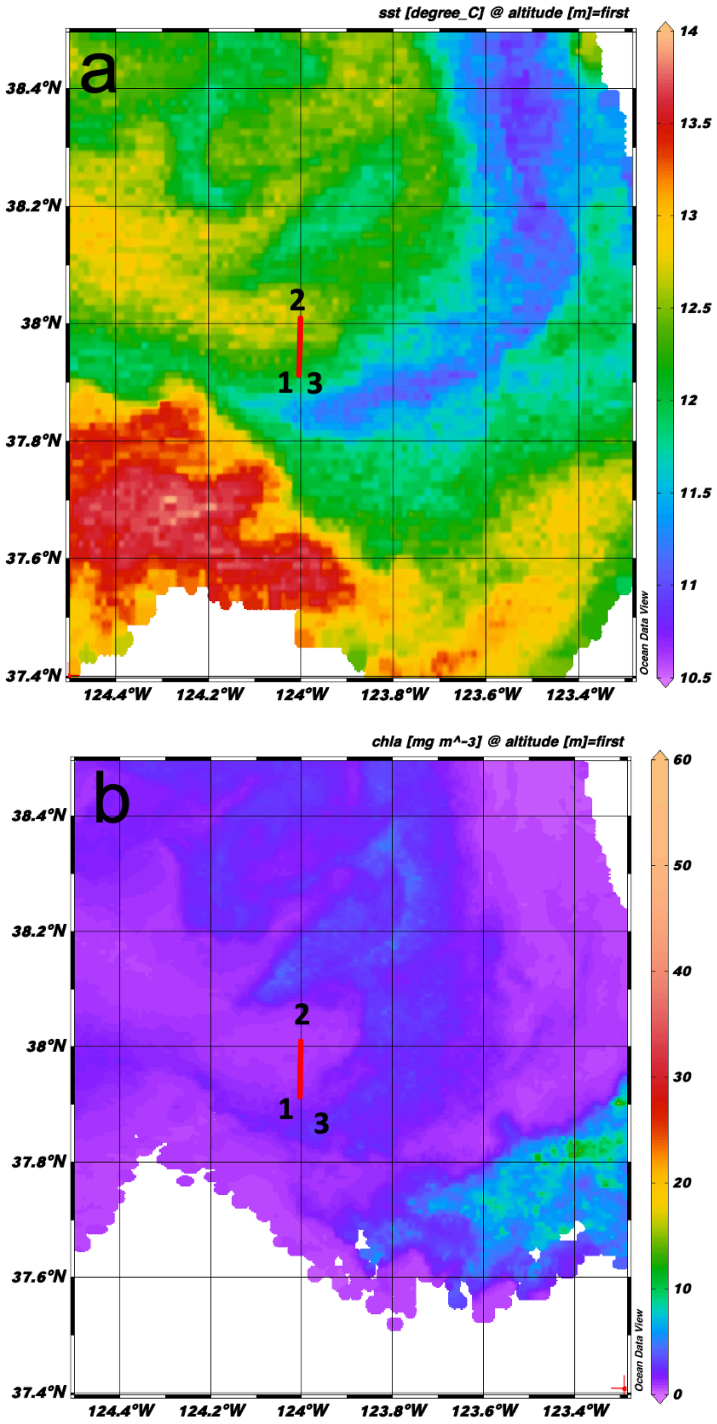

Figure 3.A1: Path for Pupcycle II transect taking place June 6th, overlayed on NOAA Coast Watch satellite imagery of sea surface temperature **(a)** and chlorophyll a **(b)**.

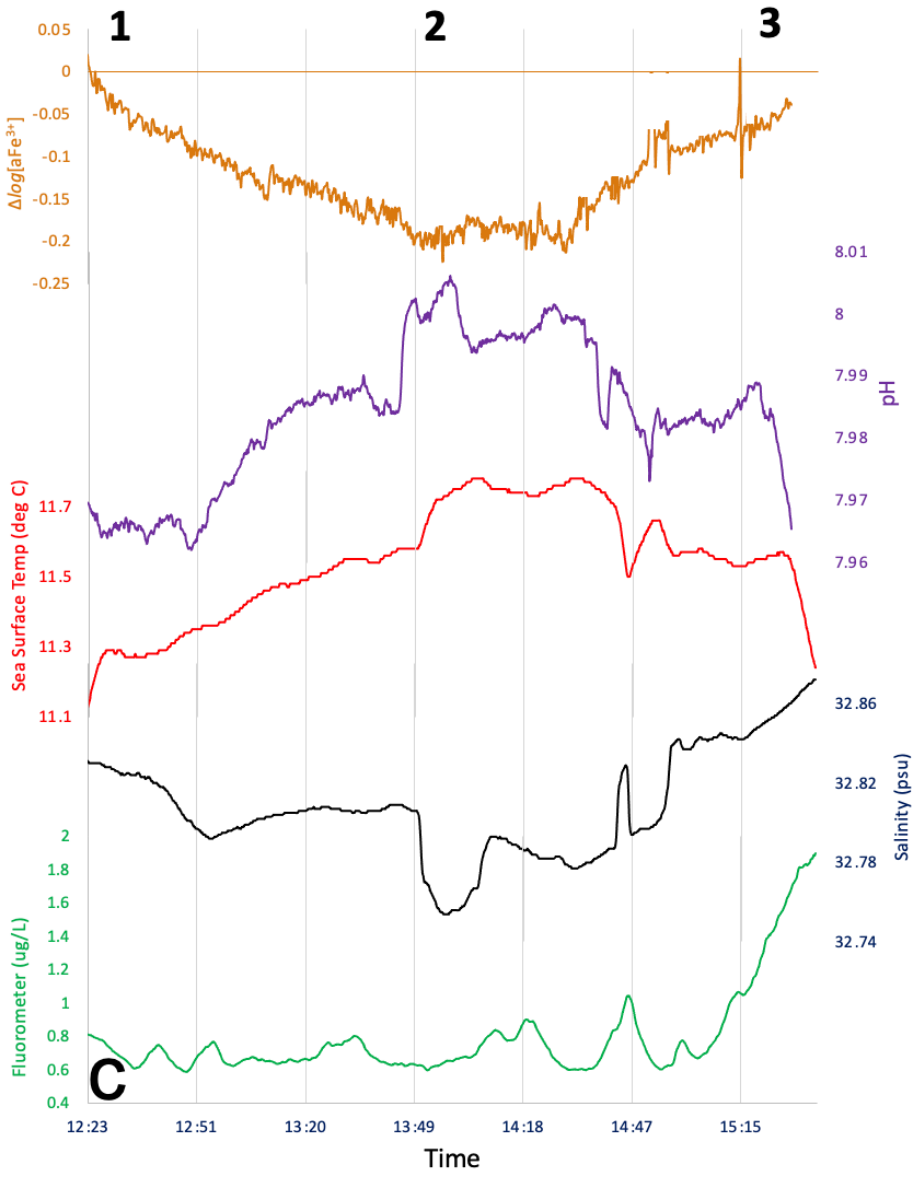

Figure 3.A1, continued: c) Fe-ISE CFA and R/V Sally Ride seawater flow-through sensor measurements over the course of the transect, with numbered time points corresponding to numbered locations in **a**, **b**.

Supplemental Field Data – CCE LTER Process Cruise P2402

During the winter of 2024, additional Fe-ISE field tests were carried out during the California Current Ecosystem (CCE) Long-term Ecological Research project (LTER) process cruise on the R/V Roger Revelle. This cruise took place from February to March 2024, and entailed several multi-day Lagrangian studies (cycles), tracking a variety of water parcels using low-profile floating drift arrays and sediment traps. While all cycles included daily trace metal rosette vertical profiles for standard trace metal analyses, the Fe-ISE CFA system was also used for analyses of discrete bottle samples at certain stations (Figure 3.A2).

Trace metal clean samples for dFe and CLE-AdCSV Fe-speciation analyses were sampled from Teflon-coated X-Niskin bottles on a powder-coated rosette, deployed on a coated hydrowire. Fe samples were handled in a Class 100 trace metal clean van and filtered in-line using acid-washed Teflon tubing and acid-washed 0.2 µm Acropak-200 capsule filters pressurized by filtered air. Samples were handled and analyzed as described in **Experimental** (see **Trace-Metal Clean Seawater Collection** and **Laboratory Determination of dFe and Fe-L Parameters of Seawater**).

Filtered samples were also collected from X-Niskins for subsequent analysis on the Fe-ISE CFA system in acid-clean 500 mL fluorinated high-density polyethylene (FLPE) bottles, and stored at room temperature for 4 – 5 hours. At the time of analysis, each sample was circulated through the Fe-ISE CFA system until a stable Fe-ISE potential was reached (<0.15 mV/min). The Fe-ISE was conditioned before and between analyses as described in **Experimental**, but using filtered seawater rather than unfiltered. The Fe-ISE was calibrated using B5 modified offshore seawater, and all data was processed as in **Experimental**. Plotted values of $\Delta\log(aFe^{3+})$ in subsequent Figures are referenced to the lowest $\log(aFe^{3+})$ value measured at

each cycle. In-situ temperature and salinity were measured using the trace metal rosette CTD (SBE19plus V2, Seabird electronics).

We point out several notable features of these depth profiles, especially as they relate to the P2507 data in the main body of this work. First, aFe^{3+} and pH are directly correlated in Cycles 2 through 4 (Figures 3.A4 to 3.A7), matching the trends of most of the P2507 profiles. Although the P2402 profiles were measured as discrete samples, strong aFe^{3+} gradients remained until Fe-ISE analysis, unlike the P2507 discrete samples (Figures 3.16, 3.17). It may be that deeper profiles of P2402 spanned larger overall gradients, or that the act of filtering limits the aFe^{3+} changes which were observed in the unfiltered P2507 bottle samples. Second, notable exceptions to this aFe^{3+}/pH coupling occur at Santa Barbara Basin (Figure 3.A3) and in Cycle 5 (Figure 3.A8, 3.A9), where aFe^{3+} and pH are *inversely* correlated and we observe aFe^{3+} minima at the surface. Santa Barbara Basin is a known benthic source of dissolved and particulate Fe (Robinson et al. 2024), which may be related to the deep-water aFe^{3+} maximum. We also note that these stations, particularly those of Cycle 5, were located in considerably more productive waters than Cycles 2 through 4. Perhaps aFe^{3+} measurements of a filtered seawater fraction are more sensitive the Fe-chelating effects of biologically produced siderophores in the surface ocean. Trends in CLE-AdCSV data are less pronounced than that of P2507 depth profiles, but this may be due to operational adjustments (increases to FeSA complex deposition time throughout profile analyses) made to P2402 samples to accommodate decreased voltammetric sensitivity in deeper samples. Multiple analytical window analyses would better capture larger gradients in ligand complexation capacity with depth.

P2402 Figures

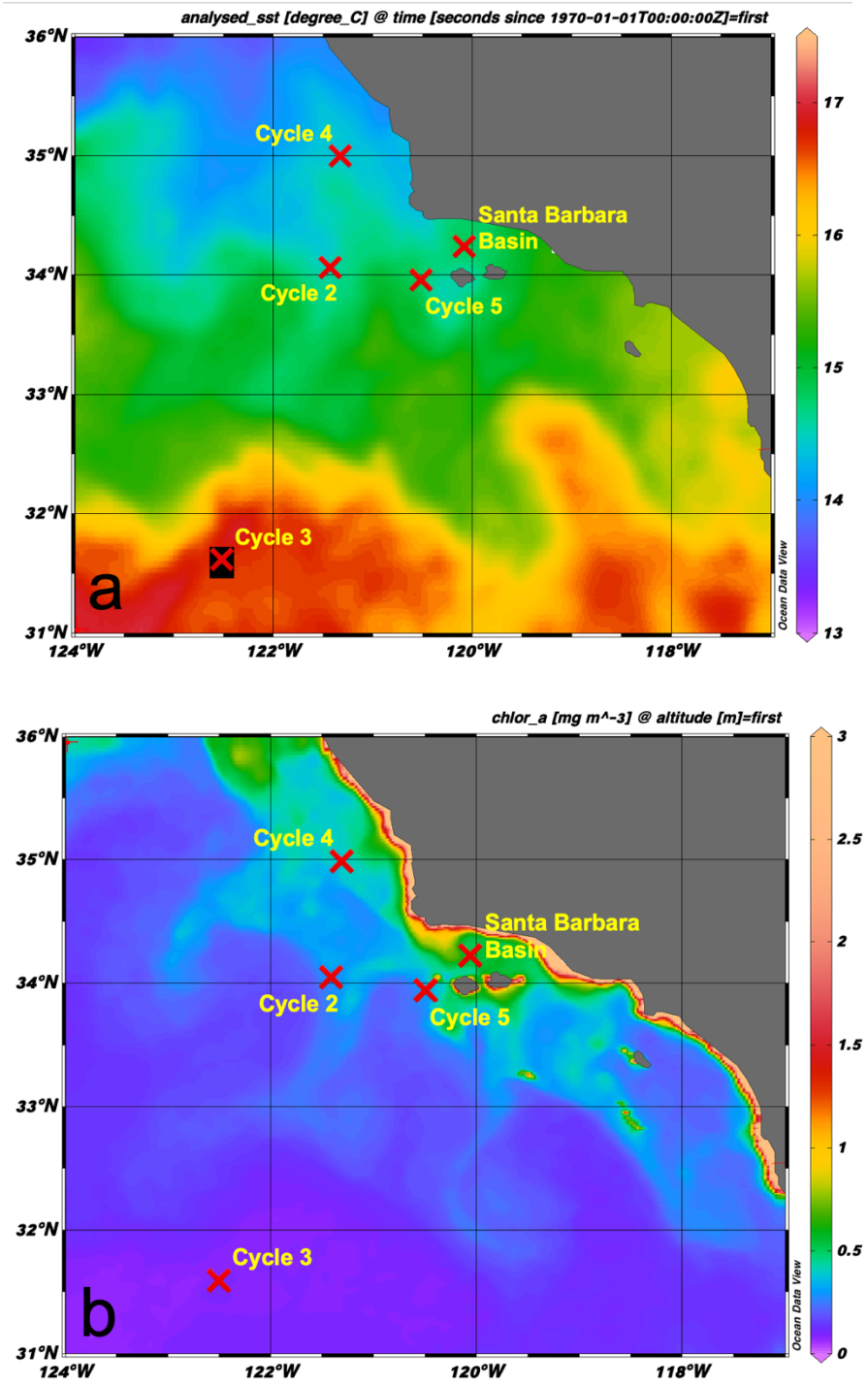

Figure 3.A2: P2402 cycle locations where Fe-ISE discrete bottle analyses were conducted for trace metal vertical profiles, overlayed on NOAA satellite imagery of sea surface temperature **(a)** and chlorophyll a **(b)**.

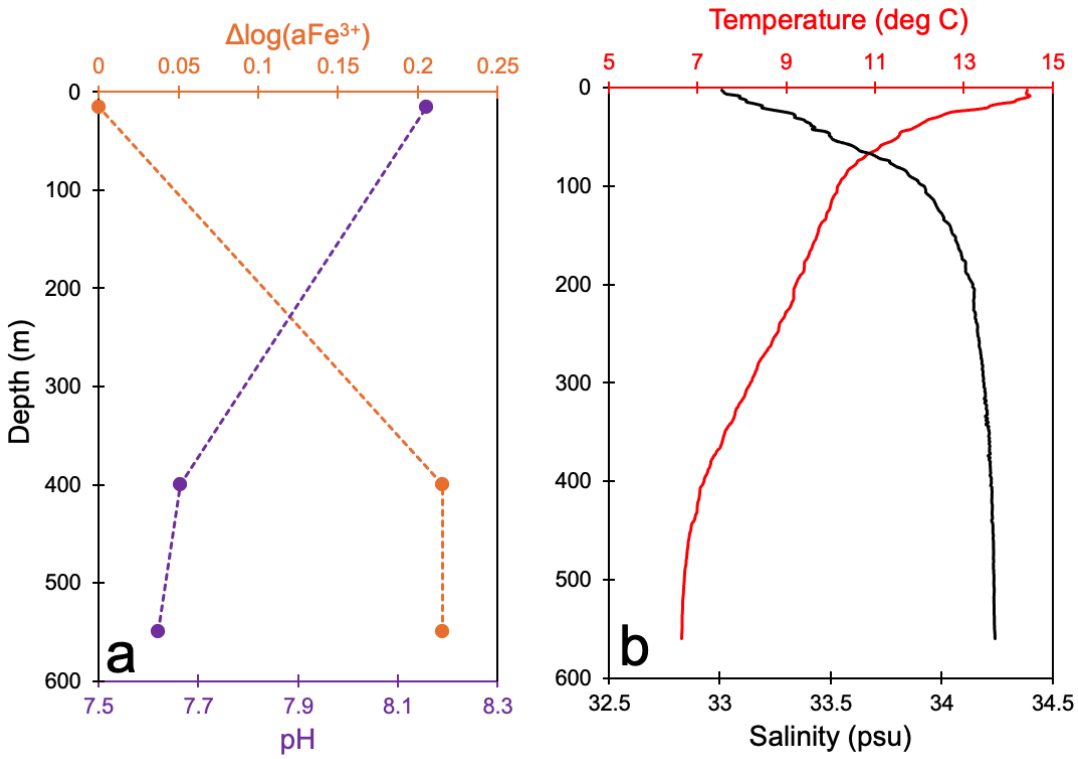

Figure 3.A3: a) Fe-ISE CFA measurements of bottle samples and **b)** CTD rosette sensor data for vertical profile at Santa Barbara Basin (Feb 24th).

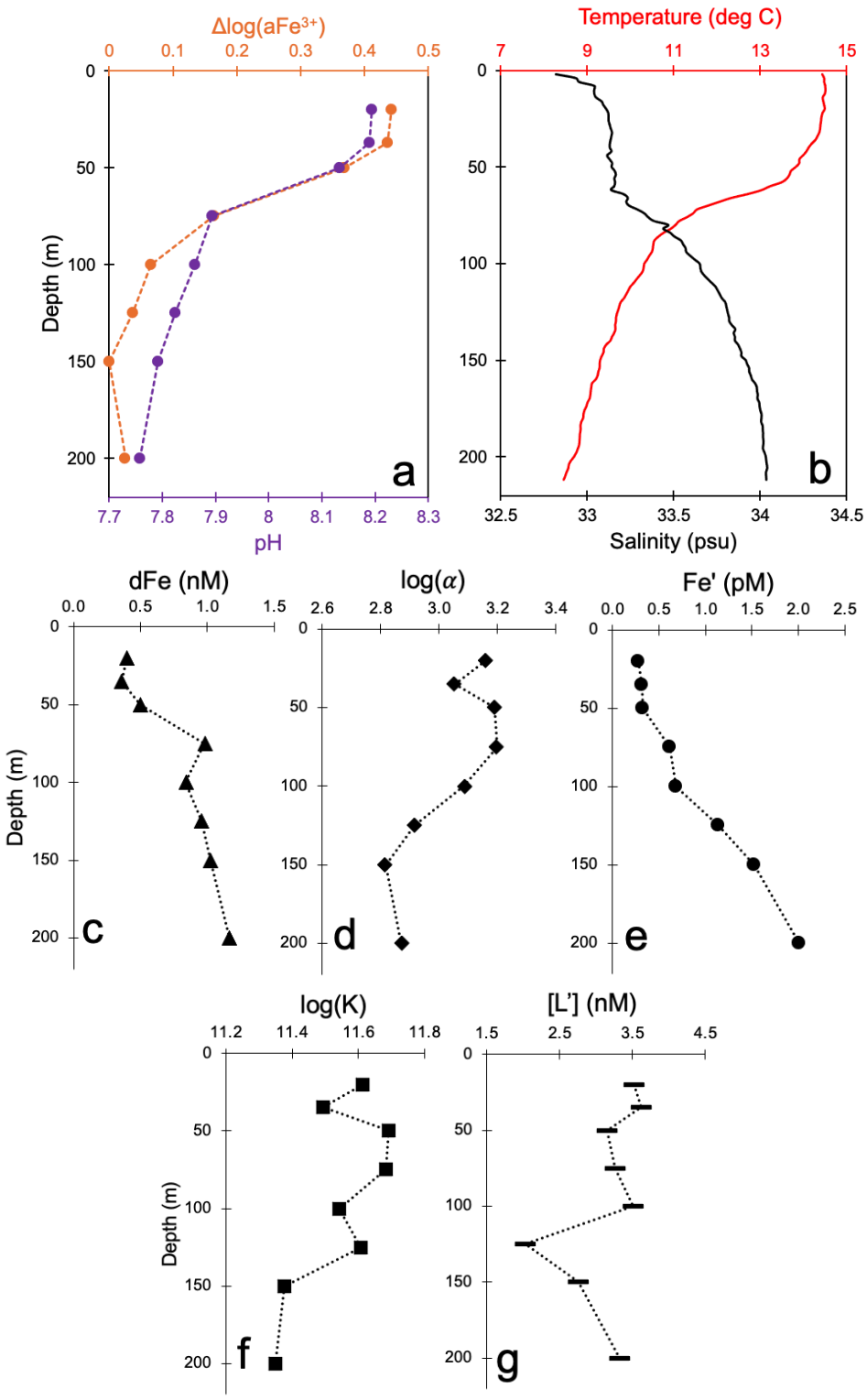

Figure 3.A4: Fe-ISE CFA measurements **(a)**, CTD rosette sensor data **(b),** total dissolved Fe concentration **(c)**, excess ligand complexation capacity **(d)**, soluble inorganic Fe concentration **(e),** thermodynamic binding constant **(f)**, and excess ligand binding site concentration **(g)** for vertical profile during Cycle 2, day 4 (Feb 27th).

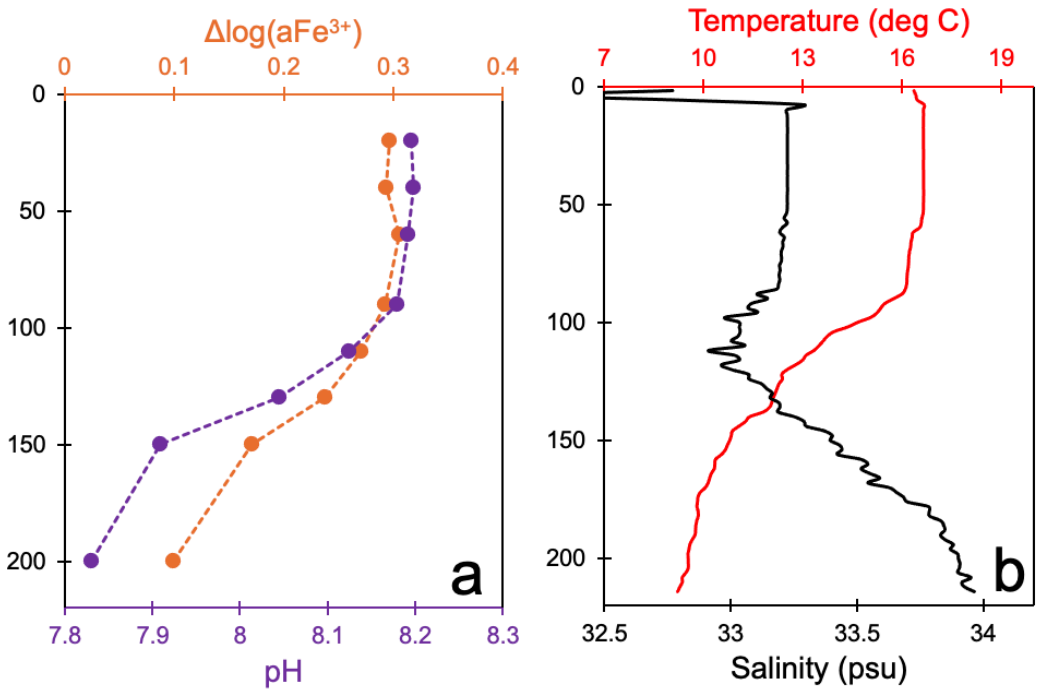

Figure 3.A5: a) Fe-ISE CFA measurements of bottle samples and **b)** CTD rosette sensor data for vertical profile during Cycle 3, day 4 (March 3rd).

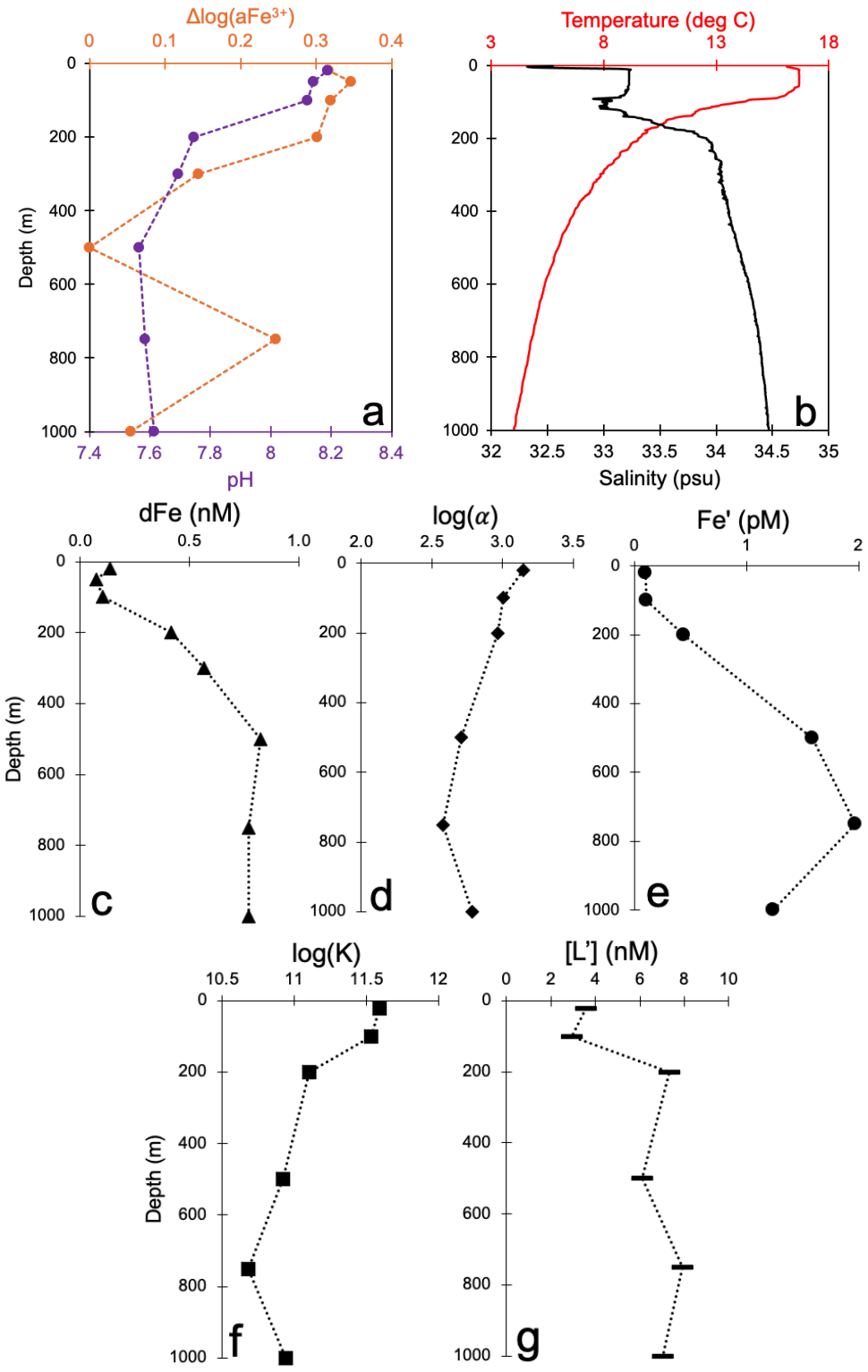

Figure 3.A6: Fe-ISE CFA measurements **(a)**, CTD rosette sensor data **(b),** total dissolved Fe concentration **(c)**, excess ligand complexation capacity **(d)**, soluble inorganic Fe concentration **(e),** thermodynamic binding constant **(f)**, and excess ligand binding site concentration **(g)** for vertical profile during Cycle 3, day 5 (March 4th).

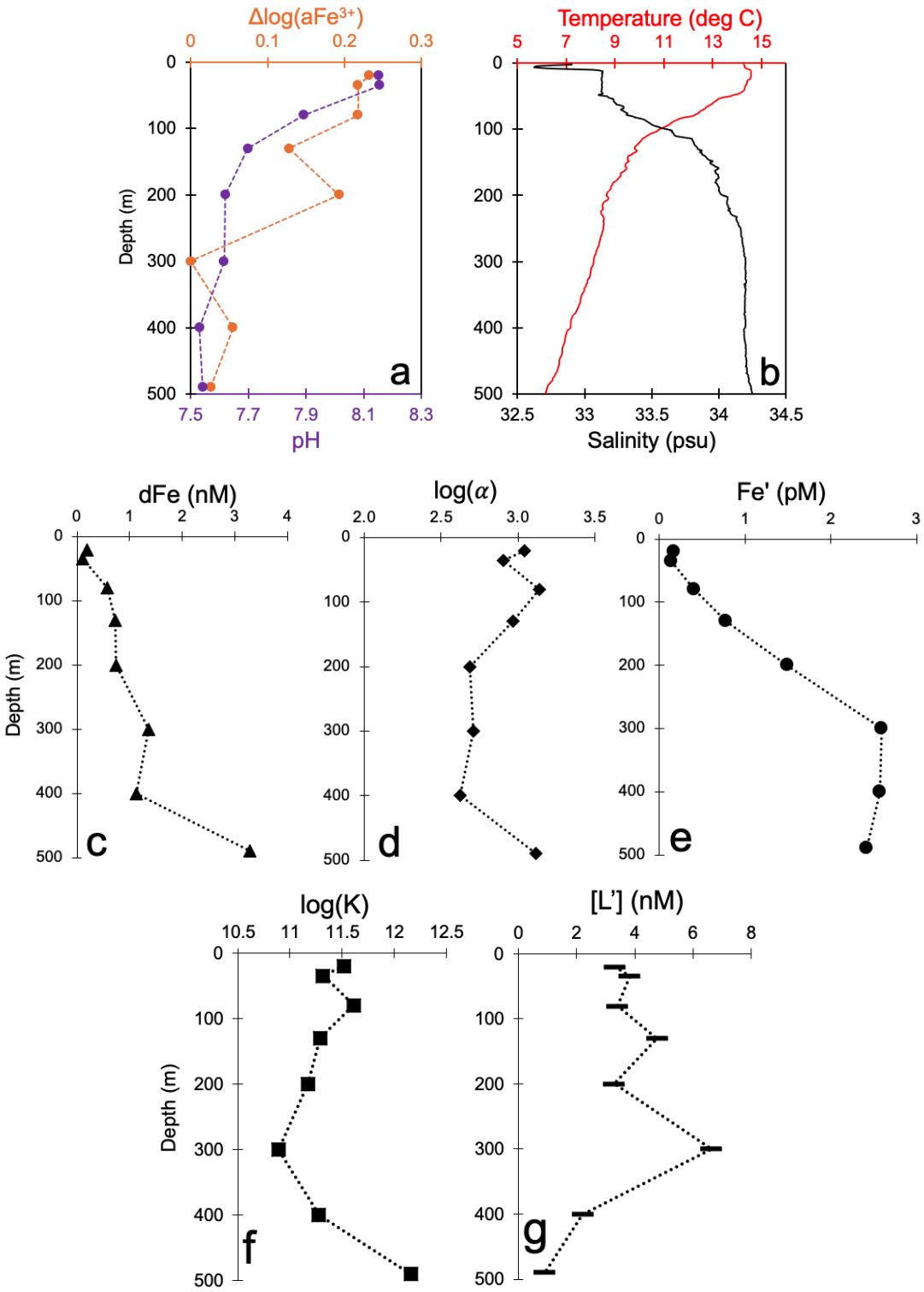

Figure 3.A7: Fe-ISE CFA measurements **(a)**, CTD rosette sensor data **(b),** total dissolved Fe concentration **(c)**, excess ligand complexation capacity **(d)**, soluble inorganic Fe concentration **(e),** thermodynamic binding constant **(f)**, and excess ligand binding site concentration **(g)** for vertical profile during Cycle 4, day 1 (March 6th).

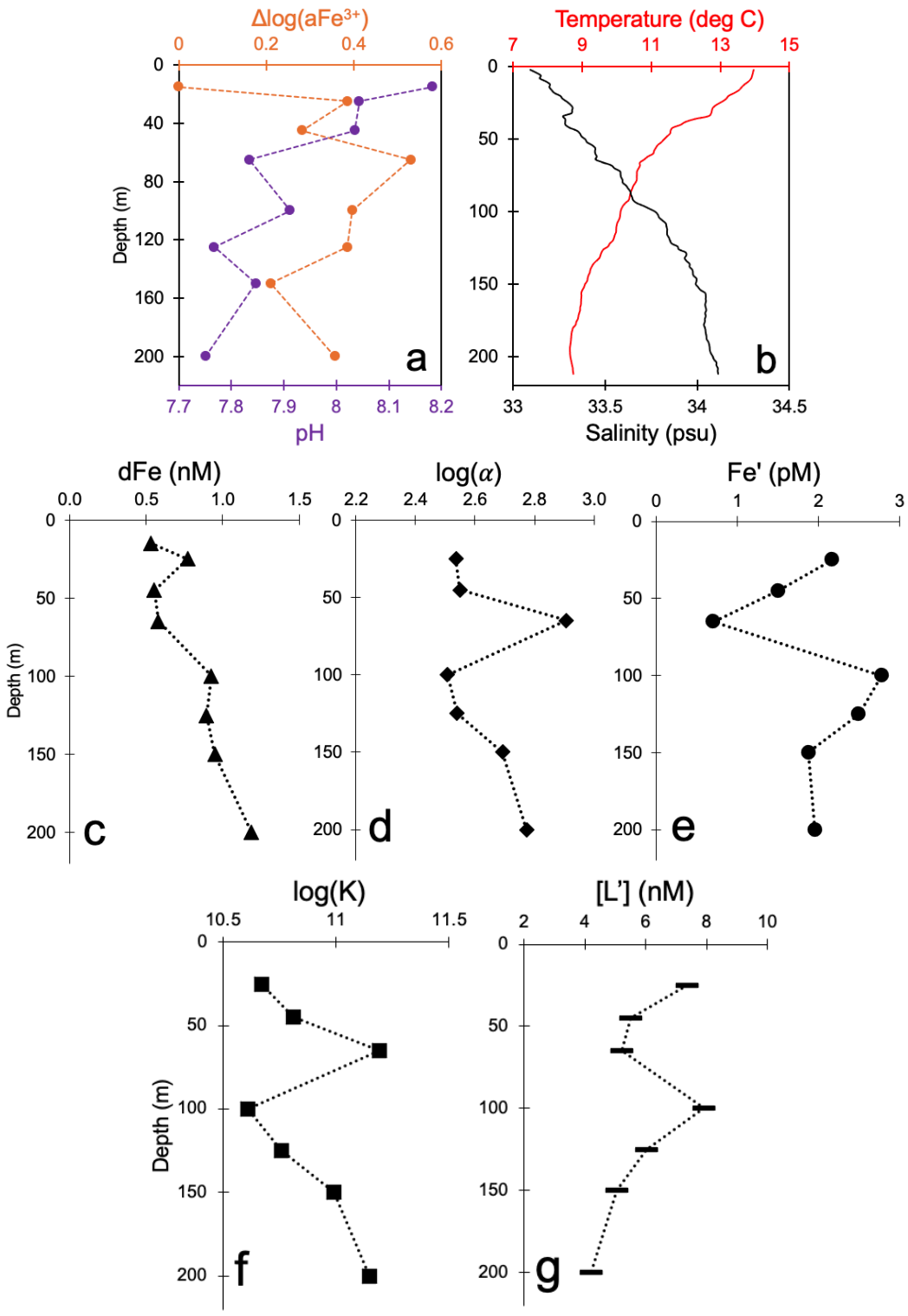

Figure 3.A8: Fe-ISE CFA measurements **(a)**, CTD rosette sensor data **(b),** total dissolved Fe concentration **(c)**, excess ligand complexation capacity **(d)**, soluble inorganic Fe concentration **(e),** thermodynamic binding constant **(f)**, and excess ligand binding site concentration **(g)** for vertical profile during Cycle 5, day 4 (March 16th).

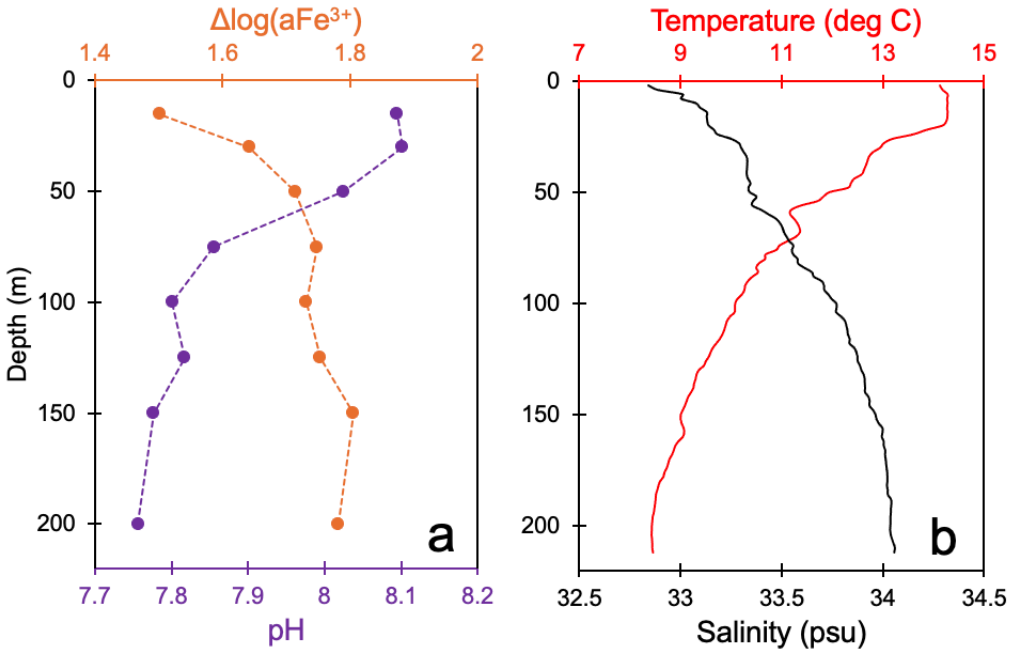

Figure 3.A9: a) Fe-ISE CFA measurements of bottle samples and **b)** CTD rosette sensor data for vertical profile during Cycle 5, day 5 (March 17th).

Conclusion

The Fe-ISE motivates us to think about Fe chemistry in an entirely new way. The chalcogenide glass matrix is electrochemically sensitive to the Fe^{3+} ion gradient at its surface. In Fe-donating solutions, which in the context of the chalcogenide Fe-ISE are limited to acidic solutions of supra-micromolar Fe concentrations, the sensor detects an “Fe-pressure” from the tendency of ions to migrate into the glass – measured as a positive electrochemical potential. Strongly Fe-chelating aqueous solutions, such as natural seawater, however, impart what is essentially an “Fe-suction” on the glass surface layers – an electromotive force pulling mobile Fe^{3+} ions from the electrode. Initial conditioning in such solutions quickly depletes the glass’s outermost surface layers of Fe in a natural balancing of the ionic differential across the membrane-solution interface. Though this differential never disappears, it does reach an equilibrium where further Fe^{3+} ionic migration becomes limited by an opposing electronic repulsion. The ionic-electronic equilibrium is quantified by the Nernst Equation, which relates Fe^{3+} ionic activity to measured voltage.

Free Fe^{3+} ion activity, (aFe^{3+}), does indeed appear to be well-correlated with Fe-ISE potential in a variety of aqueous media. But we emphasize that at the very low Fe activities of seawater, aFe^{3+} does not refer to any fraction of Fe. In theory, two seawater samples may both contain 0 total Fe, but could exhibit different potentiometric aFe^{3+} values due to differences in the aqueous species (organic chelators, hydroxide ions) which impart the Fe-suction at the chalcogenide surface, or due to thermodynamic variation affecting those species (pH, temperature). In this scenario, our model-derived picture of aFe^{3+}, calculated from a series of equilibrium binding constants, breaks down. There is no total Fe to be partitioned into various complexes, so we could not compute any free, un-complexed Fe^{3+} fraction for either sample. Yet the Fe-ISE would be able to quantify the strength of this Fe vacuum in each sample, measuring its tendency to attract any Fe if it *were* present. This is the magic of potentiometry.

We mention this as a reminder that thinking in terms of model-derived aFe^{3+} does not fully capture the meaning of the activity to which the Fe-ISE is sensitive. While model-derived aFe^{3+} does help parameterize the overall Fe-complexation capacity of strongly Fe-chelating systems, especially as they relate to one another, it is difficult to directly relate this value to any other empirically determined Fe or Fe-ligand variables. It is largely for this reason that we choose to report Fe-ISE measurements as Δ values, focusing on relative changes rather than any absolute values. It does appear that changes in modeled aFe^{3+} are remarkably well-correlated with changes in measured potentiometric activity (i.e. reproducible calibration slopes), in artificial systems and in both modified and natural seawater, as discussed in Chapters 1 and 2 of this work. Thus, we can standardize our measurements in a way that allows us to compare trends from one dataset to another.

The work in this dissertation attempted to provide a broad framework for interpreting Fe-ISE measurements of seawater. We began in Chapter 1 by examining the fundamental sensor response characteristics relevant for measurements in a dynamic oceanographic setting, such that a user could be confident in which aspects of their sensor signal were truly attributed to Fe activity, rather than simple artifacts of the analytical system. Chapter 2 expanded on the relationship between the Fe-ISE signal in seawater-based systems and aFe^{3+} as determined by aqueous speciation models, particularly in the context of pH. Optimal seawater-based Fe-ISE calibration was discussed, and we show the analytical value of Fe-ISE acidimetric titrations for assessing pH-dependent Fe-binding features of a seawater ligand pool. In Chapter 3, we used the knowledge gained from the laboratory studies of Chapters 1 and 2 to deploy the Fe-ISE as an oceanographic instrument. We presented shipboard measurements from several field expeditions, discussing trends in in-situ Fe activity observed in surface transects and vertical depth profiles. We found that the largest gradients in aFe^{3+} coincided with gradients in other in-situ hydrographic parameters (pH, salinity, temperature etc.), but could not always be explained

by those parameters alone, and aFe^{3+} correlations with these variables were often not the same when comparing surface patterns to that of depth profiles.

It is reassuring that Fe-ISE measurements can distinguish between water masses, as it suggests that the sensor is truly responding to in-situ differences. Our work in Chapters 1 and 2 attempt to establish that these differences are related to factors controlling overall Fe lability. While the binding strengths and concentrations of major Fe-chelators are certainly included in these factors, they are far from the only ones. Physico-chemical parameters such as pH, temperature, or solar irradiance, are well known to affect Fe-speciation, and the signature of these variables is clearly visible in an in-situ Fe-ISE measurement – unlike more ex-situ methods. Importantly, the Fe-ISE also appears to be responding to controls on Fe activity which have not yet been thoroughly explored. Fe-ligand exchange kinetics, rapid shifts in Fe-solubility, or quick changes in pressure or dissolved gas concentrations appear to affect Fe activity, and the Fe-ISE offers a new way to experimentally study these potential factors.

Although we hope this work provides a useful foundation for oceanographic Fe-ISE implementation, we understand that it is far from complete. Thinking about extremely low ionic activities in this way is relatively new, and using such a sensor to gain truly useful environmental information is a widely cross-disciplinary pursuit. We hope that we have opened the minds of marine chemists to the potential value of the Fe-ISE, and we encourage future research to expand our understanding of these fascinating sensors.

REFERENCES

Achterberg, E. P.; Holland, T. W.; Bowie, A. R.; Mantoura, R. F. C.; Worsfold, P. J. Determination of Iron in Seawater. *Analytica Chimica Acta* **2001**, *442* (1), 1–14. https://doi.org/10.1016/S0003-2670(01)01091-1.

Anderson, M. A.; Morel, F. M. M. The Influence of Aqueous Iron Chemistry on the Uptake of Iron by the Coastal Diatom Thalassiosira Weissflogii1. *Limnology and Oceanography* **1982**, *27* (5), 789–813. https://doi.org/10.4319/lo.1982.27.5.0789.

Anderson, R. F. GEOTRACES: Accelerating Research on the Marine Biogeochemical Cycles of Trace Elements and Their Isotopes. *Annual Review of Marine Science* **2020**, *12* (1). https://doi.org/10.1146/annurev-marine-010318-095123.

Avdeef, Alex.; Zabronsky, Jerome.; Stuting, H. H. Calibration of Copper Ion Selective Electrode Response to pCu 19. *Anal. Chem.* **1983**, *55* (2), 298–304. https://doi.org/10.1021/ac00253a027.

Baker, C. T.; Trachtenberg, I. Ion Selective Electrochemical Sensors—Fe+3, Cu+2. *Journal of The Electrochemical Society* **1971**, *118* (4). https://doi.org/10.1149/1.2408113.

Barbeau, K. Photochemistry of Organic Iron(III) Complexing Ligands in Oceanic Systems. *Photochemistry and Photobiology* **2006**, *82* (6). https://doi.org/10.1562/2006-06-16-ir-935.

Belli, S. L.; Zirino, A. Behavior and Calibration of the Copper(II) Ion-Selective Electrode in High Chloride Media and Marine Waters. *Analytical Chemistry* **1993**, *65* (19). https://doi.org/10.1021/ac00067a007.

Blake, A. C.; Chadwick, D. B.; Zirino, A.; Rivera-Duarte, I. Spatial and Temporal Variations in Copper Speciation in San Diego Bay. *Estuaries* **2004**, *27* (3). https://doi.org/10.1007/BF02803536.

Boiteau, R. M.; Fitzsimmons, J. N.; Repeta, D. J.; Boyle, E. A. Detection of Iron Ligands in Seawater and Marine Cyanobacteria Cultures by High-Performance Liquid Chromatography-Inductively Coupled Plasma-Mass Spectrometry. *Analytical Chemistry* **2013**, *85* (9). https://doi.org/10.1021/ac3034568.

Boiteau, R. M.; Repeta, D. J. Slow Kinetics of Iron Binding to Marine Ligands in Seawater Measured by Isotope Exchange Liquid Chromatography-Inductively Coupled Plasma Mass Spectrometry. *Environmental Science and Technology* **2022**, *56* (6). https://doi.org/10.1021/acs.est.1c06922.

Boiteau, R. M.; Till, C. P.; Coale, T. H.; Fitzsimmons, J. N.; Bruland, K. W.; Repeta, D. J. Patterns of Iron and Siderophore Distributions across the California Current System. *Limnology and Oceanography* **2019**, *64* (1). https://doi.org/10.1002/lno.11046.

Breitbarth, E.; Bellerby, R. J.; Neill, C. C.; Ardelan, M. V.; Meyerhöfer, M.; Zöllner, E.; Croot, P. L.; Riebesell, U. Ocean Acidification Affects Iron Speciation during a Coastal Seawater Mesocosm Experiment. *Biogeosciences* **2010**, *7* (3). https://doi.org/10.5194/bg-7-1065-2010.

Buck, K. N.; Lohan, M. C.; Berger, C. J. M.; Bruland, K. W. Dissolved Iron Speciation in Two Distinct River Plumes and an Estuary: Implications for Riverine Iron Supply. *Limnology and Oceanography* **2007**, *52* (2). https://doi.org/10.4319/lo.2007.52.2.0843.

Bundy, R. M.; Jiang, M.; Carter, M.; Barbeau, K. A. Iron-Binding Ligands in the Southern California Current System: Mechanistic Studies. *Frontiers in Marine Science* **2016**, *3* (MAR). https://doi.org/10.3389/fmars.2016.00027.

Caprara, S.; Buck, K. N.; Gerringa, L. J. A.; Rijkenberg, M. J. A.; Monticelli, D. A Compilation of Iron Speciation Data for Open Oceanic Waters. *Frontiers in Marine Science* **2016**, *3*.

Croot, P. L.; Heller, M. I. The Importance of Kinetics and Redox in the Biogeochemical Cycling of Iron in the Surface Ocean. *Frontiers in Microbiology* **2012**, *3* (JUN). https://doi.org/10.3389/fmicb.2012.00219.

Cuartero, M.; Bishop, J.; Walker, R.; Acres, R. G.; Bakker, E.; De Marco, R.; Crespo, G. A. Evidence of Double Layer/Capacitive Charging in Carbon Nanomaterial-Based Solid Contact Polymeric Ion-Selective Electrodes. *Chemical Communications* **2016**, *52* (62). https://doi.org/10.1039/c6cc04876e.

De Marco, R. Response of Copper(II) Ion Selective Electrodes in Seawater. *Analytical Chemistry* **1994**, 66, 3202-3207.

De Marco; Mackey, D. J. Calibration of a Chalcogenide Glass Membrane Ion-Selective Electrode for the Determination of Free Fe3+ in Seawater. *Marine Chemistry* **2000**, *68* (4), 283–294. https://doi.org/10.1016/S0304-4203(99)00084-5.

De Marco, R.; Clarke, G.; Pejcic, B. Ion-Selective Electrode Potentiometry in Environmental Analysis. *Electroanalysis* **2007**, *19* (19–20), 1987–2001. https://doi.org/10.1002/elan.200703916.

De Marco, R.; Eriksen, R.; Zirino, A. Electrochemical Impedance Spectroscopy Study of the Response Mechanism of the Jalpaite CuII Ion-Selective Electrode in Seawater. *Anal. Chem.* **1998**, *70* (22), 4683–4689. https://doi.org/10.1021/ac980196+.

De Marco, R.; Jiang, Z. T.; John, D.; Sercombe, M.; Kinsella, B. An in Situ Electrochemical Impedance Spectroscopy/Synchrotron Radiation Grazing Incidence X-Ray Diffraction Study of the Influence of Acetate on the Carbon Dioxide Corrosion of Mild Steel. *Electrochimica Acta* **2007**, *52* (11). https://doi.org/10.1016/j.electacta.2006.10.048.

De Marco, R.; Martizano, J. Response of the Iron Chalcogenide Glass Membrane Ion-Selective Electrode in a Seawater Ligand Mimetic Calibration Buffer. *Electroanalysis* **2007**, *19* (24), 2513–2517. https://doi.org/10.1002/elan.200704012.

De Marco, R.; Martizano, J. Response of a Copper(II) and Iron(III) Ion-Selective Electrode Bielectrode Array in Saline Media. *Talanta* **2008**, *75* (5). https://doi.org/10.1016/j.talanta.2008.01.018.

De Marco, R.; Pejcic, B. Electrochemical Impedance Spectroscopy and X-Ray Photoelectron Spectroscopy Study of the Response Mechanism of the Chalcogenide Glass Membrane Iron(III)

Ion-Selective Electrode in Saline Media. *Anal. Chem.* **2000**, *72* (4), 669–679. https://doi.org/10.1021/ac990603x.

De Marco, R.; Pejcic, B.; Wang, X. D. Continuous Flow Analysis of Iron (III) in Seawater Using a Chalcogenide Glass Ion-Selective Electrode. *Laboratory Robotics and Automation* **1999**, *11* (5), 284–288. https://doi.org/10.1002/(SICI)1098-2728(1999)11:5<284::AID-LRA7>3.0.CO;2-8.

De Marco, R.; Shackleton, J. Calibration of the Hg Chalcogenide Glass Membrane Ion-Selective Electrode in Seawater Media. *Talanta* **1999**, *49* (2). https://doi.org/10.1016/S0039-9140(99)00003-X.

Dudal, Y.; Gérard, F. Accounting for Natural Organic Matter in Aqueous Chemical Equilibrium Models: A Review of the Theories and Applications. *Earth-Science Reviews* **2004**, *66* (3–4). https://doi.org/10.1016/j.earscirev.2004.01.002.

Forsch, K. O.; Fulton, K. C.; Weiss, M. M.; Krause, J. W.; Stukel, M. R.; Barbeau, K. A. Iron Limitation and Biogeochemical Effects in Southern California Current Coastal Upwelling Filaments. *Journal of Geophysical Research: Oceans* **2023**, *128* (11). https://doi.org/10.1029/2023JC019961.

Forsch, K. O.; Hahn-Woernle, L.; Sherrell, R. M.; Roccanova, V. J.; Bu, K.; Burdige, D.; Vernet, M.; Barbeau, K. A. Seasonal Dispersal of Fjord Meltwaters as an Important Source of Iron and Manganese to Coastal Antarctic Phytoplankton. *Biogeosciences* **2021**, *18* (23). https://doi.org/10.5194/bg-18-6349-2021.

Gerringa, L. J. A.; Rijkenberg, M. J. A.; Schoemann, V.; Laan, P.; de Baar, H. J. W. Organic Complexation of Iron in the West Atlantic Ocean. *Marine Chemistry* **2015**, *177*, 434–446. https://doi.org/10.1016/j.marchem.2015.04.007.

Gerringa, L. J. A.; Gledhill, M.; Ardiningsih, I.; Muntjewerf, N.; Laglera, L. M. Comparing CLE-AdCSV Applications Using SA and TAC to Determine the Fe-Binding Characteristics of Model Ligands in Seawater. *Biogeosciences* **2021**, *18* (19), 5265–5289. https://doi.org/10.5194/bg-18-5265-2021.

Gledhill, M.; Achterberg, E. P.; Li, K.; Mohamed, K. N.; Rijkenberg, M. J. A. Influence of Ocean Acidification on the Complexation of Iron and Copper by Organic Ligands in Estuarine Waters. *Marine Chemistry* **2015**, *177*. https://doi.org/10.1016/j.marchem.2015.03.016.

Gledhill, M.; Gerringa, L. J. A. The Effect of Metal Concentration on the Parameters Derived from Complexometric Titrations of Trace Elements in Seawater—A Model Study. *Frontiers in Marine Science* **2017**, *4*.

Gledhill, M.; Zhu, K.; Rusiecka, D.; Achterberg, E. P. Competitive Interactions Between Microbial Siderophores and Humic-Like Binding Sites in European Shelf Sea Waters. *Frontiers in Marine Science* **2022**, *9*. https://doi.org/10.3389/fmars.2022.855009.

Haskell, W. Z.; Prokopenko, M. G.; Hammond, D. E.; Stanley, R. H. R.; Sandwith, Z. O. Annual Cyclicity in Export Efficiency in the Inner Southern California Bight. *Global Biogeochemical Cycles* **2017**, *31* (2). https://doi.org/10.1002/2016GB005561.

Jasinski, R.; Trachtenberg, I. Potentiometric Titration of Sulfate Using an Ion-Selective Iron Electrode. *Analytical Chemistry* **1972**, *44* (14). https://doi.org/10.1021/ac60322a030.

Jasinski, R.; Trachtenberg, I. Evaluation of the Ferric Ion Sensitive Chalcogenide Glass Electrode. *Journal of The Electrochemical Society* **1973**, *120* (9). https://doi.org/10.1149/1.2403655.

Jasinski, R.; Trachtenberg, I.; Andrychuk, D. Potentiometric Measurement of Copper in Seawater with Ion Selective Electrodes. *Analytical Chemistry* **1974**, *46* (3). https://doi.org/10.1021/ac60339a007.

Kinniburgh, D. G.; Van Riemsdijk, W. H.; Koopal, L. K.; Borkovec, M.; Benedetti, M. F.; Avena, M. J. Ion Binding to Natural Organic Matter: Competition, Heterogeneity, Stoichiometry and Thermodynamic Consistency. In *Colloids and Surfaces A: Physicochemical and Engineering Aspects*; 1999; Vol. 151. https://doi.org/10.1016/S0927-7757(98)00637-2.

Koenig, C. E.; Grabner, E. W. Reinvestigation of a Ferric Ion-Selective Electrode Based on the Chalcogenide Glass FexSe60Ge28Sb12(x = 1–10). *Electroanalysis* **1995**, *7* (11), 1090–1094. https://doi.org/10.1002/elan.1140071117.

Koopal, L. K.; Saito, T.; Pinheiro, J. P.; Van Riemsdijk, W. H. Ion Binding to Natural Organic Matter: General Considerations and the NICA-Donnan Model. In *Colloids and Surfaces A: Physicochemical and Engineering Aspects*; 2005; Vol. 265. https://doi.org/10.1016/j.colsurfa.2004.11.050.

Körtzinger, A.; Schimanski, J.; Send, U. High Quality Oxygen Measurements from Profiling Floats: A Promising New Technique. *Journal of Atmospheric and Oceanic Technology* **2005**, *22* (3). https://doi.org/10.1175/JTECH1701.1.

Kuma, K.; Nakabayashi, S.; Matsunaga, K. Photoreduction of Fe(III) by Hydroxycarboxylic Acids in Seawater. *Water Research* **1995**, *29* (6). https://doi.org/10.1016/0043-1354(94)00289-J.

Kuma, K.; Nakabayashi, S.; Suzuki, Y.; Kudo, I.; Matsunaga, K. Photo-Reduction of Fe(III) by Dissolved Organic Substances and Existence of Fe(II) in Seawater during Spring Blooms. *Marine Chemistry* **1992**, *37* (1–2). https://doi.org/10.1016/0304-4203(92)90054-E.

Kuma, K.; Nishioka, J.; Matsunaga, K. Controls on Iron(III) Hydroxide Solubility in Seawater: The Influence of pH and Natural Organic Chelators. *Limnology and Oceanography* **1996**, *41* (3). https://doi.org/10.4319/lo.1996.41.3.0396.

Laglera, L. M.; Filella, M. The Relevance of Ligand Exchange Kinetics in the Measurement of Iron Speciation by CLE-AdCSV in Seawater. *Marine Chemistry* **2015**, *173*. https://doi.org/10.1016/j.marchem.2014.09.005.

Laglera, L. M.; Filella, M. The Relevance of Ligand Exchange Kinetics in the Measurement of Iron Speciation by CLE-AdCSV in Seawater. *Marine Chemistry* **2015**, *173*. https://doi.org/10.1016/j.marchem.2014.09.005.

Lauderdale, J. M.; Braakman, R.; Forget, G.; Dutkiewicz, S.; Follows, M. J. Microbial Feedbacks Optimize Ocean Iron Availability. *Proceedings of the National Academy of Sciences of the United States of America* **2020**, *117* (9). https://doi.org/10.1073/pnas.1917277117.

Lie, A. A. Y.; Kim, D. Y.; Schnetzer, A.; Caron, D. A. Small-Scale Temporal and Spatial Variations in Protistan Community Composition at the San Pedro Ocean Time-Series Station off the Coast of Southern California. *Aquatic Microbial Ecology* **2013**, *70* (2). https://doi.org/10.3354/ame01652.

Liu, F.; Gledhill, M.; Tan, Q. G.; Zhu, K.; Zhang, Q.; Salaün, P.; Tagliabue, A.; Zhang, Y.; Weiss, D.; Achterberg, E. P.; Korchev, Y. Phycosphere pH of Unicellular Nano- and Micro-Phytoplankton Cells and Consequences for Iron Speciation. *ISME Journal* **2022**, *16* (10). https://doi.org/10.1038/s41396-022-01280-1.

Liu, F.; Tan, Q. G.; Weiss, D.; Crémazy, A.; Fortin, C.; Campbell, P. G. C. Unravelling Metal Speciation in the Microenvironment Surrounding Phytoplankton Cells to Improve Predictions of Metal Bioavailability. *Environmental Science and Technology* **2020**, *54* (13). https://doi.org/10.1021/acs.est.9b07773.

Liu, X.; Millero, F. J. The Solubility of Iron Hydroxide in Sodium Chloride Solutions. *Geochimica et Cosmochimica Acta* **1999**, *63* (19–20). https://doi.org/10.1016/S0016-7037(99)00270-7.

Lodeiro, P.; Rey-Castro, C.; David, C.; Achterberg, E. P.; Puy, J.; Gledhill, M. Acid-Base Properties of Dissolved Organic Matter Extracted from the Marine Environment. *Science of the Total Environment* **2020**, *729*. https://doi.org/10.1016/j.scitotenv.2020.138437.

Lohan, M. C.; Aguilar-Islas, A. M.; Bruland, K. W. Direct Determination of Iron in Acidified (pH 1.7) Seawater Samples by Flow Injection Analysis with Catalytic Spectrophotometric Detection: Application and Intercomparison. *Limnology and Oceanography: Methods* **2006**, *4* (JUN.). https://doi.org/10.4319/lom.2006.4.164.

Mahieu, L.; Omanović, D.; Whitby, H.; Buck, K. N.; Caprara, S.; Salaün, P. Recommendations for Best Practice for Iron Speciation by Competitive Ligand Exchange Adsorptive Cathodic Stripping Voltammetry with Salicylaldoxime. *Marine Chemistry* **2024**, *259*. https://doi.org/10.1016/j.marchem.2023.104348.

Maldonado, M. T.; Price, N. M. Utilization of Iron Bound to Strong Organic Ligands by Plankton Communities in the Subarctic Pacific Ocean. *Deep-Sea Research Part II: Topical Studies in Oceanography* **1999**, *46* (11–12). https://doi.org/10.1016/S0967-0645(99)00071-5.

Manck, L. E.; Park, J.; Tully, B. J.; Poire, A. M.; Bundy, R. M.; Dupont, C. L.; Barbeau, K. A. Petrobactin, a Siderophore Produced by Alteromonas, Mediates Community Iron Acquisition in the Global Ocean. *ISME J* **2022**, *16* (2), 358–369. https://doi.org/10.1038/s41396-021-01065-y.

Marcinek, S.; Chapoulie, A.; Salaün, P.; Smith, S.; Omanović, D. Revised Application of Copper Ion Selective Electrode (Cu-ISE) in Marine Waters: A New Meta-Calibration Approach. *Talanta* **2021**, *226*. https://doi.org/10.1016/j.talanta.2021.122170.

Maric, M.; Sohail, M.; De Marco, R. A near Edge X-Ray Absorption Fine Structure (NEXAFS) Study of the Response Mechanism of the Iron (III) Chalcogenide Glass Membrane Ion-Selective Electrode. *Electrochemistry Communications* **2014**, *41*, 27–30. https://doi.org/10.1016/j.elecom.2014.01.017.

Maric, M.; Sohail, M.; Veder, J.-P.; De Marco, R. Development of an Improved Ligand Mimetic Calibration System for the Analysis of Iron(III) in Seawater Using the Iron(III) Chalcogenide Glass Ion Selective Electrode: A Combined Mechanistic and Analytical Study. *Sensors and Actuators B: Chemical* **2015**, *207*, 907–917. https://doi.org/10.1016/j.snb.2014.09.003.

Martin, J. H. Glacial-interglacial CO2 Change: The Iron Hypothesis. *Paleoceanography* **1990**, *5* (1). https://doi.org/10.1029/PA005i001p00001.

Martin, J. H.; Fitzwater, S. E. Iron Deficiency Limits Phytoplankton Growth in the North-East Pacific Subarctic. *Nature* **1988**, *331* (6154), 341–343. https://doi.org/10.1038/331341a0.

Martin, J. H.; Fitzwater, S. E.; Gordon, R. M. Iron Deficiency Limits Phytoplankton Growth in Antarctic Waters. *Global Biogeochemical Cycles* **1990**. https://doi.org/10.1029/GB004i001p00005.

Martin, J. H.; Michael Gordon, R. Northeast Pacific Iron Distributions in Relation to Phytoplankton Productivity. *Deep Sea Research Part A, Oceanographic Research Papers* **1988**, *35* (2). https://doi.org/10.1016/0198-0149(88)90035-0.

Mellett, T.; Brown, M. T.; Chappell, P. D.; Duckham, C.; Fitzsimmons, J. N.; Till, C. P.; Sherrell, R. M.; Maldonado, M. T.; Buck, K. N. The Biogeochemical Cycling of Iron, Copper, Nickel, Cadmium, Manganese, Cobalt, Lead, and Scandium in a California Current Experimental Study. *Limnology and Oceanography* **2018**, *63*. https://doi.org/10.1002/lno.10751.

Miao, A. J.; Wang, W. X. Fulfilling Iron Requirements of a Coastal Diatom under Different Temperatures and Irradiances. *Limnology and Oceanography* **2006**, *51* (2). https://doi.org/10.4319/lo.2006.51.2.0925.

Millero, F. J. Solubility of Fe(III) in Seawater. *Earth and Planetary Science Letters* **1998**, *154* (1–4). https://doi.org/10.1016/s0012-821x(97)00179-9.

Millero, F. J.; Woosley, R.; Ditrolio, B.; Waters, J. Effect of Ocean Acidification on the Speciation of Metals in Seawater. *Oceanography* **2009**, *22* (SPL.ISS. 4). https://doi.org/10.5670/oceanog.2009.98.

Millero, F. J.; Yao, W.; Aicher, J. The Speciation of Fe(II) and Fe(III) in Natural Waters. *Marine Chemistry* **1995**, *50* (1–4). https://doi.org/10.1016/0304-4203(95)00024-L.

Millero, F. J.; Yao, W.; Aicher, J. The Speciation of Fe(II) and Fe(III) in Natural Waters. *Marine Chemistry* **1995**, *50* (1), 21–39. https://doi.org/10.1016/0304-4203(95)00024-L.

Moore, R. M.; Millward, G. E. Dissolved-Particulate Interactions of Aluminium in Ocean Waters. *Geochimica et Cosmochimica Acta* **1984**, *48* (2). https://doi.org/10.1016/0016-7037(84)90247-3.

Neira, C.; Mendoza, G.; Levin, L. A.; Zirino, A.; Delgadillo-Hinojosa, F.; Porrachia, M.; Deheyn, D. D. Macrobenthic Community Response to Copper in Shelter Island Yacht Basin, San Diego Bay, California. *Marine Pollution Bulletin* **2011**, *62* (4). https://doi.org/10.1016/j.marpolbul.2011.01.027.

Omanović, D.; Garnier, C.; Pižeta, I. ProMCC: An All-in-One Tool for Trace Metal Complexation Studies. *Marine Chemistry* **2015**, *173*, 25–39. https://doi.org/10.1016/j.marchem.2014.10.011.

Öztürk, M.; Croot, P. L.; Bertilsson, S.; Abrahamsson, K.; Karlson, B.; David, R.; Fransson, A.; Sakshaug, E. Iron Enrichment and Photoreduction of Iron under UV and PAR in the Presence of Hydroxycarboxylic Acid: Implications for Phytoplankton Growth in the Southern Ocean. *Deep-Sea Research Part II: Topical Studies in Oceanography* **2004**, *51* (22–24). https://doi.org/10.1016/j.dsr2.2000.10.001.

Pejcic, B.; De Marco, R.; Buckley, C. E.; Maitland, C. F.; Knott, R. A Small Angle Neutron Scattering and Electrochemical Impedance Spectroscopy Study of the Nanostructure of the Iron Chalcogenide Glass Ion-Selective Electrode. *Talanta* **2004**, *63* (1). https://doi.org/10.1016/j.talanta.2003.11.025.

Pejcic, B.; De Marco, R.; Prince, K. Surface Studies of a Chalcogenide Glass Ferric Ion-Selective Electrode Part 1: Influence of Ferric and Hydroxide Ions on Interfacial Kinetics. *Surface and Interface Analysis* **2002**, *33* (9). https://doi.org/10.1002/sia.1449.

Pejcic, B.; De Marco, R.; Prince, K. Surface Studies of a Chalcogenide Glass Ferric Ion-Selective Electrode Part 2. The Effects of Inorganic Ions, Organic Ligands and Seawater on Sensor Response. *Surface and Interface Analysis* **2002**, *33* (9). https://doi.org/10.1002/sia.1450.

Powell, R. T.; Wilson-Finelli, A. Photochemical Degradation of Organic Iron Complexing Ligands in Seawater. *Aquatic Sciences* **2003**, *65* (4). https://doi.org/10.1007/s00027-003-0679-0.

Rapp, I.; Schlosser, C.; Browning, T. J.; Wolf, F.; Le Moigne, F. A. C.; Gledhill, M.; Achterberg, E. P. El Niño-Driven Oxygenation Impacts Peruvian Shelf Iron Supply to the South Pacific Ocean. *Geophysical Research Letters* **2020**, *47* (7). https://doi.org/10.1029/2019GL086631.

Rivera-Duarte, I.; Rosen, G.; Lapota, D.; Chadwick, D. B.; Kear-Padilla, L.; Zirino, A. Copper Toxicity to Larval Stages of Three Marine Invertebrates and Copper Complexation Capacity in San Diego Bay, California. *Environmental Science and Technology* **2005**, *39* (6). https://doi.org/10.1021/es040545j.

Robinson, D.; Pham, A. L. D.; Yousavich, D. J.; Janssen, F.; Wenzhöfer, F.; Arrington, E. C.; Gosselin, K. M.; Sandoval-Belmar, M.; Mar, M.; Valentine, D. L.; Bianchi, D.; Treude, T. Iron "Ore" Nothing: Benthic Iron Fluxes from the Oxygen-Deficient Santa Barbara Basin Enhance Phytoplankton Productivity in Surface Waters. *Biogeosciences* **2024**, *21* (3). https://doi.org/10.5194/bg-21-773-2024.

Rose, A. L.; Waite, T. D. Kinetics of Hydrolysis and Precipitation of Ferric Iron in Seawater. *Environmental Science and Technology* **2003**, *37* (17). https://doi.org/10.1021/es034102b.

Rue, E. L.; Bruland, K. W. Complexation of Iron(III) by Natural Organic Ligands in the Central North Pacific as Determined by a New Competitive Ligand Equilibration/Adsorptive Cathodic Stripping Voltammetric Method. *Marine Chemistry* **1995**. https://doi.org/10.1016/0304-4203(95)00031-L.

Schefer, U.; Ammann, D.; Pretsch, E.; Oesch, U.; Simon, W. Neutral Carrier Based Ca2+-Selective Electrode with Detection Limit in the Sub-Nanomolar Range. *Analytical Chemistry* **1986**, *58* (11). https://doi.org/10.1021/ac00124a036.

Slagter, H. A.; Laglera, L. M.; Sukekava, C.; Gerringa, L. J. A. Fe-Binding Organic Ligands in the Humic-Rich TransPolar Drift in the Surface Arctic Ocean Using Multiple Voltammetric Methods. *Journal of Geophysical Research: Oceans* **2019**. https://doi.org/10.1029/2018JC014576.

Smith, M. J.; Manahan, S. E. Copper Determination in Water by Standard Addition Potentiometry. *Analytical Chemistry* **1973**, *45* (6). https://doi.org/10.1021/ac60328a009.

Sokalski, T.; Ceresa, A.; Zwickl, T.; Pretsch, E. Large Improvement of the Lower Detection Limit of Ion-Selective Polymer Membrane Electrodes. *Journal of the American Chemical Society* **1997**, *119* (46). https://doi.org/10.1021/ja972932h.

Spackeen, J. L.; Sipler, R. E.; Bertrand, E. M.; Xu, K.; McQuaid, J. B.; Walworth, N. G.; Hutchins, D. A.; Allen, A. E.; Bronk, D. A. Impact of Temperature, CO2, and Iron on Nutrient Uptake by a Late-Season Microbial Community from the Ross Sea, Antarctica. *Aquatic Microbial Ecology* **2018**, *82* (2). https://doi.org/10.3354/ame01886.

Stockdale, A.; Tipping, E.; Lofts, S.; Mortimer, R. J. G. Effect of Ocean Acidification on Organic and Inorganic Speciation of Trace Metals. *Environmental Science and Technology* **2016**, *50* (4). https://doi.org/10.1021/acs.est.5b05624.

Sukekava, C. F.; Downes, J.; Filella, M.; Vilanova, B.; Laglera, L. M. Ligand Exchange Provides New Insight into the Role of Humic Substances in the Marine Iron Cycle. *Geochimica et Cosmochimica Acta* **2024**, *366*. https://doi.org/10.1016/j.gca.2023.12.007.

Sunda, W.; Huntsman, S. Effect of pH, Light, and Temperature on Fe-EDTA Chelation and Fe Hydrolysis in Seawater. *Marine Chemistry* **2003**, *84* (1–2). https://doi.org/10.1016/S0304-4203(03)00101-4.

Town, R. M.; Filella, M. Dispelling the Myths: Is the Existence of L1 and L2 Ligands Necessary to Explain Metal Ion Speciation in Natural Waters? *Limnology and Oceanography* **2000**, *45* (6), 1341–1357. https://doi.org/10.4319/lo.2000.45.6.1341.

Wirth, T.; Takeshita, Y.; Davis, B.; Park, E.; Hu, I.; Huffard, C. L.; Johnson, K. S.; Nicholson, D.; Staudinger, C.; Warren, J. K.; Martz, T. Assessment of a pH Optode for Oceanographic Moored and Profiling Applications. *Limnology and Oceanography Methods* **2024**, 22 (11), 805-802. https://doi.org/10.1002/lom3.10646

Velasquez, I. B.; Ibisanmi, E.; Maas, E. W.; Boyd, P. W.; Nodder, S.; Sander, S. G. Ferrioxamine Siderophores Detected amongst Iron Binding Ligands Produced during the Remineralization of Marine Particles. *Frontiers in Marine Science* **2016**, *3*.

Vlasov, Y. G.; Bychkov, E. A. Chalcogenide Glass Chemical Sensors: Relationship between Ionic Response, Surface Ion Exchange and Bulk Membrane Transport. *Journal of Electroanalytical Chemistry* **1994**, *378* (1–2). https://doi.org/10.1016/0022-0728(94)87072-1.

Vlasov, Y. G.; Bychkov, E. A.; Legin, A. V. Chalcogenide Glass Chemical Sensors: Research and Analytical Applications. *Talanta* **1994**, *41* (6). https://doi.org/10.1016/0039-9140(94)00124-3.

Worsfold, P. J.; Lohan, M. C.; Ussher, S. J.; Bowie, A. R. Determination of Dissolved Iron in Seawater: A Historical Review. *Marine Chemistry* **2014**, *166*, 25–35. https://doi.org/10.1016/j.marchem.2014.08.009.

Ye, Y.; Völker, C.; Gledhill, M. Exploring the Iron-Binding Potential of the Ocean Using a Combined pH and DOC Parameterization. *Global Biogeochemical Cycles* **2020**, *34* (6). https://doi.org/10.1029/2019GB006425.

Zhu, K.; Achterberg, E. P.; Bates, N. R.; Gerringa, L. J. A.; Middag, R.; Hopwood, M. J.; Gledhill, M. Influence of Changes in pH and Temperature on the Distribution of Apparent Iron Solubility in the Oceans. *Global Biogeochemical Cycles* **2023**, *37* (5). https://doi.org/10.1029/2022GB007617.

Zhu, K.; Birchill, A. J.; Milne, A.; Ussher, S.; Humphreys, M. P.; Carr, N.; Mahaffey, C.; Lohan, M. C.; Achterberg, E. P.; Gledhill, M. Equilibrium Calculations of Iron Speciation and Apparent Iron Solubility in the Celtic Sea at Ambient Seawater pH Using the NICA-Donnan Model. *Marine Chemistry* **2021**, *237*. https://doi.org/10.1016/j.marchem.2021.104038.

Zhu, K.; Hopwood, M. J.; Groenenberg, J. E.; Engel, A.; Achterberg, E. P.; Gledhill, M. Influence of pH and Dissolved Organic Matter on Iron Speciation and Apparent Iron Solubility in the Peruvian Shelf and Slope Region. *Environ. Sci. Technol.* **2021**, *55* (13), 9372–9383. https://doi.org/10.1021/acs.est.1c02477.

Zirino, A.; A. VanderWeele, D.; Belli, S. L.; Roland DeMarco; Mackey, D. J. Direct Measurement of Cu(II)Aq in Seawater at pH 8 with the Jalpaite Ion-Selective Electrode. *Marine Chemistry* **1998**, *61* (3), 173–184. https://doi.org/10.1016/S0304-4203(97)00108-4.

Zirino, A.; De Marco, R.; Rivera, I.; Pejcic, B. The Influence of Diffusion Fluxes on the Detection Limit of the Jalpaite Copper Ion-Selective Electrode. *Electroanalysis* **2002**, *14* (7–8), 493–498. https://doi.org/10.1002/1521-4109(200204)14:7/8<493::AID-ELAN493>3.0.CO;2-C.